

Central Lancashire Online Knowledge (CLOK)

Title	Open Issues in Non-Gaussian Transport and Acceleration of Charged Energetic Particles in Space and Astrophysical Plasmas
Type	Article
URL	https://clock.uclan.ac.uk/id/eprint/56565/
DOI	https://doi.org/10.1007/s11214-025-01203-4
Date	2025
Citation	Effenberger, F., Walter, D., Fichtner, H., Aerdker, S., Grauer, R., Laitinen, Timo Lauri mikael, le Roux, J. A., Litvinenko, Y., Lübke, J. et al (2025) Open Issues in Non-Gaussian Transport and Acceleration of Charged Energetic Particles in Space and Astrophysical Plasmas. Space Science Reviews, 221 (5). p. 75. ISSN 0038-6308
Creators	Effenberger, F., Walter, D., Fichtner, H., Aerdker, S., Grauer, R., Laitinen, Timo Lauri mikael, le Roux, J. A., Litvinenko, Y., Lübke, J., Perri, S., Reichherzer, P., Shalchi, A., van den Berg, J. P. and Zimbardo, G.

It is advisable to refer to the publisher's version if you intend to cite from the work.
<https://doi.org/10.1007/s11214-025-01203-4>

For information about Research at UCLan please go to <http://www.uclan.ac.uk/research/>

All outputs in CLOK are protected by Intellectual Property Rights law, including Copyright law. Copyright, IPR and Moral Rights for the works on this site are retained by the individual authors and/or other copyright owners. Terms and conditions for use of this material are defined in the <http://clock.uclan.ac.uk/policies/>

Central Lancashire Online Knowledge (CLOK)

Title	Open Issues in Non-Gaussian Transport and Acceleration of Charged Energetic Particles in Space and Astrophysical Plasmas
Type	Article
URL	https://clock.uclan.ac.uk/id/eprint/56565/
DOI	https://doi.org/10.1007/s11214-025-01203-4
Date	2025
Citation	Effenberger, F., Walter, D., Fichtner, H., Aerdker, S., Grauer, R., Laitinen, T., le Roux, J. A., Litvinenko, Y., Lübke, J. et al (2025) Open Issues in Non-Gaussian Transport and Acceleration of Charged Energetic Particles in Space and Astrophysical Plasmas. Space Science Reviews, 221 (5). p. 75. ISSN 1572-9672
Creators	Effenberger, F., Walter, D., Fichtner, H., Aerdker, S., Grauer, R., Laitinen, T., le Roux, J. A., Litvinenko, Y., Lübke, J., Perri, S., Reichherzer, P., Shalchi, A., van den Berg, J. P. and Zimbardo, G.

It is advisable to refer to the publisher's version if you intend to cite from the work.
<https://doi.org/10.1007/s11214-025-01203-4>

For information about Research at UCLan please go to <http://www.uclan.ac.uk/research/>

All outputs in CLOK are protected by Intellectual Property Rights law, including Copyright law. Copyright, IPR and Moral Rights for the works on this site are retained by the individual authors and/or other copyright owners. Terms and conditions for use of this material are defined in the <http://clock.uclan.ac.uk/policies/>



Open Issues in Non-Gaussian Transport and Acceleration of Charged Energetic Particles in Space and Astrophysical Plasmas

F. Effenberger¹ · D. Walter¹ · H. Fichtner¹ · S. Aerdker¹ · R. Grauer¹ · T. Laitinen² · J.A. le Roux³ · Y. Litvinenko¹ · J. Lübke¹ · S. Perri⁴ · P. Reichherzer⁵ · A. Shalchi⁶ · J.P. van den Berg⁷ · G. Zimbardo⁴

Received: 26 August 2024 / Accepted: 30 July 2025
© The Author(s) 2025

Abstract

This review explores the anomalous transport and acceleration of charged energetic particles in heliospheric and astrophysical plasmas. Traditional diffusion-advection models can be insufficient to fully describe the observed behavior of energetic particles, prompting the need for alternative frameworks based on non-Gaussian stochastic processes and fractional differential equations to capture regimes of subdiffusion and superdiffusion of energetic particles. We discuss the theoretical basis of these non-Gaussian transport processes and examine the influence of magnetic turbulence, nonlinear diffusion, and field line random walk on particle dynamics. Superdiffusion, where the particle mean-square displacement grows faster than linear with time, and subdiffusion, with slower-than-linear growth, are observed across a range of environments from solar energetic particles to supernova remnants. This review highlights several examples from space and astrophysical plasmas that demonstrate instances of anomalous transport and acceleration, with a particular focus on its potential influence on fundamental processes such as shock acceleration and heliospheric energetic particle propagation. Long-range correlations and structures in space plasmas can impact both parallel and perpendicular transport. In the context of interplanetary shocks in the solar wind, parallel superdiffusion predominates due to a distinct pitch-angle scattering process not accounted for by quasi-linear theory, emphasizing the significance of nonlinear interactions and trapping effects. At quasi-parallel shocks in supernova remnants, parallel superdiffusion can also occur, leading to different acceleration spectra. In contrast to this superdiffusion along the magnetic field, field line random walk in combination with parallel particle diffusion can result in compound subdiffusion perpendicular to it. The review concludes with open questions and future directions for research that could deepen our understanding of particle transport in the turbulent environments of space and astrophysical plasmas.

Keywords Cosmic rays · Solar energetic particles · Particle transport · Particle acceleration · Numerical modelling · Synthetic turbulence · Review

Extended author information available on the last page of the article

1 Introduction

1.1 Motivation to Study Anomalous Transport

For the last 50 years since the introduction of the basic transport equation by Parker (1965), models for the acceleration and propagation of energetic particles in the heliosphere, the Galaxy and beyond, have adhered to the paradigm of a diffusion-advection equation describing the evolution of the particle distribution function. This equation holds, as long as the energetic particles interact with ‘scattering centers’, realized by fluctuations carried by the plasma, such that the fluctuations cause a normal Gaussian diffusion and advection of the energetic particles with the plasma. The Parker equation has been employed with great success, quantitatively computing the differential intensities of energetic test particles without altering the properties of the background plasma (see the recent review by Giacalone et al. 2022).

Since about 20 years (see, e.g., Zimbardo 2003) there is, however, increasing evidence that the diffusive transport of energetic particles can also be anomalous (as reviewed in Perri et al. 2022). Analyses of observations of energetic electrons (Perri and Zimbardo 2008a) and protons (Perri and Zimbardo 2015) as well as of the magnetic fluctuations upstream of interplanetary shocks (Perri et al. 2021), small-scale magnetic flux tubes in the interplanetary medium (le Roux and Zank 2021; le Roux 2023), and of relativistic electrons in supernova remnants (Perri et al. 2016) imply that the transport of energetic particles may not always be consistent with Gaussian diffusion but rather be sub- or superdiffusive. Signatures of the latter processes comprise modified spectra of energetic particles accelerated at shocks (Kirk et al. 1996; Perri and Zimbardo 2012a), extended or shortened acceleration times (Perri and Zimbardo 2015), increased intensity peaks at the acceleration sites (Effenberger and Litvinenko 2014; Prete et al. 2019), and spatial power laws upstream of shocks (Perri and Zimbardo 2009a). The concept of superdiffusion has not only been applied to shock acceleration processes in the heliosphere or at supernova remnants, but also to galactic superbubbles (Barghouty and Schnee 2012), to molecular clouds (Hu et al. 2022), to Galactic cosmic ray transport (Lagutin and Volkov 2024), and to galaxy clusters (Zimbardo and Perri 2018). The anomalous transport, however, cannot be described with standard Parker-type equations, but requires the consideration of so-called fractional transport equations.

Interestingly, the anomalous power-law scaling can also be a result of nonlinearities occurring in more sophisticated modelling, aimed at self-consistency. First extensions to self-consistency were made in the 1990s in two directions, with energetic particles changing the dynamics of the thermal plasma they traverse and affecting the evolution of the turbulence spectra within. The desired self-consistency is achieved by a nonlinear coupling of the linear Parker equation (possibly extended to contain momentum diffusion) to the (magneto)hydrodynamical equations describing a thermal background plasma or to a wave or turbulence transport equation. While in such coupling schemes, the nonlinearity does not directly extend to the diffusion process itself, which remains treated as normal (Gaussian) diffusion within the linear Parker equation, the alternative to the solution of coupled systems is the consideration of a single, but nonlinear diffusion-advection equation, see, e.g., Malkov et al. (2024). Notably, it has been shown that the transport resulting from such a nonlinear treatment of the diffusion term can be anomalous (e.g., Tsallis and Bukman 1996; Litvinenko et al. 2017). It appears that the topics of nonlinearity and anomaly of energetic particle transport as well as acceleration can be intrinsically linked.

1.2 Brief Overview over the Theoretical Framework of Anomalous Transport

The term ‘anomalous transport’ most often refers to ‘anomalous diffusion’. Diffusion can be quantified by considering the time evolution of the mean square displacements (MSDs) $\langle(\Delta x)^2\rangle$ as a result of an interaction or scattering process (e.g., Metzler and Klafter 2000, 2004; Eliazar and Klafter 2011):

$$\langle(\Delta x)^2\rangle = \kappa_\alpha t^\alpha \quad ; \quad 0 < \alpha < 2 \quad (1.1)$$

The different diffusion regimes can be classified with the exponent α :

$$\text{subdiffusion: } 0 < \alpha < 1$$

$$\text{Normal diffusion: } \alpha = 1$$

$$\text{superdiffusion: } 1 < \alpha < 2$$

While not always distinguished, the range for $\alpha > 2$ should be referred to as the superballistic regime ($\alpha = 2$ is the ballistic case).

One difficulty with the quantitative modeling of sub- and superdiffusion is related to the fact that the time-independent proportionality factor κ_α in Eq. (1.1) does not have the units of a normal diffusion coefficient (i.e. [length²/time] for $\alpha = 1$), in general, but a non-integer (or fractional) power of time. The corresponding transport equation has, therefore, also to be formulated for an anomalous ‘diffusion coefficient’ with fractional units. It can be shown (e.g., Metzler and Klafter 2000, for a heuristic argument see Fichtner et al. 2014) that this diffusion coefficient and the one in Eq. (1.1) are related via $\kappa_\mu = \kappa_\alpha^{1/\alpha}$ with $\mu = 2/\alpha$, and that the corresponding transport equation is a so-called fractional differential equation. In case of pure superdiffusion, the transport equation reads (for simplicity here in one space dimension):

$$\frac{\partial f}{\partial t} = \kappa_\mu \frac{\partial^\mu f}{\partial |x|^\mu} - V \frac{\partial f}{\partial x} + \frac{p}{3} \frac{\partial V}{\partial x} \frac{\partial f}{\partial p} + S(x, p, t) \quad (1.2)$$

wherein $f(x, p, t)$ is the omnidirectional phase space density of the energetic particles, x position, p momentum, t time, V the speed of the thermal plasma, and $S(x, p, t)$ a source/sink. The first term on the right-hand side generalizes the normal diffusion to superdiffusion. The fractional derivative ($1 < \mu < 2$) should be understood as the symmetric (indicated by the modulus of x) fractional Laplacian (e.g., Lischke et al. 2020) and is also known as the Riesz derivative (Riesz 1949, see later).

If superdiffusion and subdiffusion occur simultaneously, the transport equation takes the form

$${}_t D_*^\alpha f = \kappa_\mu \frac{\partial^\mu f}{\partial |x|^\mu} - V \frac{\partial f}{\partial x} + \frac{p}{3} \frac{\partial V}{\partial x} \frac{\partial f}{\partial p} + S(x, p, t) \quad (1.3)$$

where an additional fractional time derivative occurs. The latter can be understood as a Caputo derivative (e.g., Mainardi et al. 2007), for alternatives see, e.g., Tateishi et al. (2017). For numerical simulations it is useful to re-write Eq. (1.3) such that there remains a normal first-order time derivative on the left-hand side. When doing so, two alternatives have to be distinguished (Metzler and Klafter 2000), namely whether the subdiffusion-causing scattering centers (or ‘temporary particle traps’) are external to the moving medium or maintained

by it. The respective equations are

$$\frac{\partial f}{\partial t} = {}_0D_t^{1-\alpha} \left(\kappa_\mu \frac{\partial^\mu f}{\partial |x|^\mu} - V \frac{\partial f}{\partial x} + \frac{p}{3} \frac{\partial V}{\partial x} \frac{\partial f}{\partial p} \right) + S(x, p, t) \quad (1.4)$$

$$\frac{\partial f}{\partial t} = {}_0D_t^{1-\alpha} \left(\kappa_\mu \frac{\partial^\mu f}{\partial |x|^\mu} \right) - V \frac{\partial f}{\partial x} + \frac{p}{3} \frac{\partial V}{\partial x} \frac{\partial f}{\partial p} + S(x, p, t) \quad (1.5)$$

with the Riemann-Liouville fractional derivative ($1 < \alpha < 2$)

$${}_0D_t^{1-\alpha} f(t) = \frac{1}{\Gamma(\alpha)} \frac{d}{dt} \int_0^t (t-s)^{\alpha-1} f(s) ds. \quad (1.6)$$

As remarked by Metzler and Klafter (2000), only the second case is consistent with Galilei invariance. Interestingly, the first alternative implies a modified advective transport as particles are trapped at ‘scattering centers’ outside the considered medium. In that sense, there exist then also an anomalous advection. Given that the scattering centers, that are realized by the turbulence in a given astrophysical plasma, are most often maintained by the latter (i.e. are not external to it), the second alternative described by Eq. (1.5) is to be considered for those space and astrophysical applications. Note however, that an example for the exceptions of externally maintained ‘traps’ may be the inner solar wind boundary, where magnetic reconnection near current sheets associated with the so-called magnetic carpet in the corona continuously produces magnetic islands.

This distinction has consequences when applying the generalized Ito lemma (Itô 1951). According to Magdziarz and Weron (2007) the above Eq. (1.4) is, when neglecting any velocity gradient and source, equivalent to the following stochastic differential equations (SDE):

$$dx(\tau) = -V d\tau + k_\mu^{1/\mu} dL_\mu(\tau) \quad (1.7)$$

where τ is an internal time related to physical time t via a subordination, and L_μ is a Lévy process (Lévy 1926) that in the case $\mu = 2$ corresponds to the Wiener process associated with Gaussian diffusion. Therefore, for usual astrophysical applications the above SDE should not be employed with a subordination process applied to all terms including advection. The equivalence should only be exploited for the diffusion part, whereas the treatment of all effects related to advection require a different approach (e.g., a Strang splitting, Strang 1968).

A more fundamental study of anomalous transport can be carried out by solving the equations of motion (EoMs) of many particles in a prescribed turbulent medium, i.e. by so-called full-orbit simulations. For many astrophysical systems the relevant EoM is the so-called Newton-Lorentz equation (e.g., Shalchi and Dosch 2008):

$$\frac{d\vec{p}}{dt} = q(\vec{E} + \vec{v} \times \vec{B}) \quad (1.8)$$

wherein \vec{v} and \vec{p} are a particle’s velocity and momentum, q its charge, and $\vec{E} = \delta \vec{E}$ and $\vec{B} = \vec{B}_0 + \delta \vec{B}$ are the electric and magnetic field, respectively, decomposed in an average background and a fluctuating component. By solving for many particle orbits and computing their mean square displacements the nature of the transport and its dependence on the properties of the turbulence can be investigated in great detail.

Insights about anomalous diffusion regimes from full-orbit simulations will be dependent on the turbulent magnetic field model that is employed. A common approach is to consider synthetic fields that are a superposition of random-phase wave modes and that mimic the observed turbulence geometry, e.g. a dominant 2D mode in solar wind turbulence with a guide field. However, observations show also features of large-scale correlated structures in space plasma turbulence related to intermittency. Such structures can have an impact on the actual transport behaviour (e.g. Durrive et al. 2020; Lübke et al. 2024) and should be incorporated in synthetic turbulence models to gain a more complete understanding of possible anomalous propagation regimes. Intermittency has been observed in the solar wind (e.g. Bruno and Carbone 2013; Telloni et al. 2021) and the local interstellar medium (e.g. Fraternale et al. 2022) and there are observational indications that it is also ubiquitous in astrophysical plasmas, for example in molecular clouds (Falgarone et al. 2015). As discussed in Sect. 5.1.2, the presence of intermittent turbulence in a wide range of plasma environments may thus indicate that anomalous diffusion of energetic particles in astrophysical plasmas is also much more common than is usually assumed.

1.3 Structure of the Review

This review originated in a workshop titled ‘Nonlinear and Anomalous Transport of Energetic Particles in Astrophysical Environments’ that took place from 30 May to 2 June 2023 at the Ruhr-Universität Bochum, Germany. In what follows this introductory section (MA:¹ H. Fichtner, F. Effenberger; CA:² J.A. le Roux, D. Walter), rather than providing a complete overview of the relevant scientific activities, we highlight open issues in a, nonetheless, comprehensive way, and refer to earlier reviews for various details. In Sect. 2 (MA: S. Perri, G. Zimbardo, S. Aerdker, F. Effenberger, J.A. le Roux) different models of sub- and superdiffusion are discussed, in Sect. 3 (MA: D. Walter, CA: F. Effenberger, H. Fichtner, Y. Litvinenko) the topic of nonlinear diffusion and its relation to anomalous transport is presented, in Sect. 4 (MA: A. Shalchi; T. Laitinen), the relevance of field line random walk and the transition of subdiffusion to normal diffusion is investigated, and in Sect. 5 (MA: J. Lübke, P. Reichherzer, F. Effenberger; CA: R. Grauer, J.P. van den Berg) results from and issues with full-orbit simulations are reported. The final Sect. 6 (MA: F. Effenberger, H. Fichtner, D. Walter) briefly summarizes the review and lists open questions.

2 Contrasting Different Models for Super- and Subdiffusion

We present here a concise, and somewhat simplified, description of anomalous diffusion, with the purpose of contrasting the properties and the assumptions of different models of anomalous transport. The reader is referred to the cited literature for more formal treatments.

Normal diffusion is characterized by a mean square displacement (MSD) $\langle(\Delta x)^2\rangle$ growing linearly in time as $\langle(\Delta x)^2\rangle = 2Dt$ (see Eq. (1.1)), where the diffusion coefficient D can be expressed as $D = \frac{1}{3}\lambda v = \frac{1}{3}\lambda^2/\tau$, with λ the mean free path and v the random walker average speed. Also, $\lambda = v\tau$, with τ the “collision” time. On the other hand, anomalous diffusion is characterized by $\langle(\Delta x)^2\rangle \propto t^\alpha$ with $\alpha < 1$ for subdiffusion and $\alpha > 1$ for superdiffusion (see Eq. (1.1) again). Since the central limit theorem (CLT) states that in the long time limit the probability density of random walker positions has to be a Gaussian distribution, and

¹MA = main author(s)

²CA = contributing author(s)

the MSD has to grow as $2Dt$, the presence of superdiffusion implies that one or both of the basic assumptions of the CLT are not satisfied. These assumptions are (i) a finite mean square value of the free path lengths ℓ , i.e., $\langle \ell^2 \rangle = \lambda^2$, and (ii) independent, uncorrelated random displacements (e.g., Metzler and Klafter 2000, 2004; Zaburdaev et al. 2015). In this work we will consider that the elementary displacements ℓ are uncorrelated; then, we may say that we have superdiffusion when $\langle \ell^2 \rangle \rightarrow \infty$, i.e., when the mean free path diverges. In such a case the diffusion coefficient is diverging, too. Conversely, we have subdiffusion when the average time duration of the various free paths diverges, $\tau \rightarrow \infty$, so that $D \rightarrow 0$. In both cases, we have to consider a random walk process which has different statistical properties than a Gaussian random walk. This means that the probability $\Psi(\ell, \tau)$ of making an elementary free path of length ℓ in a time τ is a power-law function of ℓ , such that

$$\langle \ell^2 \rangle = \int_0^\infty d\tau \int_{-\infty}^\infty \ell^2 \Psi(\ell, \tau) d\ell = \infty. \quad (2.1)$$

If we assume that the probabilities of ℓ and τ are independent, i.e., if we assume that $\Psi(\ell, \tau) = g(\ell)\psi(\tau)$ with $\int_{-\infty}^\infty g(\ell) d\ell = 1$ and $\int_0^\infty \psi(\tau) d\tau = 1$, the divergence of $\langle \ell^2 \rangle$ implies that

$$g(\ell) \propto |\ell|^{-\mu-1} \quad (2.2)$$

for large $|\ell|$, with $1 < \mu < 2$; for small $|\ell|$, we consider that $g(\ell)$ has a non-diverging, bell-shaped form. The above expression for $g(\ell)$ means that the probability of very long paths is not exponentially small. These long free paths are called Lévy flights, and an appropriate treatment shows that the corresponding probability density function for the random walker position is given by a Lévy distribution (e.g., Zumofen and Klafter 1993; Metzler and Klafter 2000, 2004; Zaslavsky 2002; Zaburdaev et al. 2015),

$$P_{LF}(k, t) = \exp(-Ct|k|^\mu) \quad (2.3)$$

in Fourier space, and, in the limit $|x| \gg (Ct)^{1/\mu}$, in physical space

$$P_{LF}(x, t) \simeq \frac{\Gamma(\mu+1)}{\pi} \sin\left(\frac{\pi\mu}{2}\right) \frac{Ct}{|x|^{\mu+1}}. \quad (2.4)$$

Therefore, heavy tails for large $|x|$ are found in the probability density. This probability density is also the propagator of the problem, i.e., the solution of the transport equation for a delta-function initial condition, and can be contrasted with the Gaussian propagator found in the case of normal diffusion (e.g., Metzler and Klafter 2000, 2004). Further, if a power-law distribution of waiting times (or travel times) $\psi(\tau)$ such that $\langle \tau \rangle = \int_0^\infty \tau \psi(\tau) d\tau$ diverges, with $\langle \ell^2 \rangle$ being finite, subdiffusive transport can be found.

On the other hand, from the point of view of anomalous transport the Lévy flight description leads to the following problem: assuming $\langle x \rangle = 0$, if we compute the MSD at any given time t , we find

$$\langle x(t)^2 \rangle = \int_{-\infty}^\infty x^2 P_{LF}(x, t) dx = \infty, \quad (2.5)$$

that is, for $\mu < 2$ the MSD is diverging, too, and does not correspond to Eq. (1.1). This divergence is physically related to the fact that in the Lévy flight description ℓ can be covered even in an extremely short time, i.e., arbitrarily large speeds are possible, since the free

path length is independent from the time needed to cover it. This is in agreement with the factorization of $\Psi(\ell, \tau) = g(\ell)\psi(\tau)$ assumed above.

This problem can be solved by introducing Lévy walks (Shlesinger et al. 1987; Klafter et al. 1987; Metzler and Klafter 2004; Zaburdaev et al. 2015), where the probability of performing a free path of length ℓ is related to the time τ needed to cover the distance (the travel time). In the simple case of constant velocity v , the probability of displacements for large $|\ell|$ is given by

$$\Psi(\ell, \tau) = \frac{1}{2} A \delta(|\ell| - v\tau) |\ell|^{-\mu-1} \quad (2.6)$$

which also yields $\langle \ell^2 \rangle = \int \ell^2 \Psi(\ell, \tau) d\ell d\tau = \infty$ for $1 < \mu < 2$, but the δ -coupling between ℓ and τ ensures that the free paths are covered with a finite velocity v . Note that in our notation the speed v is always positive, while the displacement ℓ can be both positive or negative. Further, the δ -coupling means that ℓ and τ have the same power-law probability distribution. This implies that non-Markovianity, that is the presence of memory effects due to the presence of very long travel times, and non-locality, that is the presence of very long displacements in the random walk, go together in the case of Lévy walks. With the Lévy walk model, superdiffusion with an anomalous diffusion exponent $\alpha = 3 - \mu$ is obtained (Shlesinger et al. 1987; Klafter et al. 1987; Zumofen and Klafter 1993; Zimbardo and Perri 2013).

A derivation based on the continuous time random walk approach (that is, basically, on the Montroll-Weiss equation (Montroll and Weiss 1965)) shows that the propagator for Lévy walks is similar to that for Lévy flights, but has a cut off for $|x| > vt$, i.e., for distances larger than those which could be reached by particles which move ballistically for time t . Therefore, for $|x| < vt$ one has (Blumen et al. 1990; Zumofen and Klafter 1993; Metzler and Klafter 2004; Zimbardo and Perri 2013; Zaburdaev et al. 2015)

$$P_{LW}(x, t) \simeq \frac{\Gamma(\mu + 1)}{\pi} \sin\left(\frac{\pi\mu}{2}\right) \frac{Ct}{|x|^{\mu+1}}, \quad (2.7)$$

while the propagator goes to zero for $|x| \geq vt$. The comparison between the Lévy flights and Lévy walk propagators is given graphically in Fig. 1. The determination of the constant C is given in Zimbardo and Perri (2013) and Perri et al. (2015). With the Lévy walk propagator going to zero for $|x| > vt$, we can compute the MSD restricting the integration domain between $\pm vt$ (e.g., Perri et al. 2015),

$$\langle x^2 \rangle = \int_{-vt}^{vt} x^2 P_{LW}(x, t) dx \propto t^{3-\mu}, \quad (2.8)$$

in agreement with what is obtained by more formal derivations (Shlesinger et al. 1987; Klafter et al. 1987; Zumofen and Klafter 1993; Zimbardo and Perri 2013). In summary, we can see that the Lévy walk propagator is very similar to the Lévy flight propagator, even though they imply a different dynamical model (see also the discussion in Zaburdaev et al. 2015). From this point of view, the Lévy flight scenario can be used to describe Lévy walks to a good approximation (Perri et al. 2015). The actual Lévy walk propagator is shown graphically by Zaburdaev et al. (2015), Fig. 2. The latter study shows that spikes at $x = \pm vt$ are found in the propagator, which are due to the propagation of the ballistic fronts formed by those particles which are never scattered in the available time t — something which is reminiscent of the peak, observed in situ near the Earth, in the flux of solar energetic

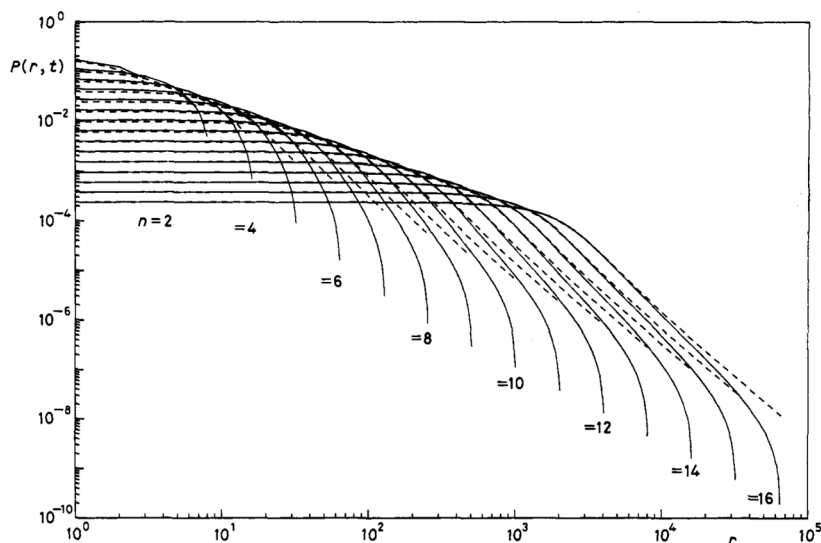
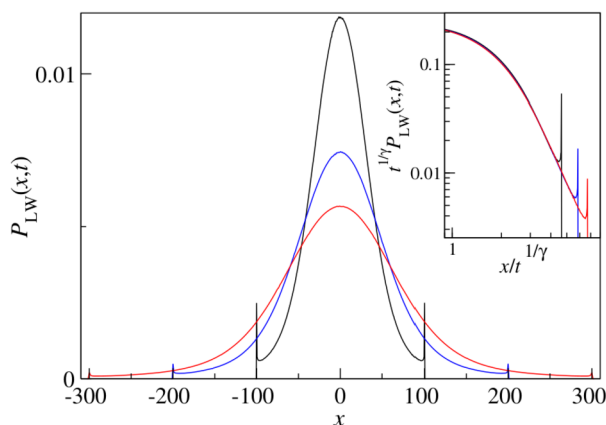


Fig. 1 Comparison between the Lévy walk propagators (solid lines) and the Lévy flight propagators (dashed lines) for $\mu = 1.5$ and for different dimensionless times given by $t = 2^n - 1$, with n indicated close to each curve. The propagator flattens and broadens as time goes by. Adopted from Blumen et al. (1990)

Fig. 2 Lévy walk propagator for $\mu = 1.5$ (here, $\mu \equiv \gamma$) for three different times $t = 100, 200$ and 300 in dimensionless units. Note the propagator spikes at the ballistic propagation fronts. The inset shows the same propagator in log-log axes, multiplied by the scaling factor $t^{1/\gamma}$, which allows to identify the power-law tails typical of Lévy distributions. Adopted from Zaburdaev et al. (2015)



particles accelerated near the sun, due to scatter-free particles (e.g., Lin 1974; Reames 1999; Lin 2005; Trotta and Zimbardo 2011).

Below we show how, in spite of the fact that Lévy walks and Lévy flights imply a different particle dynamics, the two processes lead to very similar results when the motion of energetic particles around interplanetary (IP) shocks are considered. We show this agreement first for analytical models, and then for numerical simulations.

2.1 Energetic Particle Profile at Shocks Obtained by the Lévy Walk Propagator

Perri and Zimbardo (2007, 2008b) considered the behaviour of energetic particles accelerated by interplanetary (IP) shock waves, which are measured in situ by many spacecraft.

Assuming a one-dimensional shock, which is a reasonable assumption at large heliocentric distances, we can express the density $n(x, E, t)$ of particles of a given energy E , either upstream or downstream of the source, as (Kirk et al. 1996; Ragot and Kirk 1997)

$$n(x, E, t) = \int_{-\infty}^{\infty} dx' \int_{-\infty}^t dt' P(x - x', t - t') S(x', t') \quad (2.9)$$

where the injected flux at the source, which is the moving shock, can be modeled as $S(x, t) = S_0(E) \delta(x - V_{\text{sh}} t)$. Now, Perri and Zimbardo (2007, 2008b) proposed to use the Lévy walk propagator in the long time regime, Eq. (2.7), so that well upstream of the shock we have

$$n(x, E, t) = \int_{-\infty}^{\infty} dx' \int_{-\infty}^t dt' A \frac{t - t'}{(x - x')^{\mu+1}} S_0(E) \delta(x' - V_{\text{sh}} t') \quad (2.10)$$

where the constant A gathers the constants in Eq. (2.7) and we assumed the shock to be coming from $t = -\infty$. A first integration over x' allows to exploit the δ -function; then, for convenience in the integration we set the shock start time as t_0 :

$$n(x, E, t) = \int_{t_0}^t dt' A S_0(E) \frac{t - t'}{(x - V_{\text{sh}} t')^{\mu+1}}. \quad (2.11)$$

Introducing as an integration variable $z = x - V_{\text{sh}} t'$, upon integrating we obtain

$$n(x, E, t) = \frac{A S_0(E)}{V_{\text{sh}}^2} \left[\frac{x - V_{\text{sh}} t}{-\mu} [(x - V_{\text{sh}} t)^{-\mu} - (x - V_{\text{sh}} t_0)^{-\mu}] + \frac{1}{\mu - 1} [(x - V_{\text{sh}} t)^{1-\mu} - (x - V_{\text{sh}} t_0)^{1-\mu}] \right]. \quad (2.12)$$

Taking the limit $t_0 \rightarrow -\infty$, which corresponds to a time asymptotic steady state (Kirk et al. 1996), and considering that $1 < \mu < 2$, we are left with

$$n(x, E, t) = \frac{A S_0(E)}{V_{\text{sh}}^2} \frac{(x - V_{\text{sh}} t)^{1-\mu}}{\mu(\mu - 1)}, \quad (2.13)$$

that is, a power-law decay both in space and time with slope $\beta = \mu - 1$ for $t < 0$, i.e., before the shock passing for $x = 0$. If we choose the observer position in $x = 0$, we have just a power law in time (Perri and Zimbardo 2007, 2008b, 2009b).

In principle, this result holds for positions well upstream of the shock, since we used the propagator form valid for $|x| \gg (C t^{1/\mu})$, with C depending on the value of the anomalous diffusion coefficient. In practice, the value of C can be determined by the break in the upstream power-law profile, see Perri and Zimbardo (2015) and Perri et al. (2015) for the appropriate treatment. In addition, the determination of the power-law break position shows that it is actually rather close to the shock (Prete et al. 2021). We note that such extended power-law shock precursors are frequently observed in IP space, and in some cases also at supernova remnant shocks (Perri et al. 2016; Perri 2018).

Turning to the region downstream of the shock, we can use the same expression (2.9) to obtain the ratio between the density n_0 at the shock peak and the density far downstream. These two densities are equal in the case of normal diffusion, but are found to be different in the case of either subdiffusion or superdiffusion. We consider that, under steady state

conditions, the flux of injected particles at the shock Φ_0 equals the outbound flux far downstream, $\Phi_0 = n_2 V_2$. On the other hand, we can obtain the density n_0 at the shock by setting $x = V_{\text{sh}} t$ in Eq. (2.9), that is, having an observer moving with the shock. In the downstream frame, $V_{\text{sh}} = V_2$. From now on, we drop the dependence on energy in $n(x, E, t)$ and $S_0(E)$ for brevity. Then we have

$$\begin{aligned} n_0 \equiv n(V_{\text{sh}} t, t) &= \int_{-\infty}^{\infty} dx' \int_{-\infty}^t dt' P(V_{\text{sh}} t - x', t - t') S(x', t') \\ &= \int_{-\infty}^t dt' S_0 P(V_{\text{sh}} t - V_{\text{sh}} t', t - t') = S_0 \int_0^{\infty} dz P(V_{\text{sh}} z, z) \end{aligned} \quad (2.14)$$

where we introduced the integration variable $z = t - t'$. Using the scaling properties of the Lévy walk propagator, considering the normalization condition

$$\int_{-\infty}^{\infty} P_{LW}(x, t) dx = 1$$

and the parity of P_{LW} with respect to x , we obtain (Kirk et al. 1996; Perri and Zimbardo 2012a; Zimbardo and Perri 2013, 2018)

$$\frac{n_2}{n_0} = 2 \frac{\mu - 1}{\mu} = 2 \frac{2 - \alpha}{3 - \alpha}. \quad (2.15)$$

It can be seen that in the case of superdiffusion, $\mu < 2$ and $\alpha > 1$, we have $n_2 < n_0$, which means that the density far downstream is lower than that at the shock, at variance with the case of normal diffusion. The opposite, i.e., $n_2 > n_0$, is found in the case of subdiffusion (Kirk et al. 1996).

In summary, we can see that for the energetic particles accelerated at the shock, superdiffusive transport leads to a power-law profile rather than an exponential profile upstream of the shock, and to far downstream densities lower than the density at the shock. Both properties are routinely observed by spacecraft at IP shock crossing (Giacalone 2012; Prete et al. 2021).

2.2 Energetic Particle Profiles Around Shocks Obtained by Fractional Transport Equations

A complementary approach to the study of anomalous diffusion is based on the use of transport equations which contain fractional derivatives (see, for instance, Metzler and Klafter 2000, 2004; Zaslavsky 2002; del-Castillo-Negrete et al. 2004; Webb et al. 2006; Perrone et al. 2013; le Roux and Zank 2021). Typically, a fractional time derivative of order $\beta < 1$ leads to subdiffusion and a fractional space derivative of order $\mu < 2$ leads to Lévy flights and superdiffusion, see the above references. Several definitions of fractional derivative have been given; here, we adopt the spatial symmetric fractional derivative in Riesz's form (e.g., Litvinenko and Effenberger 2014), defined by

$$\frac{\partial^\mu f(x)}{\partial |x|^\mu} = \frac{1}{\pi} \sin\left(\frac{\pi}{2}\mu\right) \Gamma(1 + \mu) \int_0^{\infty} \frac{f(x + \xi) - 2f(x) + f(x - \xi)}{\xi^{1+\mu}} d\xi, \quad (2.16)$$

with $0 < \mu < 2$, which clearly shows the nonlocal character of transport, since the function $f(x)$ at positions $x + \xi$ and $x - \xi$ is involved in the integral. We can get a quick grasp of

the effects of fractional derivatives by considering a simplified version of Eq. (1.2)

$$\frac{\partial f(x, t)}{\partial t} = \kappa_\mu \frac{\partial^\mu f(x, t)}{\partial |x|^\mu}, \quad (2.17)$$

where the anomalous diffusion coefficient κ_μ has dimensions $(\text{length})^\mu/\text{time}$. Let us search for solutions by Fourier transforming the x coordinate. Then, in Fourier space we obtain

$$\frac{\partial \hat{f}(k, t)}{\partial t} = -\kappa_\mu |k|^\mu \hat{f}(k, t), \quad (2.18)$$

in agreement with the general rule for the Fourier transform of Riesz derivatives (Metzler and Klafter 2000; del-Castillo-Negrete et al. 2004; Perrone et al. 2013; Isliker et al. 2017b). We can solve with respect to time to find

$$\hat{f}(k, t) = \exp[-\kappa_\mu |k|^\mu t], \quad (2.19)$$

which, for $\mu < 2$, is the Fourier transform of a symmetric Lévy distribution, as shown above by Eq. (2.3).

The first application of fractional transport equations to the study of cosmic ray transport (without acceleration) around a shock has been carried out by Litvinenko and Effenberger (2014), who studied a still simplified version of Eq. (1.2)

$$\frac{\partial f}{\partial t} + V \frac{\partial f}{\partial x} = \kappa_\mu \frac{\partial^\mu f}{\partial |x|^\mu} + S_0 \delta(x). \quad (2.20)$$

where V is the advection velocity and the spatial derivative corresponds to Riesz formula; also, S_0 represents the flux of particles injected at the shock, and the equation is written in the shock frame. By taking the Fourier transform of this equation, they find that a general solution depending on space and time is given by

$$f(x, t) = \frac{S_0}{2\pi} \int_{-\infty}^{\infty} \frac{1 - \exp[(-iV k - \kappa_\mu |k|^\mu)t]}{\kappa_\mu |k|^\mu + iV k} \exp(ikx) dk. \quad (2.21)$$

Taking the limit of large distances, $|x| \gg (\kappa t)^{1/\mu}$, and changing to the frame of reference of the observer upstream of the shock, Litvinenko and Effenberger (2014) find

$$f(x, t) \simeq \frac{\Gamma(\mu - 1)}{\pi} \sin\left(\frac{\pi}{2}\mu\right) \frac{\kappa_\mu S_0}{V_{\text{sh}}^2} \left[\frac{1}{(x - V_{\text{sh}}t)^{\mu-1}} - \frac{x + (\mu - 1)V_{\text{sh}}t + \alpha V_{\text{sh}}t_0}{(x + V_{\text{sh}}t_0)^\mu} \right]. \quad (2.22)$$

Considering a shock starting from $x = -\infty$, which in their notation corresponds to $t_0 \rightarrow \infty$, the above expression coincides with the result obtained by use the Lévy walk propagator, given by Eq. (2.13), in the same limit of shock coming from $x = -\infty$. Keeping in mind the diversity of the approaches, this agreement is remarkable, and confirms the robustness of these results.

Furthermore, Litvinenko and Effenberger (2014) compare the solutions for the energetic particle profiles upstream and downstream of the shock obtained by various methods and approximations, see the captions of Fig. 3. Notably, they pointed out that “An interesting feature of the solution is the peak at the injection site $x = 0$, which is not present for Gaussian diffusion.” This peak at injection matches well with the finding, described in Sect. 2.1, that the far downstream density is lower than the density at the shock in the case of superdiffusion. It also matches the results of the numerical simulations described in the next subsections.

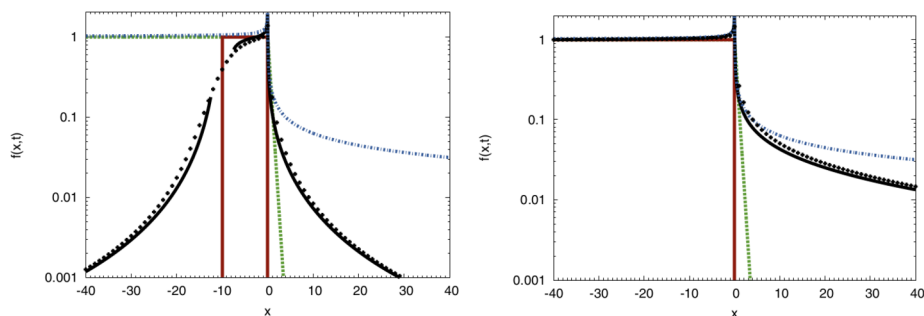


Fig. 3 Solutions for the energetic particle profiles around the shock at $x = 0$ obtained by Litvinenko and Effenberger (2014). Left panel: short times after the shock onset; right panel: for larger times after the shock onset. The solutions are obtained by means of several methods, like the Fourier transform in the weak diffusion limit (solid black lines), a series solution (black symbols), an approximate steady-state solution (blue dash-dots). The dashed green line represents the solution for normal diffusion, and the brown lines represent an advection only, non-diffusive solution. Adopted from Litvinenko and Effenberger (2014)

2.3 Test Particle Numerical Simulations and Comparison with Observations

The transport properties of particles in the presence of magnetic turbulence in space plasmas can be studied by means of numerical simulations (e.g., Giacalone and Jokipii 1999; Qin et al. 2002a,b; Zimbardo et al. 2006; Pommois et al. 2007; Shalchi and Kourakis 2007b; Pucci et al. 2016; Trotta et al. 2020, and many others). In particular, test particle simulations allow to investigate the effect of specific “ingredients” on particle propagation. To study anomalous transport in a region of space where a shock is present, we can also consider stochastic differential equations (e.g., Strauss and Effenberger 2017). This method can be used both for Lévy flights and Lévy walks; here we present first the scheme for Lévy flights.

2.3.1 Simulation of Lévy Flights

For the Lévy flights model, we use the equivalence of Fokker-Planck type equations and SDEs (Itô 1951). The corresponding SDE for the spatial displacement dx is given by Eq. (1.7) without subordination, so that $\tau = t$ and

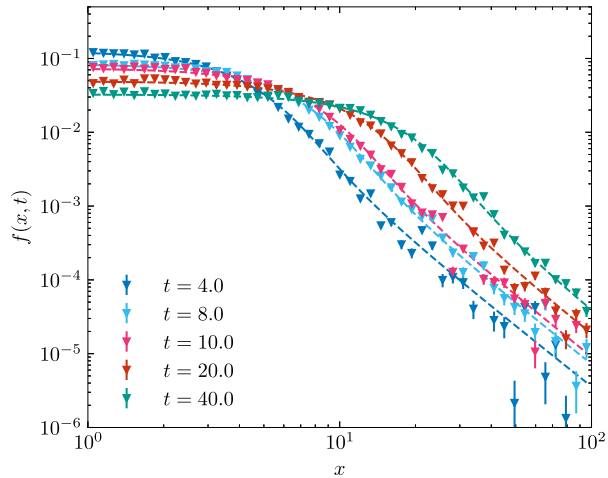
$$dx(t) = V dt + \kappa_\mu^{1/\mu} dL_\mu(t), \quad (2.23)$$

with the fractional diffusion coefficient κ_μ and Lévy process $L_\mu(t)$ (see, e.g., Magdziarz and Weron 2007, for more details on the equivalence of fractional Fokker-Planck equations and Lévy SDEs). Note, that Eq. (2.23) describes the evolution of a phase-space element or *pseudo-particle* and not actual particle trajectories. The distribution function $f(x, t)$ is obtained by averaging over multiple such samples. We use a modified version of the cosmic ray propagation framework CRPropa 3.2 (Alves Batista et al. 2022; Merten et al. 2017) to model Lévy flights (Merten and Aerdker 2025). The diffusive transport module utilizes an Euler-Maruyama scheme to solve Eq. (2.23).

Each simulation time step $\Delta t = t_{n+1} - t_n$ a random number $\eta_{\mu,t}$ is drawn from the μ -stable Lévy distribution. The pseudo-particle position x_n is then updated according to

$$x_{n+1} - x_n = V \Delta t + \sqrt{2\kappa_\mu^{1/\mu}} \Delta t^{1/\mu} \eta_{\mu,t}, \quad (2.24)$$

Fig. 4 Fourier series (dashed line) and SDE (triangles) solution of the distribution function for a delta-injection of pseudo-particles at $t = 0$ over time. The fractional dimension is $\mu = 1.7$. Adopted from Effenberger et al. (2024)



where the Chambers-Mallows-Stuck algorithm (Chambers et al. 1976) is used to generate Lévy random numbers $\eta_{\mu,t}$. Essentially, the enhanced tails of the Lévy distribution lead to Lévy flights. For $\mu = 2$ Brownian motion is recovered, which allows to easily compare Gaussian and anomalous diffusion.

In the simplest case of pure fractional diffusion ($V = 0$), the power-law asymptotics of the superdiffusive process becomes visible. Figure 4 shows the distribution function f (for $\mu = 1.7$) decaying over time. The SDE approach is compared to a Fourier series approximation as discussed in Stern et al. (2014). Note the similarity to the Lévy flight propagators shown in Fig. 1.

With that, the spatial transport of particles at shocks is modeled by Effenberger et al. (2024). Pseudo-particles are injected at the shock at $x = 0$. They are advected downstream with the background flow V and may diffuse back upstream. With continuous injection at the shock a stationary solution develops. CRPropa 3.2 does not allow for such continuous injection, pseudo-particles are injected at $t = 0$ and propagated until the simulation ends.³ One advantage of the SDE approach is its independence on a source term. Thus, assuming a stationary background, the distribution function $f(x, T)$ at time T can be obtained by integrating over the contributions $f(x, T_i)$ stored at times $T_i < T$ during the simulation. For more details we refer to (Aerdker et al. 2024; Merten and Aerdker 2025). While this constraint may seem disadvantageous, the structure of CRPropa becomes important when acceleration at the shock is taken into account, or when modeling superdiffusive transport parallel and perpendicular to magnetic field lines.

In Fig. 5 the resulting distribution functions for different fractional dimensions μ are shown. The lower the fractional dimension, the more distinct is the peak right at the shock. The results are in excellent agreement with the Fourier series approximation (see Sect. 2.2). Note, that the advection V is constant and, thus, there is no particle acceleration. Units are normalized so that $x_0 = v_0 t_0$; $x_0 = 1$ AU and $v_0 = 400$ km/s results in $t_0 \approx 4.3$ days. Figure 6 shows the impact of the fractional dimension μ as well as anomalous diffusion coefficient κ_μ on the upstream side compared to Gaussian diffusion. While the fractional dimension changes the slope of the power-laws in space, the anomalous diffusion coefficient changes

³So far, there is no explicit time dependency in CRPropa 3.2. Instead, the trajectory length is often used to infer back to the time, assuming that pseudo-particles move with constant speed.

Fig. 5 Fourier series (lines) and SDE (symbols) solution at simulation time $t = 100$ close to the shock at $x = 0$ for different values of μ . The solution for Gaussian diffusion is shown by the dotted line. Adopted from Effenberger et al. (2024)

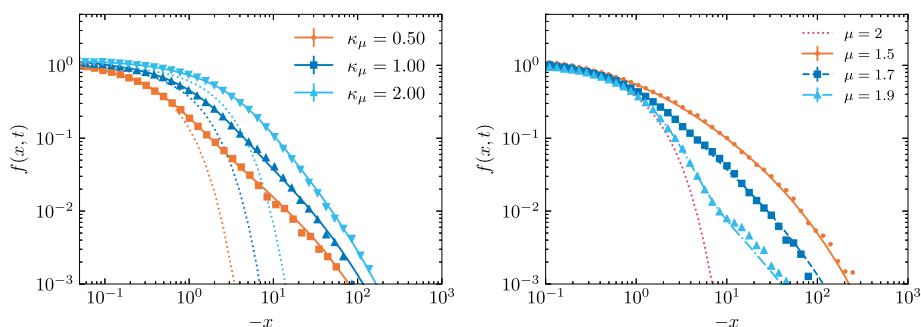
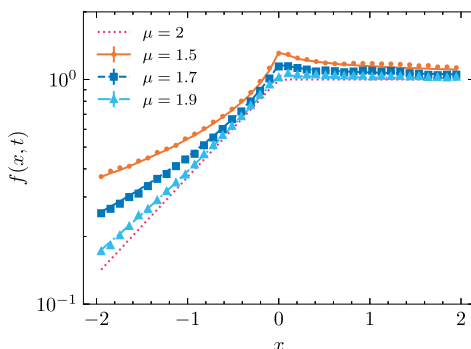


Fig. 6 Upstream Fourier-series solution (line) compared to the corresponding SDE solution (symbols) at $t = 100$. Left: Different values of κ_μ with $\mu = 1.7$. Right: Different values of the fractional dimension μ with $\kappa_\mu = 1$. Results for Gaussian diffusion are shown by the dotted lines for comparison. Adopted from Effenberger et al. (2024)

the position of the turn-over from a Gaussian-like to a power-law distribution. This may be used to fit both, anomalous diffusion coefficient and fractional dimension, to observations.

Particle acceleration at a 1D planar shock is modeled by a varying background flow $V(x)$ for the shock and by solving the ordinary differential equation

$$dp(t) = -\frac{p}{3} \frac{\partial V}{\partial x} dt \quad (2.25)$$

along with the SDE (2.23). In this macroscopic picture (Drury 1983), acceleration at the shock results from the diverging background flow $V(x)$. The energy spectrum at the shock is determined by the interplay of advection and diffusion, which is related to the escape probability, and the compression ratio $q = V_1/V_2$. For a strong shock with $q = 4$ this leads to the well known spectral slope $s = 2 - 3q/(q - 1) = -2$ when Gaussian diffusion is considered. Lévy flights change the probability to escape the shock. The upstream power-law distribution indicates that particles are more efficiently scattered back over the shock, leading to a lower particle number density far downstream. This is discussed in more detail in Aerdker et al. (2025).

In general, there are no constraints on the time step for the Euler-Maruyama scheme as it is numerically stable. In the macroscopic picture the shock must have a finite width, otherwise Eq. (2.25) diverges at the shock. The finite shock width then leads to constraints on the time step. For Gaussian diffusion, we refer to e.g. Kruells and Achterberg (1994),

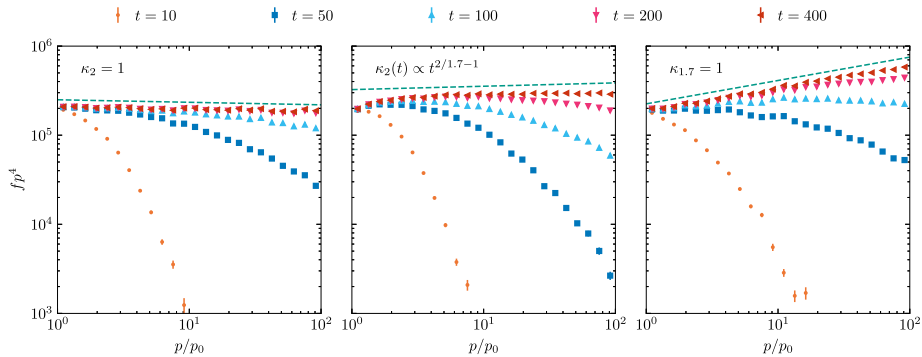


Fig. 7 Time evolution of the weighted spectrum $f(p, t)p^4$ at the shock for Gaussian diffusion, $\kappa_2 = 1$ (left), time-dependent diffusion, $\kappa_2(t) \propto t^{2/1.7-1}$ (middle) and Lévy flights with $\mu = 1.7$ and $\kappa_{1.7} = 1$ (right). Note that the time-dependent diffusion coefficient and Lévy flights have the same mean squared displacement. The spectra are fitted at simulation time $t = 800$, the corresponding slope is shown by the dashed line. Figure adopted from Aerdker et al. (2025)

Achterberg and Schure (2011), Strauss and Effenberger (2017), Aerdker et al. (2024). In summary, the shock width must be small compared to the diffusion length scale κ/V to model a shock and the time step must be sufficiently small so that pseudo-particles encounter the changing background flow. The first constraint can be seen as a physical argument: Diffusion must be high enough to allow particles to diffusive back against the background flow. The second is a numerical constraint and determined by the chosen shock width.

Aerdker et al. (2025) compare the time-evolution of the energy spectrum at the shock considering Lévy flights, Gaussian diffusion and Gaussian diffusion with a time-dependent diffusion coefficient $\kappa(t) = \kappa_0 t^{2/\mu-1}$. The time-dependency is chosen such that the mean squared displacement of the Gaussian process mimics that of a Lévy flight process with a fractional dimension μ . Differences in the spectrum and differential number density are then solely determined by the different processes, and not by different mean squared displacements at a given time.

Figure 7 shows the resulting momentum spectra at a shock with compression $q = 4$ at different simulation times until the stationary solution for $p/p_0 < 100$ is reached. For Gaussian diffusion, the acceleration time scale is given by $\tau_{\text{acc}} = 3/(V_1 - V_2)(\kappa_1/V_1 + \kappa_2/V_2)$, with upstream (1) and downstream (2) advection and diffusion coefficients, respectively. The increasing diffusion coefficient over time slows down the acceleration process, while the spectral slope remains unchanged. For Lévy flights the spectrum is harder and the acceleration is faster compared to the time-dependent Gaussian process.

The resulting spectral slopes can be compared to Lévy walk models. With the propagator approach Perri and Zimbardo (2012a) obtain the power-law slope as

$$\gamma = P_{\text{esc}} \frac{E}{\Delta E} = 6 \frac{2\mu - 2}{3\mu - 2} \frac{1}{q - 1} + 1, \quad (2.26)$$

for superdiffusive shock acceleration (see also Kirk et al. (1996) for the subdiffusive case). Here the spectral slope is determined by the relative energy gain $\Delta E/E$ at a planar shock with compression ratio q and the escape probability P_{esc} . Note, that the parameter μ used here is different from the notation used in Perri and Zimbardo (2012a). This is due to the different relations between the mean squared displacement and the fractional dimension for Lévy flights ($\alpha = 2/\mu$) and Lévy walks ($\alpha = 3 - \mu$).

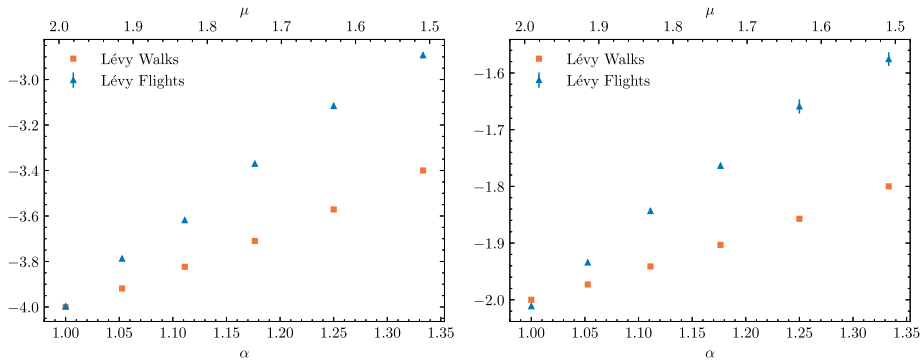


Fig. 8 Spectral slopes obtained from Lévy flight simulations with different fractional dimensions μ corresponding to a mean squared displacement increasing with t^α . The results for Lévy flights are compared to Lévy walks given by Eq. 2.26. Left: compression ratio $q = 2$, right: compression ratio $q = 4$

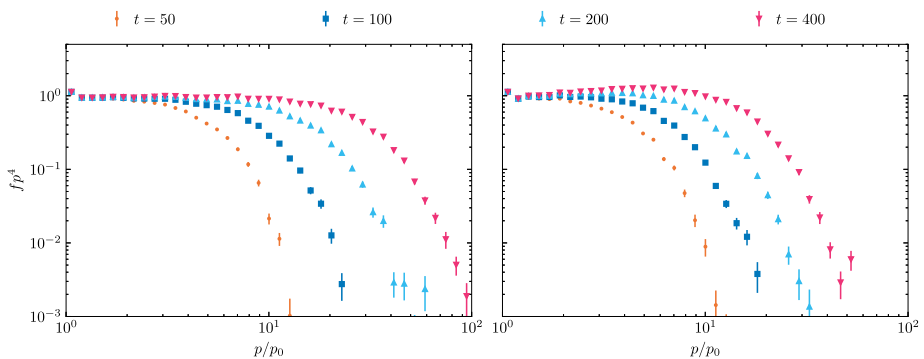


Fig. 9 Time evolution of the weighted spectrum $f(p, t)p^4$ at the shock for energy-dependent normal diffusion. Gaussian diffusion (left) is compared to Lévy flights (right). Both have the same values $\kappa_{\mu,0} = 1$ and $\mu = 1$. Note, that $\kappa_{\mu,0}$ has different units depending on the fractional dimension μ . Adopted from Aerdker et al. (2025)

Figure 8 shows the spectral slope resulting from Lévy flights and Lévy walks for different fractional dimensions μ and compression ratios q . We compare processes with the same time dependence of the mean squared displacement α .

Given by the spectrum of the magnetic field turbulence, superdiffusion likely is momentum dependent. With the SDE approach momentum-dependent Lévy flights are modeled like described previously. The anomalous diffusion coefficient in Eq. 2.23 now is momentum dependent, and

$$\kappa_\mu(p) = \kappa_0 \left(\frac{p}{p_0} \right)^\alpha. \quad (2.27)$$

with $\alpha > 0$.

Figure 9 shows the resulting momentum spectra at the shock for Gaussian diffusion and Lévy flights. The acceleration time scale τ_{acc} depends on the diffusion coefficient, thus, acceleration is slowed down over time, when particles reach higher momentum and the

(anomalous) diffusion coefficient increases. Due to the inherently higher mean squared displacement the impact on the acceleration time scale is stronger for the Lévy flights. Note, that the Gaussian diffusion and Lévy flight process have the same value $\kappa_0 = 1$ here but different units. Perri and Zimbardo (2012a) scale the diffusion coefficient for Lévy walks with the fractional dimension μ , leading to a smaller anomalous diffusion coefficient. With that, superdiffusive acceleration is faster compared to Gaussian diffusion.

2.3.2 Simulation of Lévy Walks

Now we present a numerical scheme for simulating Lévy walks. Following the approach of Trotta and Zimbardo (2015), Prete et al. (2019) describe in a one dimensional simulation the effects of advection and Lévy random walk, by writing the particle displacement dx as

$$dx = V_{\text{bulk}} dt + v_{\text{ran}} dt, \quad (2.28)$$

where dt is the integration time step, V_{bulk} equals the advection velocity V_1 for $x < 0$ (upstream), and V_2 for $x > 0$ (downstream), with a stationary shock at $x = 0$. A large number of particles, typically 10^6 are injected at $x = 0$ and then are followed for “sufficiently long times” (see later). The random velocity v_{ran} is chosen as

$$v_{\text{ran}} = (2\xi - 1)v, \quad (2.29)$$

where $\xi \in [0, 1]$ is a random number and v the particle speed, which depends on energy only and is constant in the simulations by Prete et al. (2019, 2021). Special care is necessary for generating a new random velocity, as this depends on the desired scattering time. In the case of normal diffusion, a constant scattering time τ is chosen, with the integration time step much smaller than τ : when the integration time increases by an amount τ , a new random velocity is generated and the integration goes on. This effectively describes normal diffusion, see Figs. 1–4 in Prete et al. (2019), and changing τ corresponds to changing the diffusion coefficient, given that $D = \frac{1}{3}v^2\tau$.

On the other hand, for anomalous diffusion a new random velocity is generated when the integration time is increased by a time τ which is extracted from a Lévy distribution as $\psi(\tau) \simeq A v^{-\mu-1} \tau^{-\mu-1}$, which is obtained from Eq. (2.6) upon integrating on ℓ . In practice, a string of scattering times τ_i is generated for each particle before running the simulation. Both long and short scattering times are included, as implied by the power-law probability distribution. When the integration time is increased by the next of such τ_i , a new random velocity is generated. The probability of making a displacement of length ℓ in a time τ is given by Eq. (2.6) for $\tau > \tau_0$, while it equals $\Psi(\ell, \tau) = \frac{1}{2}A\delta(|\ell| - v\tau)$ for $\tau < \tau_0$. Hence, τ_0 is a break time in the power-law distribution of scattering times. Sample trajectories are shown in Fig. 10. It is worth noticing that the distribution of free path lengths ℓ , as well as that of scattering times τ , in a Lévy walk is not totally scale free; rather, there must exist a minimum free path length $\ell_0 = v\tau_0$ below which the power law $\Psi \sim |\ell|^{-\mu-1}$ no longer holds, otherwise the probability density $\Psi(\ell, \tau)$ would not have a finite normalization. Conversely, the condition $\int \Psi(\ell, \tau) d\ell d\tau = 1$ allows us to determine the normalization constant A as

$$A = \frac{1}{\tau_0} \left(\frac{\mu}{\mu + 1} \right) \quad (2.30)$$

Fig. 10 Sample trajectories of particles undergoing a Lévy walk (time on the vertical axis). Particles injected at the shock position $x = 0$, and their motion is described by Eq. (2.28). Notice that both short and long displacements are found. Adopted from Prete et al. (2021)

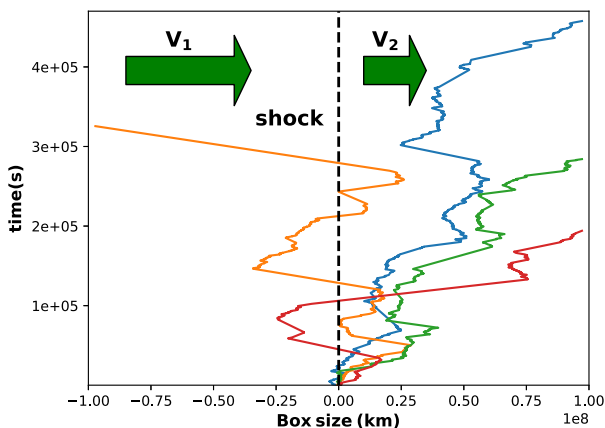
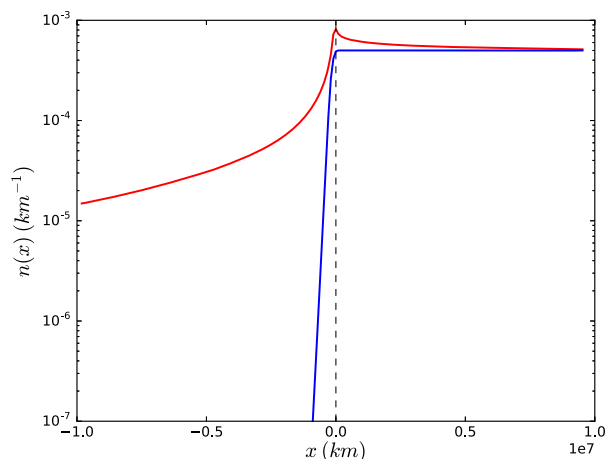


Fig. 11 Density profiles for particles injected at the shock for normal diffusion (blue line) and superdiffusion with $\alpha = 1.5$ (red line). Adopted from Prete et al. (2019)



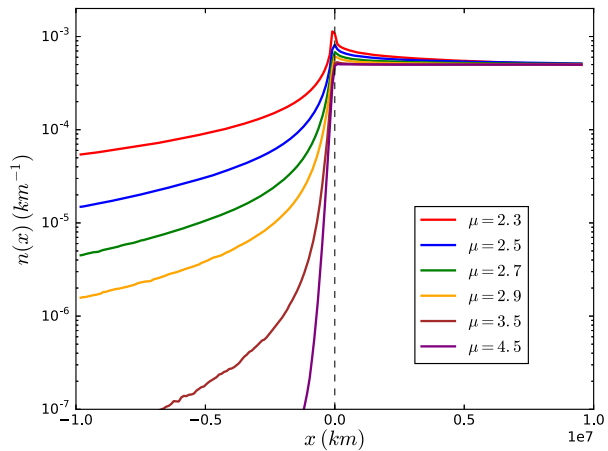
As shown by Trotta and Zimbardo (2015), the Lévy distributed free path times can be generated by a random number $\xi \in [0, 1]$ by means of the expression

$$\tau = \tau_0 \left[\frac{1}{(\mu + 1)(1 - \xi)} \right]^{1/\mu}. \quad (2.31)$$

It can be seen that when $\xi \rightarrow 1$ very long free path times are generated. The particle velocity is not changed during a given free path time τ_i , but only when a new τ_{i+1} is to be used: in this way the space-time δ -coupling of Lévy walks is enforced. Such a scheme permits to reproduce superdiffusion (Trotta and Zimbardo 2015; Prete et al. 2019, 2021; Trotta et al. 2020) as well as the shape of energetic particles spatial profiles around the shock (see Figs. 11 and 12).

In particular, we note that the features predicted by the analytical models for superdiffusion described above, i.e., a power-law profile far upstream of the shock and a decreasing density downstream of the shock, are easily reproduced by the numerical simulations, as clearly shown in Fig. 11, where it is possible to notice the differences in the density profiles between a normal (blue line) and a superdiffusive regime (red line). Further, we consider

Fig. 12 Energetic particle profile around the shock at $x = 0$ for several values of the power-law exponent μ . Adopted from Prete et al. (2019); note that in this figure from Prete et al. (2019) μ corresponds to our $\mu + 1$



that the various approach presented here lead to the same results because in the stationary, long time limit the difference between Lévy walks and Lévy flights is vanishing, as shown by the propagators.

The simple test particle model described above is, thus, able to give in output different spatial density profiles of energetic particles by changing the model parameters, as shown by Fig. 12. Motivated by the rich variety of particle flux profiles detected in-situ by spacecraft during IP shock crossings (Giacalone 2012; Perri et al. 2015; Zimbardo et al. 2020; Perri et al. 2021), Prete et al. (2019, 2021) made a comparison between the outcomes of numerical simulations in regimes of superdiffusion and satellite observations of ion fluxes at IP shock waves. We point out that for such a comparison the spatial dependence coming from simulations has to be recast into a time dependence (as is typical of spacecraft *in situ* measurements which produce time series) via the straightforward transformation $t = x/V_i^{sh}$, being $i = 1, 2$ an index indicating the upstream or the downstream sides, where V_i^{sh} is the upstream or downstream plasma speed in the shock rest frame. Notice that in the test particle simulations all the quantities have been calculated in the shock frame, too, therefore it is necessary to pay attention when making a comparison with quantities in the spacecraft frame. The simulation results have been tested against shocks with different macroscopic quantities, such as the compression ratio $r = n_2/n_1$, namely the ratio between the particle number density downstream and upstream, the Alfvénic Mach number $M_A = V_{sh}/V_A$, being $V_A = B/\sqrt{4\pi\rho}$ the Alfvén speed, and the shock geometry, evaluated by means of the angle between the shock normal and the upstream magnetic field direction, i.e., θ_{Bn} . Based on the thermal ion reflection process at shocks, shocks with $\theta_{Bn} > 45^\circ$ are termed quasi-perpendicular, while for $\theta_{Bn} < 45^\circ$ the shock is termed quasi-parallel. Prete et al. (2021) explored three different shock geometries, namely quasi-parallel, oblique, and quasi-perpendicular, for three shock crossings by the Advanced Composition Explorer (ACE) spacecraft. Parameters of the numerical models, such as the upstream and the downstream speeds, the compression ratio of the shock, and the particle energies have been set by using the observed values for each shock crossing. Figure 13 shows the comparison between ion fluxes as detected by the ACE/EPAM/LEMS120 experiment as a function of the time “distance” from the shock front (located at $t = 0$) in four energy bins (panels from (a) to (d)). This was the ACE shock crossing on 2000 June 8 and it was an oblique shock event with $\theta_{Bn} \sim 45^\circ$ and relatively high compression ratio, i.e., $r \sim 3$. The black solid lines indicate the outcomes from the numerical model for particles having an energy equal to the center of the energy bin in-

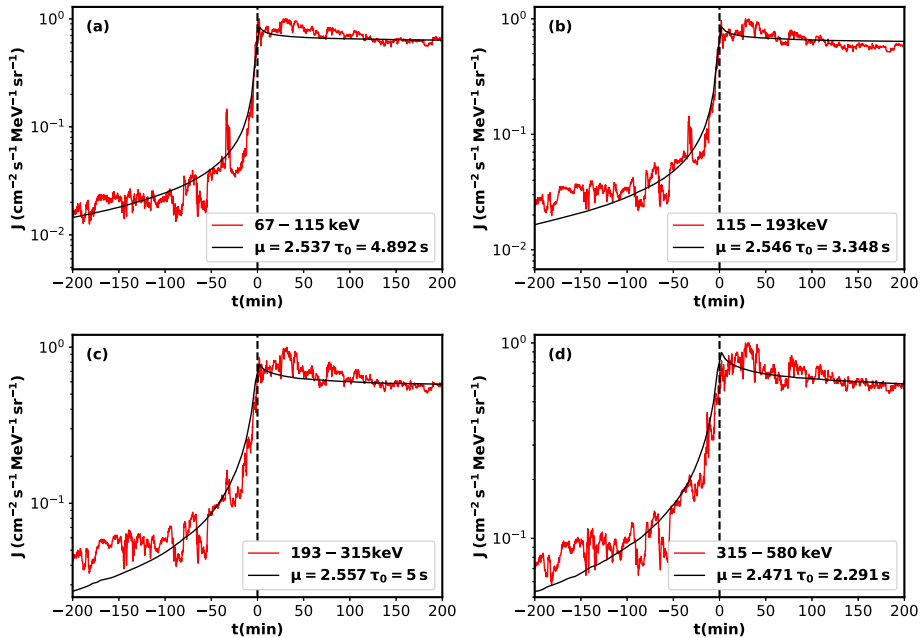


Fig. 13 Energetic ion fluxes around the shock wave detected by ACE on 2000 June 8. Data at 12 s time resolution have been used from the ACE/EPAM/LEMS120 experiment. Each panel refers to a given energy bin. The vertical dashed line indicates the shock time, so that the upstream region is on the left and the downstream region is on the right. The solid black lines are the density profiles obtained running the test particle model with the superdiffusive parameters indicated in the figure legend and the particle energy and the shock properties as coming from the observations of the event. Adopted from Prete et al. (2021). In this figure, too, as in Fig. 12, the reported μ corresponds to $\mu + 1$ in the present paper

icated in each panel. The parameters μ and τ_0 chosen in the runs are also reported. The comparison displays a very good agreement between observed densities and modelled densities both upstream and downstream. Similar results have also been obtained for other shock crossings, and confirm the superdiffusive character of energetic particle transport for these events.

Although the comparison is satisfactory, there are several caveats that need to be taken into account: first of all the model describes an infinite planar shock, where all possible curvature effects are neglected; the magnetic field is not included so that it is not possible to have any control on the shock geometry; the runs are performed in a rest frame in which the shock is stationary (shock rest frame), thus all time variations related to the shock propagation, front corrugation (Johlander et al. 2016; Kajdič et al. 2019) are not considered; no acceleration process at shock is modeled. Thus, the model reported in Prete et al. (2019) can be considered as a first-order numerical model for energetic particle propagating around IP shocks, and superdiffusive transport allows to reproduce the observed fluxes in a reasonable way, but not all of the relevant physical effects are taken into account.

2.4 Superdiffusive Transport in Hybrid Simulations

Beyond test particle simulations, a quasi 1D hybrid numerical experiment with fluid electrons and protons as macroparticles has been used to compare different techniques for the

analysis of particle transport around a quasi-parallel shock wave (Trotta et al. 2020). In particular, the MSD of an ensemble of supra-thermal protons, accelerated locally at the shock, has been tracked both upstream and downstream. Further, since the numerical simulation is limited by the box size, while Eq. (1.1) is defined for very long times, in order not to capture transients in the particle transport only, an extension of the MSD method has been applied. This is called time-averaged mean square displacement (TAMSD), and it is used in heterogeneous systems and in case of poor statistics (see Trotta et al. (2020) and references therein). TAMSD use single particle trajectories and time averages instead of ensemble averages, namely

$$\overline{\Delta x^2}(\tau) = \frac{1}{T - \tau} \sum_{t=1}^{T-\tau} (x(t + \tau) - x(t))^2, \quad (2.32)$$

where τ is a time window, T is the total time of particle tracking, and x is the particle position. Because of the Central Limit Theorem, for a Brownian motion and for a very large number of time records, MSD and TAMSD should converge. Trotta et al. (2020) making an ensemble average of Eq. (2.32), found indeed a good agreement between the two techniques upstream and downstream of the shock. While it is interesting to compare such techniques in non-homogeneous systems, such as the plasma around shocks, the emergence of superdiffusive transport of energetic protons upstream, mainly due to reflected protons streaming back into the upstream region, has been reported. Both techniques recovered a value of the scaling exponent $\alpha \sim 1.4$ for long times, after a transient of $\alpha \sim 1.9$. Evidences of anomalous transport were also observed downstream, although a tendency to recover diffusion for long times was detected. However, thanks to the novel TAMSD method based on single particle trajectories, it was possible to check the co-existence of different types of particle transport within the downstream, spanning from subdiffusion, due to a trapping within strong magnetic field fluctuations formed just after the shock transition, to superdiffusion caused by particles moving rapidly away from the shock front. We note that this is consistent with the model of truncated Lévy flights presented in Sect. 2.6. Examples of such particles are shown in Fig. 14, adopted from Trotta et al. (2020).

It is true that the simulated system around a quasi-parallel shock has finite size and that the results on particle transport can be influenced by this; however, few attempts made in varying the box sizes did not affect the final results, although the limitation in size remains an open question when dealing with Eq. (1.1) that imply asymptotic times. On the other hand, shock waves in astrophysics can be considered finite-size systems, limited by their typical lifetime and loss mechanisms (i.e., interplanetary shocks, supernova remnant shocks, etc.), thus the detection of superdiffusive transport around such systems, both when using test particle and self-consistent approaches, gives an indication on the natural emergence of anomalous transport under particular conditions.

2.5 Non Locality and Uphill Transport

The test-particle treatments of energetic particle transport around a shock wave show that the particle density profile has a peak at the shock location, that is, the density at the shock is larger than the densities both upstream and downstream. The latter feature, although frequently observed in spacecraft in situ data, is rather puzzling from the theoretical point of view. We note in passing that these shock peaks should not be confused with the short-lived shock spikes, that have been discussed already by Decker (1983), who explained them with single-encounter shock-drift acceleration. Here, we rather concentrate on longer-lived

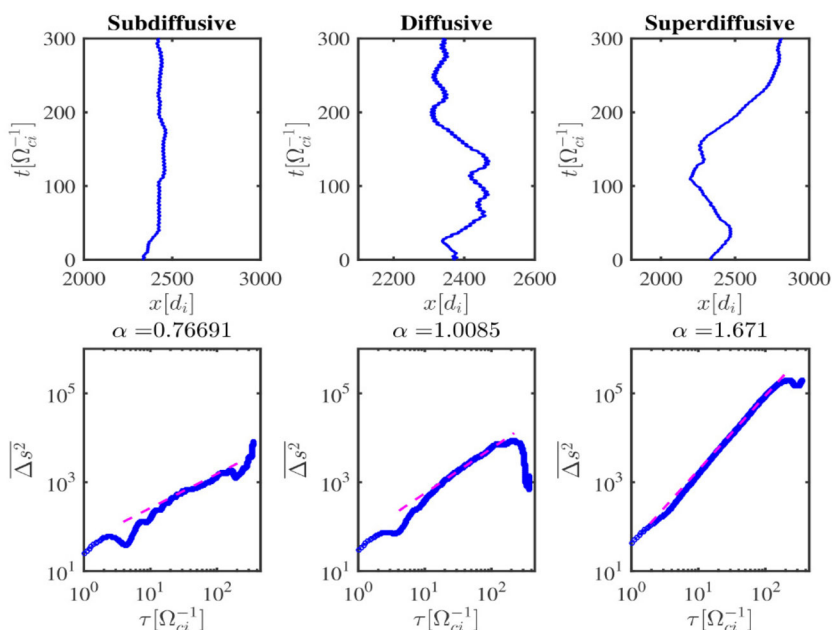


Fig. 14 Examples of protons moving within the downstream region of the simulation box. Particle trajectories are reported in the top panels, while the single particle TAMSDs are plotted in the bottom panels. Three different types of transport can be recognized, as also shown by the magenta dashed lines in the bottom panels, indicating the best power-law fits. The power-law slopes α are also displayed in the figure. Adopted from Trotta et al. (2020)

peaks resulting from repeated scattering across the shock that is, thus, multiply encountered. Therefore, let us consider the advection-diffusion expression for the flux J in one dimension,

$$J = Vf - D \frac{\partial f}{\partial x}, \quad (2.33)$$

where we used the standard flux-gradient relation for the diffusive flux. In steady state, upstream of the shock the total flux is zero, $J = 0$, that is, the advection flux (which is positive with the signs as in Figs. 10 and 11) is balanced by diffusive flux which is negative because $\partial f / \partial x > 0$. Conversely, downstream of the shock the total flux must equal the injected flux S_0 , in agreement with Eq. (2.20), but in the case of a decreasing particle density downstream (i.e., $\partial f / \partial x < 0$) both the advection flux and the diffusive flux are positive and decreasing with x ; conversely, the solution of Eq. (2.33) implies a density f growing with x . This leads to the conclusion that downstream the diffusive flux should be zero, $\partial f / \partial x = 0$, and the density profile flat (Drury 1983), so that $J = V_2 f = S_0$.

We can solve this puzzle by remembering that fractional derivatives are non local operators which involve not only the derivative $\partial f / \partial x$ at the position where the flux is being calculated, but also the derivative, or the function f , in a wide region of space. In the words of del-Castillo-Negrete (2006) we have:

“The standard diffusion paradigm assumes a local relationship between the flux and the gradient, $J = -D \partial f / \partial x$. This leads to “downhill” transport, i.e., transport in the direction opposite to the gradient. [...] However, in the case of fractional diffusion, the flux is an

integral operator that depends on the global properties of the profile and this can yield to a nontrivial, multivalued flux-gradient relation. In particular, fractional diffusion operators can give rise to “uphill transport.” By this we mean that, at specific regions of the space, the flux has the same direction as the gradient.”

It is such an uphill transport that allows to balance the advection flux with the diffusive flux even downstream of the shock, as we show in the following. We also note that for laboratory plasmas uphill transport may have the amazing property of improving plasma and energy confinement. This has been shown in several laboratory plasma toroidal experiments, where particle density and/or temperature increase on the torus axis as the result of off-axis fueling or heating. In particular, Luce et al. (1992) and Petty and Luce (1994) find that in the DIII-D tokamak off-axis energy injection due to electron cyclotron heating leads to inward energy transport and a strong central (on-axis) electron temperature peak. The central electron temperature is found to increase gradually with time, indicating that a transport related mechanism is the origin of the peaked electron temperature profile (Petty and Luce 1994). In the W7-AS stellarator, Stroth et al. (1999) find evidence for inward particle transport: since this transport is observed in a current-free stellarator, it cannot be related to a toroidal electric field causing $E \times B$ drift. An inward particle flux and a centrally peaked density profile were also observed in the Tore Supra tokamak in a steady-state plasma lasting 4 minutes without toroidal electric field (Hoang et al. 2003). These experimental results have been interpreted in terms of non-local transport associated with turbulence. In particular, van Milligen et al. (2004) have shown by a probabilistic non-local transport model with two-side off-axis injection that, when the particle step probability is Gaussian, a flat density profile is obtained between the two injection sites; conversely, when the particle step probability is a Lévy distribution, a peaked density profile is obtained in the center, between the two injection sites. In practice, the central region quickly fills up with particles starting from the injection sites and making the long steps allowed by the Lévy distribution.

It is worth noting that the breakdown of the standard Fourier’s law and/or Fick’s law when the gradient scale and the mean free path become comparable was recognized in the Eighties, and convolution integrals were proposed to express non local heat transport in the presence of steep temperature gradients (Bell 1983; Luciani et al. 1983). (We may notice that energetic particle densities around a shock wave are very likely to correspond to steep gradients.) Still in the plasma fusion field, Ida et al. (2015) point out that to take into account non locality, the heat flux $q(r)$ should be given by

$$q(r) = - \int \kappa(r, r') \frac{\partial T}{\partial r'} dr' \quad (2.34)$$

where T is the temperature and r is the radial distance from the torus major radius, thus using a non-local formulation of the Fourier law for the heat flux. A similar expression for the electron flux in solar flares has been considered by Bian et al. (2017), who propose a bi-exponential kernel $\kappa(|x - x'|) \simeq \exp(-|x - x'|/\lambda(v))$. Also, a similar, non local form of Ficks’s law is considered by Müller et al. (2023) to model the experimental results on turbulent particle transport in the TJ-K stellarator.

A transport equation with fractional spatial derivatives may be obtained, for instance, by considering a fractional Fick’s law for the flux J , where the standard gradient can be substituted by a fractional derivative of order $\beta < 1$, i.e., in one dimension,

$$J = -\kappa_\beta \frac{\partial^\beta f}{\partial |x|^\beta}. \quad (2.35)$$

Then, using the continuity equation, a fractional transport equation similar to Eq. (2.17), with $\mu = \beta + 1$, is obtained. Several authors have considered the issue of a fractional Fick's law (Zanette 1998; Chaves 1998; Paradisi et al. 2001; Calvo et al. 2007). For particle transport around a shock, we start from Eq. (2.20), we consider steady state, $\partial f / \partial t = 0$, and integrating with respect to x from $-\infty$ to x we obtain

$$V_1 f - \kappa_\mu \frac{\partial^\beta f}{\partial |x|^\beta} = 0 \quad (2.36)$$

for the upstream region, $x < 0$, with $\beta = \mu - 1$; and

$$V_2 f - \kappa_\mu \frac{\partial^\beta f}{\partial |x|^\beta} = S_0 \quad (2.37)$$

for the downstream region, $x > 0$. In particular, Zimbardo et al. (2017) have shown that, if the Riesz fractional derivative is changed for the Caputo fractional derivative, which is appropriate to treat boundary value problems (del-Castillo-Negrete 2006), the upstream density profile can be described by Mittag-Leffler functions and far upstream the power-law scaling $(x - V_{sh}t)^{1-\mu}$ is recovered.

Turning to downstream, the red profile in Fig. 11 shows that the density is relatively flat far downstream, but if we stay at a point x not too far from the shock the downstream density profile is decreasing with x . Now, the evaluation of the fractional derivative involves regions both to the left and to the right of x , and we can see that moving upstream on the left, a strong density decrease is found which will contribute to positive values of $\partial^\beta f / \partial |x|^\beta$. Thus, globally, the fractional derivative for $x > 0$ will be positive and the diffusive flux negative, that is, uphill with respect to the density profile. This allows for the peak in the profile of $f(x)$, i.e., $V_2 f > S_0$, even when going from downstream towards the shock. An experimental validation, using spacecraft data, of the presence of uphill transport downstream of shocks is reserved for future work.

2.6 A Tempered Fractional Transport Theory

The theory reviewed in this subsection was developed to describe the interaction of energetic particles with quasi-two-dimensional turbulence in the solar wind. Nearly incompressible MHD turbulence theory (Zank and Matthaeus 1992, 1993; Zank et al. 2017), MHD simulations (e.g., Shebalin et al. 1983; Dmitruk et al. 2004), and inner heliospheric observations (Matthaeus et al. 1990; Bieber et al. 1996) suggested for a long time the existence of a dominant, non-propagating quasi-two-dimensional (quasi-2D) turbulence component in the solar wind containing coherent small-scale magnetic flux rope (SMFR) structures. In support of this view, an unprecedented number of SMFRs were identified more recently in the inner heliosphere with especially the Grad-Shafranov method (Zheng and Hu 2018), but also using the wavelet analysis and the Magnetic Helicity-PVI method (Zhao et al. 2020; Pecora et al. 2021). Furthermore, 2D MHD turbulence simulations featuring a sea of magnetic islands perpendicular to the mean magnetic/guide field separated by abrupt boundaries in the form of small-scale current sheets generate a probability distribution function (PDF) of the perpendicular magnetic field component increments that is statistically strongly non-Gaussian with prominent power-law tails produced by intermittent large field component increments at island boundaries (Greco et al. 2009). The PDF of the simulation by Greco et al. reproduced quite well the PDF of ACE spacecraft observations of perpendicular field component increments at 1 AU. The non-Gaussian PDF of out-of-plane current densities of SMFRs

identified in Wind data and reconstructed with the Grad-Shafranov method also agrees with the PDF of the current densities of the 2D MHD turbulence simulation of Greco et al (see Zheng and Hu (2018)). These strong-tailed PDFs provide additional support for a strong presence of SMFRs separated by small-scale current sheets in the inner heliosphere. To this it can be added that MHD turbulence simulations feature open meandering magnetic field lines in between the closed SMFR structures (e.g., Servidio et al. 2011). Both simulations of magnetic field-line wandering (Zimbardo et al. 2000) and data analysis of slow solar wind magnetic turbulence (Bruno et al. 2004) suggest that the meandering field lines in between SMFRs are superdiffusive whereas the closed field lines of SMFRs can be considered as subdiffusive.

Recent evidence of solar energetic particles (SEPs) being trapped between the boundaries of two neighboring SMFRs was found close to the Sun in Parker Solar Probe data during Orbit 5 between 0.2–0.45 AU (Pecora et al. 2021). SEP trapping by SMFRs was reported previously (Ruffolo et al. 2003; Trenchi et al. 2013). This implies that SEPs quasi-trapped in SMFRs are statistically undergoing subdiffusive transport in the perpendicular direction. SEPs following the superdiffusive magnetic field lines in between SMFRs can be thought of propagating superdiffusively across the mean magnetic field. Thus, perpendicular SEP propagation can be viewed as a competition between subdiffusive and superdiffusive transport where the net effect depends on the filling factor of quasi-2D turbulence by SMFR structures. In a transport theory for anomalous SEP transport this competition can be captured by specifying the statistics of the SEP disturbed trajectories to correspond to the strong non-Gaussian statistics associated with quasi-2D MHD turbulence in the solar wind, as discussed above. A useful way to model such statistics for the disturbed particle trajectories is to specify a stable Lévy PDF that features a power-law tail (le Roux and Zank 2021).

To this it can be added that results of simulations indicate systematic energy gain of energetic particles while being trapped in contracting magnetic islands (Drake et al. 2006), suggesting that energy gain could potentially be superdiffusive statistically if suprathermal particles interact with numerous dynamic SMFR structures. This is confirmed by a number of publications that reported superdiffusive spatial and momentum transport of energetic particles when particle trajectories are traced in MHD turbulence simulation results containing SMFRs separated by small-scale current sheets (Islaker et al. 2017a,b, 2019; Nakanotani et al. 2022).

However, anomalous energetic particle transport can be viewed as an intermediate time-scale phenomenon, because in complex biological, financial, neutral and plasma fluid dynamical systems, anomalous diffusion crosses over into normal diffusion after a certain correlation time (Ito and Miyazaki 2003; Vallaey et al. 2017). Examples of such transitions in the inner heliosphere are: (i) SEPs escaping from solar flare sites arriving early at 1 AU can be thought of as superdiffusive, while those that arrive later are more diffusive (Fisk and Axford 1969), and (ii) simulations of energetic particle propagation in turbulence where the 2D turbulence component dominates the slab component exhibits a transition of perpendicular subdiffusion to normal perpendicular diffusion. There are reports of particle superdiffusion transitioning into subdiffusion in magnetically confined plasmas (Cartea and Del-Castillo-Negrete 2007), and in the case of energetic particle trajectories traced in MHD simulation results featuring SMFRs separated by small-scale current sheets in the solar coronal plasma (Islaker et al. 2019). It is important that a credible theory for anomalous energetic particle transport includes a transition from anomalous transport during intermediate times toward a diffusive or different anomalous transport regime at late times. This can be accomplished by specifying an exponentially truncated Lévy PDF for the statistics of the disturbed particle trajectories in response to interacting with intermittent quasi-2D turbulence as is discussed

further below. This is supported by the fact that the best fit to the PDF of magnetic field magnitude magnetic fluctuations in the slow solar wind was found to be an exponentially truncated Lévy distribution that sensibly capture the upper limit in the size of the magnitude fluctuations (Bruno et al. 2004).

le Roux and Zank (2021) showed how one can derive from first principles a fractional focused transport equation containing standard fractional derivatives to model the anomalous diffusion of energetic particles interacting with intermittent quasi-2D turbulence containing SMFRs and meandering field lines in between in the inner heliospheric supermagnetosonic solar wind on the basis of the standard focused transport equation. This was achieved by adjusting the closure approach of Sánchez et al. (2006), applied to fluid turbulence in fusion plasmas, to this problem. Furthermore, le Roux (2022) converted the fractional focused transport equation into fractional Parker and Gleeson-Axford transport equations based on the expectation that particle pitch-angle distribution will become nearly isotropic when energetic particles on longer time scales interact with numerous SMFRs and propagate distances surpassing the correlation length of meandering field lines.

However, the anomalous transport theory of le Roux and Zank (2021) suffers from the following shortcomings: (1) The asymptotic power law of a standard Lévy stable distribution was specified in the derivation to model the non-Gaussian statistics of the disturbed energetic particle trajectories in ordinary, momentum, and pitch-angle space generated when energetic particles interact with intermittent quasi-2D turbulence. The problem is that the second moment (variance) and higher moments of the Lévy distribution for the particle step size are infinite, indicating over-efficient non-local transport that is scale-free. (2) The theory does not naturally allow for a transition of anomalous transport to normal diffusion, or to a different anomalous diffusion state. (3) Solutions of the fractional Parker transport equation indicated a breakdown in the interplay between advection and anomalous diffusion so that the competition between these two transport processes is not properly maintained at late times. To address these shortcomings, the derivation of the fractional transport theory of le Roux and Zank (2021) and le Roux (2022) is revisited. A brief outline of the derivation is presented in which a key difference is that an exponentially truncated Lévy distribution is specified to model the statistics of the disturbed particle trajectories. The outcome of the derivation is a tempered fractional focused equation containing non-standard tempered fractional derivatives presented below that addresses the above-mentioned concerns.

2.6.1 Derivation of a Tempered Fractional Kinetic Transport Theory from First Principles - Key Aspects

To derive from first principles a kinetic transport theory to model the anomalous diffusion of energetic particles interacting with intermittent quasi-2D turbulence, including a transition to a normal diffusion or different anomalous diffusion state, requires a number of key elements:

1. Since quasi-2D turbulence contain intermittent, strong perpendicular magnetic field component increments, as discussed above, strong disturbances are induced in, e.g., the perpendicular component $\delta V_{2Di} \approx v\mu\delta B_{2Di}/B_0$ of the particle velocity, where v is the particle speed, μ is the cosine of the particle's pitch angle, and δB_{2Di} is the magnetic field turbulence component in the 2D plane perpendicular to the guide/background magnetic field \mathbf{B}_0 . Thus, the kinetic transport equation for anomalous transport is derived following a nonlinear perturbation approach in which, e.g., the particle's disturbed perpendicular velocity component correlation function decays, as a consequence of the decay in the correlation function of δB_{2Di} ($\delta V_{2Di} \propto \delta B_{2Di}$) along the disturbed particle trajectory through

quasi-2D turbulence (Lagrangian correlation function). In a traditional quasi-linear theory, this correlation function is specified to decay instead along the undisturbed guiding center trajectory (weak random wave turbulence). Furthermore, in the nonlinear derivation, the Lagrangian correlation functions are more complicated. E.g., the disturbed perpendicular particle velocity correlation function also includes the perpendicular gradient of the ensemble-averaged particle distribution function along the disturbed transverse guiding center trajectory to form a correlation function with a triple product ensemble average. For comparison, in quasi-linear theory one finds the usual correlation function with a double product ensemble average only referring to the correlation of the disturbed perpendicular guiding center velocity. In le Roux and Zank (2021), based on the approach of Sánchez et al. (2006), it is shown how this complication can be overcome by switching to a Eulerian approach to deal with triple product ensemble averages. This approach is also followed in this paper.

2. Non-Gaussian power-law statistics must be specified to model, e.g., the statistics of disturbances in the perpendicular particle velocity in response to the non-Gaussian power-law statistics associated with intermittent quasi-2D turbulence. For this purpose, the large argument asymptotic of an exponentially truncated Lévy stable PDF is assumed for the rescaled disturbed transverse particle velocity component $\delta \tilde{V}_{2Di} = \delta V_{2Di} \Delta t^{1-H}$ (Sánchez et al. 2006), e.g., where H is the so-called Hurst index given by $H = \beta/\alpha$ that refers to the ratio of the fractional index β , linked to the tempered fractional time derivative, over the fractional index α , connected to the tempered fractional spatial derivative, that both appear in the transport term derived finally for tempered perpendicular anomalous diffusion. The expression for the PDF is

$$P(\delta \tilde{V}_{2Di}) = A_\alpha \sigma_{x_i}^\alpha e^{-\lambda |\delta \tilde{V}_{2Di}|} / |\delta \tilde{V}_{2Di}|^{1+\alpha}, \quad (2.38)$$

where the fractional index $0 < \alpha < 2$, A_α is a constant that depends on α given by

$$A_\alpha = \frac{1}{\pi} \Gamma(1 + \alpha) \sin(\alpha\pi/2) = \frac{\alpha(1 - \alpha)}{2\Gamma(2 - \alpha) \cos(\alpha\pi/2)}, \quad (2.39)$$

(Sánchez et al. 2006), $\sigma_{x_i}^\alpha = \langle |\delta \tilde{V}_{2Di}|^\alpha \rangle = \langle |\delta V_{2Di}|^\alpha \rangle \langle \tau_{cor} \rangle^\alpha / \langle \tau_{cor} \rangle^{\alpha H}$, where $\langle \tau_{cor} \rangle$ is the average time scale which energetic particles require before seeing decorrelated magnetic fields when interacting with quasi-2D turbulence, and λ^{-1} is the characteristic perpendicular particle velocity component value above which the power-law PDF decays exponentially. The exponential rollover is the new element in the anomalous transport theory that was not included in the previous version of the theory presented in le Roux and Zank (2021). This new addition ensures that unphysically large disturbances in the perpendicular particle velocity components, e.g., are avoided, thus overcoming the problem of infinite second or higher moments of the standard Lévy distribution that resulted in scale-free non-local spatial transport in the previous version of the theory (le Roux and Zank 2021). It is this exponential truncation that enables a transition of, e.g., the anomalous perpendicular diffusion of energetic particle transport to more normal perpendicular diffusion as the power-law statistics of the disturbed transverse particle velocities get replaced by more Gaussian-like statistics beyond the critical scale λ^{-1} . This statistical description is further elaborated in the theoretical derivation by specifying that the disturbed perpendicular particle velocity component $\delta V_{2Di} = \Delta x_i / \Delta t$, where Δx_i can be interpreted as the perpendicular component of the particle step size if $\Delta t = \tau_{cor}$. Then, the rescaled disturbed perpendicular particle velocity (not in units of particle velocity)

becomes

$$\delta \tilde{V}_{2Di} = \Delta x_i / \Delta t^H. \quad (2.40)$$

The purpose for the rescaling now becomes clear because, since $\langle |\Delta x_i|^\alpha \rangle \propto \Delta t^{\alpha H}$ for general perpendicular anomalous transport, it follows that $\sigma_{x_i}^\alpha$, which closely related to the anomalous perpendicular diffusion coefficient, is independent of Δt , as expected. In the case of energetic particle interaction with the coherent SMFR component of quasi-2D turbulence, one can introduce a simple scattering model. When particles propagate inside coherent SMFRs structures, it is assumed that they have disturbed but coherent particle trajectories. Particle scattering occurs when they propagate through the abrupt SMFR boundaries characterized by strong discontinuities in the perpendicular magnetic component increments, because of small-scale current sheets separating neighbouring SMFRs (Greco et al. 2009). Accordingly, one can think of the particle waiting time (scattering time) Δt as the trapping time in or escape time from SMFR structures, and the perpendicular step size component Δx_i as determined by the SMFR transverse crossing distance which is approximately equal to the perpendicular size of SMFRs. Consequently, in the derivation there occurs a separation of the original exponentially truncated Lévy PDF for $\delta \tilde{V}_{2Di}$ into an exponentially truncated Lévy PDF for the step size and an exponentially truncated PDF for the waiting time that can be considered to be independent:

$$\begin{aligned} P(\Delta x_i) &= A_\alpha e^{-\lambda_x |\Delta x_i|} / |\Delta x_i|^{1+\alpha}, \\ P(\Delta t) &= A_{2-\beta} e^{-\lambda_t (\Delta t)} / (\Delta t)^{1+(2-\beta)}. \end{aligned} \quad (2.41)$$

In this aspect the theoretical development is similar to the classical continuous-time random walk model for anomalous particle diffusion in which the step-size and waiting-time PDFs are assumed to be independent (Montroll and Weiss 1965). Note that both PDFs include an exponential truncation so that beyond a critical step size and waiting time Gaussian-like statistics for the particle step size and Poisson-type statistics for the particle waiting time are gradually restored.

- As a consequence of the strong energetic particle response to intermittent quasi-2D turbulence, the perpendicular spatial scale over which the ensemble-averaged energetic particle distribution $\langle f \rangle$ varies can be approximated to be equal to the quasi-2D turbulence correlation length scale l_{2D} in the transverse direction. This means that the perpendicular gradient of $\langle f \rangle$ about a correlation length l_{2D} removed from position x_i deviates significantly from the gradient at position x_i so that

$$\frac{\partial \langle f \rangle}{\partial x_i}(x_i - \Delta x_i, t, p, \mu) \approx \frac{\partial \langle f \rangle}{\partial x_i}(x_i - l_{2D}, t, p, \mu) \neq \frac{\partial \langle f \rangle}{\partial x_i}(x_i, t, p, \mu), \quad (2.42)$$

where p is the particle momentum and μ is the cosine of the particle pitch angle. Thus, spatial lags in $\langle f \rangle$, and more generally, lags in time, momentum, and pitch angle, must be retained in this nonlinear approach and cannot be ignored as is done in standard quasi-linear theory. Retaining these lags is a key element that enables modelling of anomalous diffusion of energetic particles in terms of fractional derivatives in the transport theory for anomalous diffusion. Consequently, in the derivation of the new transport equation for tempered anomalous diffusion, the exponentially truncated Lévy distributions specified initially in the derivation result finally in transport terms for anomalous diffusion featuring tempered fractional derivatives containing non-local spatial, momentum, pitch-angle, and memory effects of particle transport that are taken into account by integration. For

example, for $1 < \alpha < 2$ there appears in the derived perpendicular anomalous diffusion term a left Caputo tempered fractional derivative given by

$$\begin{aligned} & {}^C_{x_{ia}} D_{x_i}^{\alpha-1, \lambda_x} \langle f \rangle (x_i, t, p, \mu) \\ &= \frac{1}{\Gamma(2-\alpha)} \int_0^{x_i - x_{ia}} d(\Delta x_i) \frac{e^{-\lambda_x(\Delta x_i)}}{(\Delta x_i)^{\alpha-1}} \frac{\partial \langle f \rangle}{\partial x_i} (x_i - \Delta x_i, t, p, \mu), \end{aligned} \quad (2.43)$$

in which non-local transport effects are taken into account by integrating the perpendicular gradient $\partial \langle f \rangle / \partial x_i$ over the spatial interval $x_i - x_{0i}$. Note that the exponential rollover in the exponentially truncated step-size Lévy distribution specified above features in the tempered fractional derivative, thus ensuring that non-local transport effects beyond a certain critical spatial scale λ_x^{-1} is ignored. As a consequence, anomalous perpendicular diffusion on intermediate spatial scales undergoes a transition to more normal diffusion or a different anomalous diffusion state on large scale spatial scales (Cartea and Del-Castillo-Negrete 2007; Vallaey et al. 2017).

2.6.2 A Brief Outline of the Derivation

The derivation of the transport equation for tempered anomalous transport started with the standard focused transport equation (Skilling 1975a) for the evolution of a nearly gyrotropic energetic particle distribution $\langle f \rangle (x_i, t, p, \mu)$ as a function of particle position x_i , time t , momentum p (speed v), and cosine of pitch angle μ given by

$$\frac{\partial \langle f \rangle}{\partial t} + \langle V_i \rangle_\phi \frac{\partial \langle f \rangle}{\partial x_i} + \left\langle \frac{dp}{dt} \right\rangle_\phi \frac{\partial \langle f \rangle}{\partial p} + \left\langle \frac{d\mu}{dt} \right\rangle_\phi \frac{\partial \langle f \rangle}{\partial \mu} = \frac{\partial}{\partial \mu} \left(D_{\mu\mu}^A \frac{\partial \langle f \rangle}{\partial \mu} \right), \quad (2.44)$$

where the particle's gyro-phase-averaged velocity in the fixed frame is expressed as

$$\langle V_i \rangle_\phi = v\mu b_i + U_i, \quad (2.45)$$

the particle's gyro-phase-averaged momentum rate of change in the solar wind flow frame is given by

$$\frac{1}{p} \left\langle \frac{dp}{dt} \right\rangle_\phi = -\frac{1}{2}(1-\mu^2) \frac{\partial U_i}{\partial x_i} - \frac{1}{2}(3\mu^2-1)b_i b_j \frac{\partial U_i}{\partial x_j} + \mu \left(\frac{qE_i}{p} - \frac{1}{v} \frac{dU_i}{dt} \right) b_i, \quad (2.46)$$

and the associated gyro-phase-averaged μ -rate of change in the solar wind frame is

$$\left\langle \frac{d\mu}{dt} \right\rangle_\phi = \frac{1}{2}(1-\mu^2) \left[v \frac{\partial b_i}{\partial x_i} + \mu \frac{\partial U_i}{\partial x_i} - 3\mu b_i b_j \frac{\partial U_i}{\partial x_j} + 2 \left(\frac{qE_i}{p} - \frac{1}{v} \frac{dU_i}{dt} \right) b_i \right]. \quad (2.47)$$

In the focused transport equation, U_i refers to the non-uniform solar wind flow velocity, μ is the cosine of the particle's pitch angle, b_i indicates the unit vector along the non-uniform heliospheric magnetic field, E_i is the electric field, and dU_i/dt is the acceleration of the solar wind flow velocity as seen following the flow. The focused transport equation also includes a transport term for particle diffusion in μ -space containing a diffusion coefficient $D_{\mu\mu}^A$ that models gyroresonant particle interactions with relatively small-scale parallel propagating Alfvén waves (Schlickeiser 1989).

A quasi-linear theory type perturbation analysis was used to distinguish the response of the energetic particle distribution to the large-scale solar wind flow and magnetic field on

long spatial and time scales, and to the random flow and magnetic fields of non-propagating quasi-2D turbulence containing SMFR structures with meandering field lines in between on intermediate spatial and time scales. An important distinction between this perturbation approach for non-propagating quasi-2D turbulence with nonlinear coherent SMFR structures and the standard perturbation approach for small amplitude propagating MHD waves with random phases is that, while the large-scale average of the SMFR flow velocity over numerous SMFRs is specified to be zero, this was not assumed to be necessarily the case for the large-scale average of gradients in the SMFR velocity. This extension facilitates the modeling of energetic particle acceleration during a situation where multiple SMFRs are simultaneously contracting, such as expected during early-time magnetic reconnection at a large-scale current sheet. Furthermore, $E_i b_i$ refers to the parallel electric field (the component of the electric field that is non-motional or non-ideal). However, on intermediate scales (MHD scales) the motional electric field is typically considered to be the dominant electric field component and one should think of the motional electric field components parallel and perpendicular to the average/guide magnetic field in contracting and merging SMFRs to be responsible for accelerating energetic particles (Dmitruk et al. 2004). In this theory, the turbulent motional electric field in individual SMFRs $-\delta \mathbf{U} \times \delta \mathbf{B}$ parallel to the average/guide field \mathbf{B}_0 , is used to model the effect of the “parallel” SMFR electric field on energetic particles on intermediate spatial and time scales (le Roux and Zank 2021) because both the SMFR flow velocity $\delta \mathbf{U}$ and the twist component of the magnetic field $\delta \mathbf{B}$ are modelled to exist predominantly in the 2D plane perpendicular to \mathbf{B}_0 (quasi-2D model for dynamic SMFRs).

Implementation of the perturbation analysis method, and the above-mentioned three key elements needed for the development of a tempered anomalous transport theory, led to the derivation of a tempered fractional focused transport equation discussed below, and tempered fractional Parker and Gleeson-Axford transport equations as well (not shown), containing tempered fractional derivatives for modeling the response of energetic particles to intermittent quasi-2D turbulence (for more details of the derivation method, see le Roux and Zank (2021) and le Roux (2022)).

2.6.3 The Tempered Fractional Focused Transport Equation

Compactly expressed, the tempered fractional focused transport equation for the evolution of the average energetic particle distribution function $\langle f \rangle(x_i, t, p, \mu)$ is

$$\begin{aligned} & \frac{\partial \langle f \rangle}{\partial t} + \frac{\partial}{\partial x_i} ([\langle V_i \rangle_{SW} + \langle V_i \rangle_{2D}] \langle f \rangle) + \frac{1}{p^2} \frac{\partial}{\partial p} \left(p^2 \left[\left\langle \frac{dp}{dt} \right\rangle_{SW} + \left\langle \frac{dp}{dt} \right\rangle_{2D} \right] \langle f \rangle \right) \\ & + \frac{\partial}{\partial \mu} \left(\left[\left\langle \frac{d\mu}{dt} \right\rangle_{SW} + \left\langle \frac{d\mu}{dt} \right\rangle_{2D} \right] \langle f \rangle \right) \\ & = \frac{\partial}{\partial \mu} \left(\langle D_{\mu\mu}^A \rangle \frac{\partial \langle f \rangle}{\partial \mu} \right) \\ & + {}_0 D_t^{1-\beta, \lambda_t} \left[\frac{\partial}{\partial x_{i\perp}} \left(\kappa_{\perp}^{2D[\beta, \alpha]} (-x_{i\perp} D_{x_{i\perp b}}^{\alpha-1, \lambda_x} + x_{i\perp a} D_{x_{i\perp}}^{\alpha-1, \lambda_x}) \langle f \rangle \right) \right] \\ & + \frac{1}{p^2} \frac{\partial}{\partial p} \left(p^2 D_{pp}^{2D[\beta, \alpha]} \left(-p D_{p_b}^{\alpha-1, \lambda_p} + p_a D_p^{\alpha-1, \lambda_p} \right) \langle f \rangle \right) \end{aligned}$$

$$+ \frac{\partial}{\partial \mu} \left(D_{\mu\mu}^{2D[\beta,\alpha]} \left(-_{\mu} D_{\mu_b}^{\alpha-1,\lambda\mu} + {}_{\mu_a} D_{\mu}^{\alpha-1,\lambda\mu} \right) \langle f \rangle \right) \Big], \quad (2.48)$$

which is valid for $0 < \alpha < 2$ and $0 < \beta < 2$. On the left-hand-side of the fractional transport equation are the terms containing differential advective particle fluxes in ordinary, momentum and in μ -space, respectively. One can see the decomposition of the advective fluxes into that generated by particle interaction with the background solar wind flow and magnetic field (terms with the subscript “SW”) and the fluxes produced by particle interaction with the mean quasi-2D turbulence flow, magnetic field, and motional electric field (terms with subscript “2D”). The expressions for the advection velocities were derived from the basic expressions for the advection velocities in the standard focused transport equation presented above (for more information, see le Roux and Zank (2021)). These advective transport terms have normal derivatives and are unchanged from those presented in the previous version of the anomalous focused transport theory of le Roux and Zank (2021) that contain standard fractional derivatives in the anomalous diffusion terms.

What is new are the anomalous diffusion terms on the right-hand-side that include tempered fractional time, spatial, momentum, and μ -derivatives whereas previously in le Roux and Zank (2021) they contained normal fractional derivatives. For example, the anomalous momentum diffusion term include ${}_p D_p^{\alpha-1,\lambda_p}$, which is a left Riemann-Liouville tempered fractional momentum derivative, and ${}_p D_{p_b}^{\alpha-1,\lambda_p}$ that is a right Riemann-Liouville tempered fractional momentum derivative. All the fractional derivatives differ from the standard fractional derivatives because they include an exponential rollover term as discussed above. It should be noted that for $1 < \alpha < 2$, all the derivatives with index $\alpha - 1$ were originally derived as left and right Caputo tempered fractional derivatives that were transformed into Riemann-Liouville fractional derivatives, and for $0 < \alpha < 1$ they are actually left and right Riemann-Liouville tempered fractional integrals that were expressed as Riemann-Liouville fractional derivatives to enable a more compact expression of the anomalous diffusion terms. For more information about tempered fractional derivatives, see Li et al. (2019), for example. It should be mentioned that there are no mixed-derivative terms for anomalous transport on the right hand side of the transport equation. These terms have on purpose be ignored because currently it is not clear how to derive them with the current approach. This is an unsolved problem that needs to be addressed in future theoretical work.

With this extension of the anomalous transport theory, one can model naturally a transition from anomalous diffusion to more normal diffusion at later times (if the tempered fractional time derivatives/integrals are neglected), or a transition to a different anomalous diffusion state, as discussed above. It can be shown that when the fractional indices $\beta \rightarrow 1$, and $\alpha \rightarrow 2$, the tempered fractional time derivatives/integrals vanish by becoming one, while the tempered fractional spatial, momentum, and μ -derivatives/integrals become normal so that normal diffusion terms are recovered.

The transport coefficients in the anomalous diffusion terms can be compactly expressed as follows:

$$\begin{aligned} \kappa_{\perp}^{2D[\beta,\alpha]} &= C(\beta, \alpha) \langle |\delta V_{2Di}|^{\alpha} \rangle \langle \tau_{cor} \rangle^{\alpha-\beta}, \\ D_{\mu\mu}^{2D[\beta,\alpha]} &= C(\beta, \alpha) \left\langle \left| \delta \left(\frac{d\mu}{dt} \right)_{2D} \right|^{\alpha} \right\rangle \langle \tau_{cor} \rangle^{\alpha-\beta}, \\ D_{pp}^{2D[\beta,\alpha]} &= C(\beta, \alpha) \left\langle \left| \delta \left(\frac{dp}{dt} \right)_{2D} \right|^{\alpha} \right\rangle \langle \tau_{cor} \rangle^{\alpha-\beta}, \end{aligned} \quad (2.49)$$

where the function $C(\beta, \alpha)$ is defined by

$$C(\beta, \alpha) = \frac{h(\beta, \alpha)(1 - \alpha)\Gamma(\beta)}{2\cos(\alpha\pi/2)}. \quad (2.50)$$

In the expression for $C(\beta, \alpha)$, the function $h(\beta, \alpha)$ is unknown, but $h(\beta, \alpha) \rightarrow 1$ in the limit when $\alpha \rightarrow 2$ (normal spatial, momentum, and μ -derivatives). The expressions for $\langle |\delta V_{2Di}|^\alpha \rangle$, $\langle |\delta(d\mu/dt)_{2D}|^\alpha \rangle$, $\langle |\delta(dp/dt)_{2D}|^\alpha \rangle$, derived from the basic expressions for the particle advection velocities in ordinary, μ , and momentum space in the standard focused transport presented above, can be found in Appendix A, Eqs. (A9)–(A10) of le Roux (2024). For more details about the derivation of these expressions, see Appendix A in le Roux et al. (2018) and Appendix B in le Roux and Zank (2021). Furthermore, the expressions for the average energetic particle correlation time $\langle \tau_{cor} \rangle$, when related to particle trapping in SMFRs, are presented in Appendix A of le Roux and Zank (2021). If particles are predominantly following superdiffusive meandering field lines between SMFRs (Bruno et al. 2004), the particle correlation time can be associated with particles surpassing a 2D turbulence correlation length scale across the mean magnetic field $\langle \tau_{cor} \rangle = l_c / \langle |\delta V_{2Di}|^2 \rangle^{1/2}$, where l_c is the 2D turbulence correlation scale length and the average perpendicular disturbed particle velocity component $\langle |\delta V_{2Di}|^2 \rangle^{1/2}$ is given by expression (A10) in Appendix A of le Roux (2024) by specifying $\alpha = 2$. Note that normal diffusion coefficients can be recovered by letting $\beta \rightarrow 1$, and $\alpha \rightarrow 2$ in the anomalous diffusion coefficient expressions, whereby $C(\beta, \alpha) \rightarrow 1/2$ because $h(\beta, \alpha) \rightarrow 1$.

2.6.4 Connection to Fractional Diffusion-Advection Equations in the Literature

By simplifying the fractional focused transport equation for the limiting case of one-dimensional perpendicular spatial transport in the x -direction assuming spatially uniform transport coefficients while neglecting momentum and pitch-angle variations, we get an equation for particles undergoing tempered anomalous diffusion in a uniform external (prescribed) solar wind flow velocity field given by

$$\frac{\partial \langle f \rangle}{\partial t} + U_{0x} \frac{\partial \langle f \rangle}{\partial x} = {}_0D_t^{1-\beta, \lambda_t} \kappa_\perp^{2D[\beta, \alpha]} ({}_x D_x^{\alpha, \lambda_x} + {}_x D_{x_b}^{\alpha, \lambda_x}) \langle f \rangle, \quad (2.51)$$

where U_{0x} is the solar wind flow velocity in the x -direction. Note that the solar wind advection term is normal whereas the perpendicular anomalous diffusion term includes both a tempered fractional time and tempered fractional spatial derivatives. The equation has the same form as Eq. (1.5) above with the difference that the fractional derivatives in Eq. (1.5) are not tempered fractional derivatives. Therefore, the equation fits the categorization as a more general version of the Galilei invariant fractional diffusion-advection equation discussed by Metzler and Klafter (2000) in the sense that the spatial derivatives are fractional instead of normal and all the fractional derivatives are tempered instead of being standard fractional derivatives.

The equation describes how the perpendicular spatial transport of energetic particles are affected by quasi-2D turbulence, a low-frequency turbulence component advected with the solar wind flow that contains SMFR structures (trapping centers) and superdiffusive meandering magnetic field lines between these structures, as discussed above. By specifying the fractional time index $\beta = \alpha H < 1$, one models tempered perpendicular subdiffusive transport as a consequence of energetic particle trapping in SMFR structures (evidence for energetic particle trapping in SMFRs can be found in observations discussed by Trenchi

et al. (2013) and Pecora et al. (2021), e.g.), while specifying the fractional spatial index $1 < \alpha < 2$ enables modeling of tempered perpendicular superdiffusion due to energetic particles following tempered superdiffusive meandering field lines in between SMFRs (Zimbardo et al. 2000; Bruno et al. 2004). This competition between tempered subdiffusive and superdiffusive transport can be controlled. If tempered superdiffusion dominates tempered subdiffusion, e.g., this can be modeled by setting $\beta = \alpha H < 1$ and $1 < \alpha < 2$ in such a way that $1/2 < H < 1$ (the standard superdiffusive range). As a side note, a simplified version of this tempered fractional focused transport equation can be found in Baeumer and Meerschaert (2010) with the difference that in the equation of Baeumer and Meerschaert (2010) there is not a tempered fractional time derivative attached to the anomalous diffusion term, suggesting that the equation did not include particle trapping effects.

An interesting feature of this equation is that when $\beta < 1$, the tempered fractional time derivative reduces the efficiency of the tempered anomalous diffusion term at late times, an effect of particle trapping in SMFRs (this can be seen by applying dimensional analysis to the anomalous diffusion term). Consequently, solar wind advection will increasingly dominate tempered superdiffusion of energetic particles at late times. Thus, upstream of a perpendicular shock the accelerated particle distribution will decay over an increasingly short spatial scale with time until the distribution will abruptly cutoff upstream as the purely advective transport limit is reached. It is only by removing SMFRs trapping effects by specifying $\beta = 1$ that a steady-state balance between advection and tempered superdiffusion can be accomplished upstream. It should be noted that the Galilei invariant fractional diffusion-advection equation, which our fractional transport equation is an example of, has been critized by Cairoli et al. (2018) as capable of producing unphysical (negative) solutions for the distribution function. Furthermore, the underlying cause of the unexpected advection-dominated late-time solution predicted by our fractional transport equation upstream of a perpendicular shock appears to be related to the fact that the tempered fractional time derivative is present in the anomalous diffusion term but not in the solar wind advection term. As an alternative, Metzler and Klafter (2000) also discuss a Galilei-variant type of fractional diffusion-advection equation based on a non-uniform external (prescribed) velocity field that has the structure of a fractional Fokker-Planck equation in the literature (e.g., Magdziarz and Weron 2007). In this case the fractional time derivative associated with the diffusion term also appears in the advection term (see Eq. (1.4) and its discussion above) which restores a sustained competition between advection and anomalous diffusion upstream of the shock at late times. As shown in more detail in le Roux (2024), the tempered fractional focused transport equation we derived can be converted by the method of addition into a more general tempered version of the fractional Fokker-Planck equation typically discussed in the literature (e.g., Metzler and Klafter 2000; Magdziarz and Weron 2007). This yields the tempered fractional focused transport equation

$$\begin{aligned} \frac{\partial \langle f \rangle}{\partial t} = & {}_0 D_t^{1-\beta, \lambda_t} \left[-\langle \tau_{cor} \rangle^{1-\beta} \frac{\partial}{\partial x_i} ([\langle V_i \rangle_{sw} + \langle V_i \rangle_{2D}] \langle f \rangle) \right. \\ & - \frac{\langle \tau_{cor} \rangle^{1-\beta}}{p^2} \frac{\partial}{\partial p} \left(p^2 \left[\left\langle \frac{dp}{dt} \right\rangle_{sw} + \left\langle \frac{dp}{dt} \right\rangle_{2D} \right] \langle f \rangle \right) \\ & - \langle \tau_{cor} \rangle^{1-\beta} \frac{\partial}{\partial \mu} \left(\left[\left\langle \frac{d\mu}{dt} \right\rangle_0 + \left\langle \frac{d\mu}{dt} \right\rangle_{2D} \right] \langle f \rangle \right) \\ & \left. + \langle \tau_{cor} \rangle^{1-\beta} \frac{\partial}{\partial \mu} \left(\langle D_{\mu\mu}^A \rangle \frac{\partial \langle f \rangle}{\partial \mu} \right) \right] \end{aligned}$$

$$\begin{aligned}
& + \frac{\partial}{\partial x_{i\perp}} \left(\kappa_{\perp}^{2D[\beta,\alpha]} \left(-_{x_{i\perp}} D_{x_{i\perp}b}^{\alpha-1,\lambda_x} + _{x_{i\perp}a} D_{x_{i\perp}}^{\alpha-1,\lambda_x} \right) \langle f \rangle \right) \\
& + \frac{1}{p^2} \frac{\partial}{\partial p} \left(p^2 D_{pp}^{2D[\beta,\alpha]} \left(-_p D_{pb}^{\alpha-1,\lambda_p} + _{pa} D_p^{\alpha-1,\lambda_p} \right) \langle f \rangle \right) \\
& + \frac{\partial}{\partial \mu} \left(D_{\mu\mu}^{2D[\beta,\alpha]} \left(-_{\mu} D_{\mu b}^{\alpha-1,\lambda_{\mu}} + _{\mu a} D_{\mu}^{\alpha-1,\lambda_{\mu}} \right) \langle f \rangle \right) \Big]. \quad (2.52)
\end{aligned}$$

By simplifying the equation for one-dimensional perpendicular spatial transport in the x -direction assuming spatially uniform transport coefficients while neglecting particle momentum and pitch-angle variations, we get

$$\begin{aligned}
\frac{\partial \langle f \rangle}{\partial t} = {}_0 D_t^{1-\beta,\lambda_t} \Bigg[& - \frac{U_{0x}}{\langle \tau_{cor} \rangle^{\beta-1}} \frac{\partial \langle f \rangle}{\partial x} \\
& + \kappa_{\perp}^{2D[\beta,\alpha]} \left(_{xa} D_x^{\alpha,\lambda_x} + _x D_{xb}^{\alpha,\lambda_x} \right) \langle f \rangle \Big]. \quad (2.53)
\end{aligned}$$

Thus, we reproduced the basic structure of the Galilean variant fractional diffusion-advection or fractional Fokker-Plank equation presented by Metzler and Klafter (2000) in the limit of a uniform external (prescribed) velocity field (see also Eq. (1.4) above). However, our transport equation is more general in the sense that the spatial derivatives are fractional instead of normal and all the fractional derivatives are tempered instead of being standard fractional derivatives.

By assuming $\beta < 1$ to invoke energetic particle trapping by SMFR structures, and applying dimensional analysis to the advection and anomalous diffusion terms, it is clear that both these transport terms become increasingly inefficient at late times due to particle trapping, but in such a way that the competition between these terms are not affected (both terms have the same fractional time derivative). This should enable one to maintain a competition between tempered solar wind advection and perpendicular anomalous diffusion upstream of perpendicular shocks at late times to avoid total domination by solar wind advection at late times that will result in a cutoff in the upstream particle distribution. However, the problem with this version of the transport equation is that the diminished efficiency of solar wind advection at late times implies that the SMFR trapping centers are stationary (see Metzler and Klafter (2000) and the discussion of Eq. (1.4) above). This means that SMFRs are not advected with the solar wind flow which is inconsistent with of SMFRs as part of a non-propagating quasi-2D turbulence mode advected with the solar wind flow. On this basis one has to conclude that the tempered fractional transport equation, as originally derived in a Galilei invariant form with normal advection terms, is more suitable for modeling energetic particle interaction with quasi-2D turbulence. Thus, one has to consider the possibility that particle trapping in SMFRs upstream of the shock does indeed result in a growing absence of energetic particles upstream as advection of particles to downstream increasingly dominates in time. This implies that if an unusual low amount of energetic particles are observed upstream of some heliospheric shock events, a possible explanation could be that there is a significant presence of SMFRs upstream that result in particle trapping.

2.7 Summary of Section 2

After a brief exposition of sub- and superdiffusion, in general, the latter was discussed in the context of shock acceleration employing both a propagator formalism for Levy walks and

a fractional transport equation. The main differences between the cases of superdiffusive and of standard (Gaussian) diffusive shock acceleration consist in (i) spatial power laws upstream (as opposed to exponential profiles), (ii) the number density far downstream being lower than that at the shock where a characteristic local peak is formed, and (iii) the energy spectra of accelerated particles being harder than those obtained for the case of normal diffusion. All of these findings are consistent with data obtained with various spacecraft. Finally, it was sketched how a fractional transport equation can actually be derived from first principles, thereby establishing a so-called tempered fractional transport theory.

3 Nonlinear Aspects of Particle Transport and Acceleration

When investigating the transport and acceleration of energetic particles it is very likely to come across nonlinear concepts of diffusion. In the following there will be a short overview of possible nonlinear description methods and their ramifications on the behaviour of charged energetic particles. The nonlinearities will arise from the ambition to describe both the transport of particles and the influences they have on the background medium they traverse. A special focus will lie on the work done by Litvinenko et al. (2017), Litvinenko et al. (2019), Walter et al. (2020) and Walter et al. (2022) where the diffusion coefficient of the particles will have a dependence on the particles distribution functions gradient. This model will first be applied to particle transport consisting of diffusion and advection and to models of shock acceleration after that.

3.1 Gradient Connection and Diffusive Transport

As far back as Bell (1978) there were attempts to link the transport of energetic particles to the collective behaviour of waves in the background plasma they traverse. These waves, that on the one hand serve as the scattering centres of the diffusing particles are influenced by said particles on the other hand.

Bell (1978) described this intertwined system with two differential equations, one transport equation for the particle distribution f and the other one a wave equation for the energy distribution of the MHD-waves \mathcal{F} in the background plasma. The link between these two properties would be realised through the diffusion coefficient D in the f -equation and the growth-rates Γ in the \mathcal{F} -equation.

Years later Ptuskin et al. (2008) made simplifying assumptions to the growth and dissipation rates of the waves and ended up with a diffusion coefficient that depends on the particle distribution functions gradient ∇f in the following form:

$$D \sim |\nabla f|^{-\nu} \quad (3.1)$$

with $\nu = \frac{1}{2}; \frac{2}{3}$, representing exponential dependencies for two different dissipation rates, $\nu = \frac{1}{2}$ for moving magnetic mirrors and $\nu = \frac{2}{3}$ for a Kolmogorov type of dissipation.

In Litvinenko et al. (2017) this Ansatz was generalized to arbitrary values of $0 < \nu < 1$ to take into account different kinds of wave amplification and dissipation and it was applied first to diffusive transport models. For example for a purely diffusive transport like:

$$\frac{\partial f}{\partial t} = \frac{\partial}{\partial x} \left(\kappa \left| \frac{\partial f}{\partial x} \right|^{-\nu} \frac{\partial f}{\partial x} \right) \quad (3.2)$$

$$f(x, t = 0) = \delta(x) \quad (3.3)$$

For this kind of transport Litvinenko et al. (2017) were able to apply similarity solutions and provided a formula for the time evolution of the distribution function in the form of:

$$f = t^{-\frac{1}{2(1-\nu)}} \cdot g(\xi) \quad (3.4)$$

$$\xi = xt^{\frac{-1}{2(1-\nu)}} \quad (3.5)$$

$$g = \left[a_\nu + \frac{\nu}{2-\nu} (2-2\nu)^{-\frac{(1-\nu)}{\nu}} \xi^{\frac{2-\nu}{1-\nu}} \right] \quad (3.6)$$

with a_ν being a constant of integration.

These solutions show an anomalous scaling behaviour for the mean square displacement, to be more precise it is:

$$\langle x^2 \rangle \sim t^{\frac{1}{1-\nu}} \quad (3.7)$$

A visualization of the nonlinear diffusive behaviour can be seen in Fig. 15. As explained in Litvinenko et al. (2017) this corresponds to a superdiffusive behaviour. Furthermore, a stationary solution could be found for a constant advection speed and a steady δ -source. The solution showed a power-law behaviour in the upwind domain of the system of the form

$$f \sim x^{\frac{\nu-1}{\nu}} \quad (3.8)$$

Two exemplaric sketches can be seen in Fig. 16. This result is of special interest, because data analysis on particles accelerated at interplanetary shocks show distributions, that resemble power-laws as the ones above, see Fig. 17, which displays fits to power laws upstream of shocks observed with the Ulysses spacecraft (Perri et al. 2022), and for more information Perri and Zimbardo (2007), Perri and Zimbardo (2015), or Malkov et al. (2024) and Sect. 2 above. Interestingly, while the nonlinear diffusion produces upstream power laws similar to those obtained for the case of anomalous superdiffusion, the characteristic peak at the shock obtained for the latter case is absent for the former. This indicates that the ‘anomalous’ behaviour in both cases is principally different. This can be understood from two facts. First, in the nonlinear case the diffusion itself remains Gaussian, so that the acceleration process is not changed fundamentally. Second, while in the superdiffusive case the power laws result from a constant diffusion coefficient upstream, these power laws need a position-dependent diffusion coefficient in the nonlinear case (Litvinenko et al. 2017; Malkov et al. 2024).

The concept of $D = D(\nabla f)$ was further expanded upon in Litvinenko et al. (2019) and Walter et al. (2020). The first publication provided an approximation of a nonlinear diffusive system with a non-time-constant source. The distribution function f was, thereby given in the form of:

$$f = c_1 \exp \left\{ -\frac{|\xi|}{\chi} \right\} + c_2 \exp \left\{ -\frac{\xi^2}{\chi^2} \right\} \quad (3.9)$$

This allowed Litvinenko et al. (2019) to approximate solutions of diffusive transport of the form:

$$\frac{\partial f}{\partial t} = \frac{\partial}{\partial x} \left(\left| \frac{\partial f}{\partial x} \right|^{-\nu} \frac{\partial f}{\partial x} \right) + S(t) \delta(x) \quad (3.10)$$

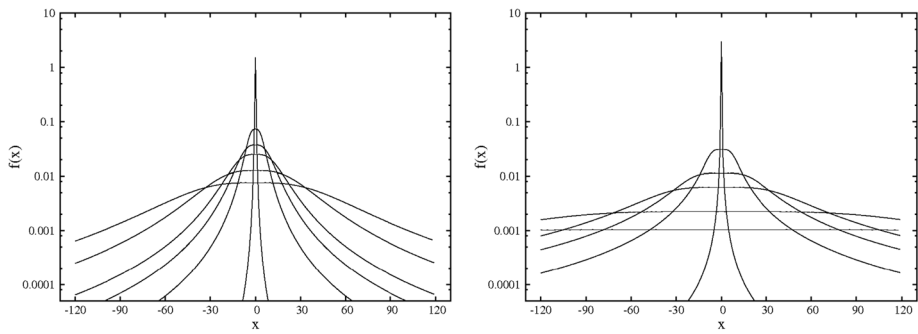


Fig. 15 Example of two diffusive processes using a nonlinear diffusion formulation. The left panel shows the diffusive process for $\nu = \frac{1}{2}$, the right panel for $\nu = \frac{2}{3}$. Both plots show the result for $t = 0.001, 2, 4, 6, 12, 20$. Adopted from Litvinenko et al. (2017)

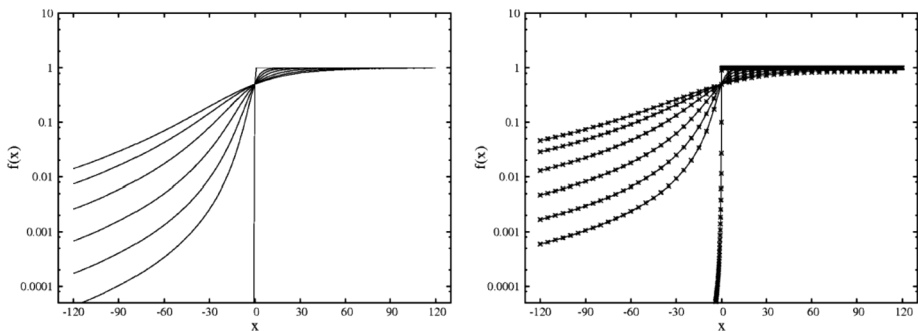


Fig. 16 Plot of a diffusion advection system with nonlinear diffusion. The left panel shows the results for $\nu = \frac{1}{2}$, the right panel for $\nu = \frac{2}{3}$. The times show are $t = 0.001, 5, 10, 20, 40, 70, 100$. Adopted from Litvinenko et al. (2017)

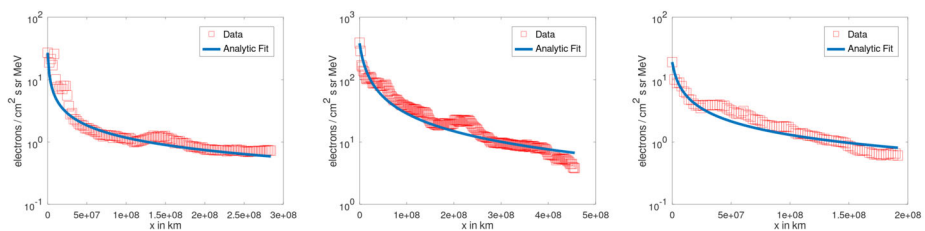


Fig. 17 Differential intensity of energetic electrons accelerated at corotating interaction regions as observed by the Ulysses spacecraft in the upstream region. Left: 11. Oct. 1992, 234 keV, $\nu = 0.60$, middle: 22. Jan. 1993, 89 keV, $\nu = 0.47$, and right: 10. May 1993, 55 keV, $\nu = 0.57$. The panels show the data for these three events (red symbols) along with the solutions of the nonlinear diffusion equation fitted to the data (blue lines). For the data see, e.g., Perri et al. (2015)

In Fig. 18 there are results plotted for the source

$$S(t) = S_0 \times \begin{cases} t & 0 < t < 1 \\ 2 - t & 1 < t < 2 \end{cases} \quad (3.11)$$

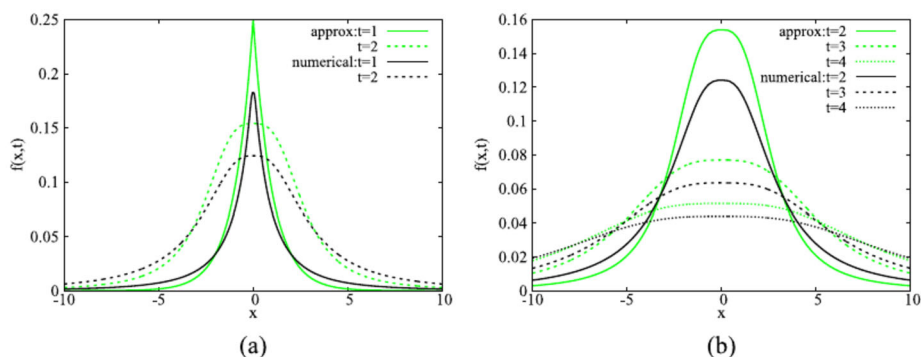


Fig. 18 Comparison of numerical results and analytical calculations for the nonlinearity parameter $\nu = \frac{1}{2}$ at different times t for a source given by Eq. (3.11). Adopted from Litvinenko et al. (2019)

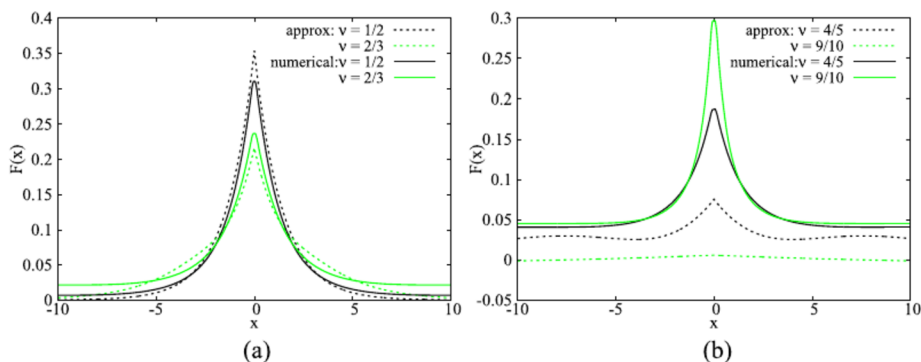


Fig. 19 Comparison of numerical results and analytical calculations at the time $t = 1$ for different nonlinearity parameters ν for a source given by Eq. (3.12). Adopted from Litvinenko et al. (2019)

and in Fig. 19 for a source like

$$S(t) = S_0 t^\alpha \quad (3.12)$$

The approaches of Litvinenko et al. (2017) and Litvinenko et al. (2019) however were expanded upon by Walter et al. (2020) where a more general expansion technique that is based on fundamental solutions was introduced and used to study diffusion-advection effects for different forms of nonlinearity and geometries.

The core premise of the method presented was to expand the transport solution at question into a series of equations by making the Ansatz as in Bender et al. (1989) and Bender et al. (1991):

$$f = f_0 + \nu f_1 + \nu^2 f_2 \quad (3.13)$$

Inserting this into a diffusion advection equation of the form

$$\frac{\partial f}{\partial t} + U \frac{\partial f}{\partial x} = \frac{\partial}{\partial x} \left(D \frac{\partial f}{\partial x} \right) + Q \quad (3.14)$$

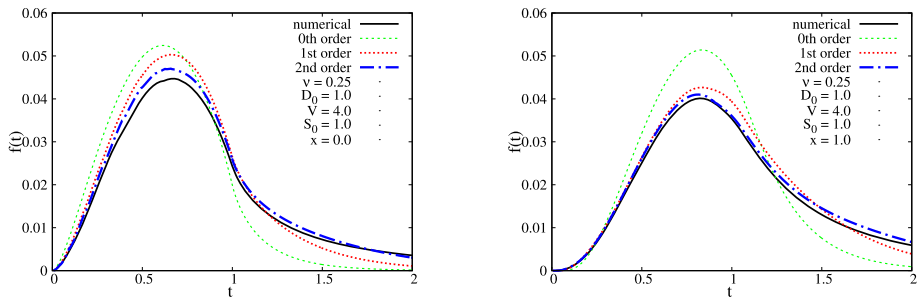


Fig. 20 Illustration of the expansion-approximation technique for given parameter set at $x = 0$ (left) and $x = 1$ (right). All other parameters can be found in the respective panels. The source was assumed to have the form $Q(x, t) = (t - t^2) \delta(x)$. Adopted from Walter et al. (2020)

with $D \sim \kappa \left| \frac{\partial f}{\partial x} \right|^{-\nu}$ and U being a constant advection velocity one ends up with a set of equations that look like:

$$\mathcal{L} f_0 = Q \quad (3.15)$$

$$\mathcal{L} f_1 = -\kappa \left(1 + \ln \left(\left| \frac{\partial f_0}{\partial x} \right| \right) \right) \frac{\partial^2 f_0}{\partial x^2} \quad (3.16)$$

$$\begin{aligned} \mathcal{L} f_2 = & -\kappa \left(\frac{\partial f_1}{\partial x} \left(\frac{\partial f_0}{\partial x} \right)^{-1} - \frac{1}{2} \ln^2 \left(\left| \frac{\partial f_0}{\partial x} \right| \right) - \ln \left(\left| \frac{\partial f_0}{\partial x} \right| \right) \right) \frac{\partial^2 f_0}{\partial x^2} \\ & - \kappa \left(1 + \ln \left(\left| \frac{\partial f_0}{\partial x} \right| \right) \right) \frac{\partial^2 f_1}{\partial x^2} \end{aligned} \quad (3.17)$$

$$\mathcal{L} f_3 = \dots \quad (3.18)$$

$$\mathcal{L} = \frac{\partial}{\partial t} + U \frac{\partial}{\partial x} - \kappa \frac{\partial^2}{\partial x^2} \quad (3.19)$$

As can be seen, the equations have all the exact same general form with the differential operator \mathcal{L} on the left hand side and a source on the right hand side that only depends on lower orders of f . The solution to every single one of these equation can, therefore, be obtained by a convolution of the right hand side with the fundamental solution Γ of \mathcal{L} that has the form:

$$\Gamma = \frac{1}{\sqrt{4\pi\kappa t}} \exp \left\{ -\frac{(x - Ut)^2}{4\kappa t} \right\} \quad (3.20)$$

Because the integral is usually not solvable via analytical means, it is necessary to solve it numerically. Luckily this can be done by using very basic numerical schemes. This has been done in Walter et al. (2020) a few examples can be seen in Fig. 20. Additionally Walter et al. (2020) also looked at different formulations of nonlinear diffusion, e.g. a non-diverging gradient dependence of the form:

$$D = \frac{\kappa}{\lambda + \nu^n \hat{\kappa} \left| \frac{\partial f}{\partial x} \right|^\nu} \quad (3.21)$$

In Walter et al. (2020) this system was discussed for $n = 1 = \hat{\kappa}$ and the resulting operator and set of equation read as follows:

$$\mathcal{L}f_0 = Q \quad (3.22)$$

$$\mathcal{L}f_1 = -\kappa \frac{\left(1 + \ln \left| \frac{\partial f_0}{\partial x} \right| \right)}{(1 + \lambda)^2} \frac{\partial^2 f_0}{\partial x^2} \quad (3.23)$$

$$\mathcal{L}f_2 = \dots \quad (3.24)$$

$$\mathcal{L} = \frac{\partial}{\partial t} + U \frac{\partial}{\partial x} - \frac{\kappa}{1 + \lambda} \frac{\partial^2}{\partial x^2} \quad (3.25)$$

The method could also be applied to non-gradient nonlinearities, in Walter et al. (2020) the example given by Kath and Cohen (1982) for $D \sim f^v$ was discussed and could be addressed in the same manner. More interesting for astrophysical purposes, however, was the application of the method onto a spherical system. For this purpose the diffusion advection equation was rewritten into:

$$\frac{\partial f}{\partial t} = \frac{1}{r^2} \frac{\partial}{\partial r} \left(r^2 D \frac{\partial f}{\partial r} \right) + Q \quad (3.26)$$

The set of equations that arises when $D = \kappa \left| \frac{\partial f}{\partial r} \right|^{-v}$ and $f = \sum_i f_i v^i$ has the following entries:

$$\mathcal{L}_{\text{rad}} f_0 = Q \quad (3.27)$$

$$\mathcal{L}_{\text{rad}} f_1 = -\frac{2\kappa}{r} \ln \left(\left| \frac{\partial f_0}{\partial r} \right| \right) \frac{\partial f_0}{\partial r} - \kappa \left(1 + \ln \left(\left| \frac{\partial f_0}{\partial r} \right| \right) \right) \frac{\partial^2 f_0}{\partial r^2} \quad (3.28)$$

$$\mathcal{L}_{\text{rad}} f_2 = \dots \quad (3.29)$$

$$\mathcal{L}_{\text{rad}} = \frac{\partial}{\partial t} - \frac{2\kappa}{r} \frac{\partial}{\partial r} - \kappa \frac{\partial^2}{\partial r^2} \quad (3.30)$$

By modifying results obtained by Webb and Gleeson (1977) it was possible to give a Greens function and a Greens formula:

$$G(r', r, t - t') = \frac{r}{r'} \frac{1}{2\sqrt{\pi}(t - t')} \times \left[\exp \left\{ -\frac{(r' - r)^2}{4(t - t')} \right\} - \exp \left\{ -\frac{(r' + r)^2}{4(t - t')} \right\} \right] \quad (3.31)$$

$$f_n(r, t) = \frac{1}{r^2} \int_0^t dt' \int_0^\infty dr' r'^2 Q_n(r', t') G(r', r, t - t') \quad (3.32)$$

Exemplaric results can be seen in Fig. 21. Now that we have talked in depth about the gradient nonlinearity and its effect on the transport of particles, we can now turn our attention to the question of how such a nonlinearity influences diffusive acceleration processes.

3.2 Gradient Connection and Shock Acceleration

After establishing the general properties of nonlinear transport in the section above and the references therein it is now time to turn the attention to the question of acceleration under

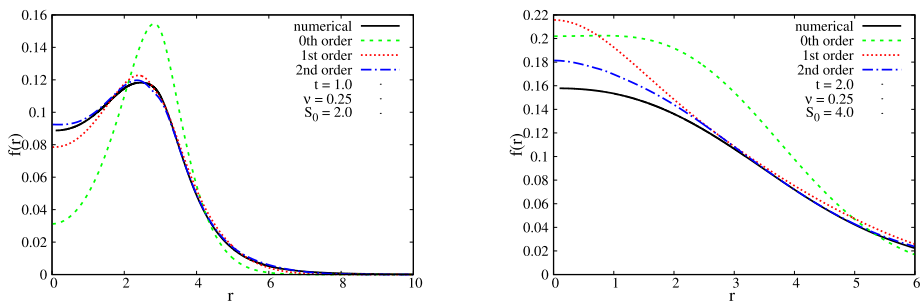


Fig. 21 Illustration of the expansion-approximation technique for $\kappa = 1$ and a source of the form $Q(x, t) = (t - t^2) \delta(r - 3)$. Adopted from Walter et al. (2020)

the influence of the nonlinear diffusion established. A first attempt to apply this kind of diffusion onto shock acceleration in particular was made by Walter et al. (2022).

Although not much hard analytical progress could be made, one central point was shown in a analytical calculation. The stationary shock spectrum, that arises when there is an infinitely large acceleration time and that is given by elementary means as $f \sim p^{-\frac{3U_1}{U_1 - U_2}}$, with U_1 being the upstream velocity and U_2 being the downstream velocity does not change for a nonlinear diffusion coefficient of the form given by Ptuskin et al. (2008) and generalized by e.g. Litvinenko et al. (2017). This was shown in a straightforward calculation in the same manner as in Drury (1983) for the strictly linear case, during which the nonlinear modifications cancelled each other out.

However, given the reference time scaling given by:

$$\langle t \rangle = \frac{3}{U_1 - U_2} \int_{p_0}^p \left(\frac{\kappa_1}{U_1} + \frac{\kappa_2}{U_2} \right) \frac{dp'}{p'} \quad (3.33)$$

we can make a solid argument that the time-scaling should change, because the average mean time to accelerate a particle from a starting momentum p_0 to momentum p is dependent on the diffusion coefficients, that are now subject to change when formulated nonlinear. More precisely, the acceleration time should get lower with decreasing diffusion coefficient.

Unfortunately there was no closed analytical solution available for a nonlinear shock acceleration system, so in Walter et al. (2022) it was necessary to rely on numerical results. Following will be a short overview of the used numerical setup before going into some of the already obtained results.

The nonlinear diffusion coefficient used in Walter et al. (2022) was of the form

$$D = \frac{\kappa}{1 + v \hat{\kappa} \left| \frac{\partial f}{\partial x} \right|^v} \quad (3.34)$$

and was applied to a simple shock model that was described by

$$\frac{\partial f}{\partial t} + U \frac{\partial f}{\partial x} = \frac{\partial}{\partial x} \left(D \frac{\partial f}{\partial x} \right) + \frac{1}{3} \frac{dU}{dx} \frac{\partial f}{\partial s} + Q \quad (3.35)$$

$$U = \frac{U_1 + U_2}{2} + \frac{U_1 - U_2}{2} \tanh[-\gamma(x - x_s)] \quad (3.36)$$

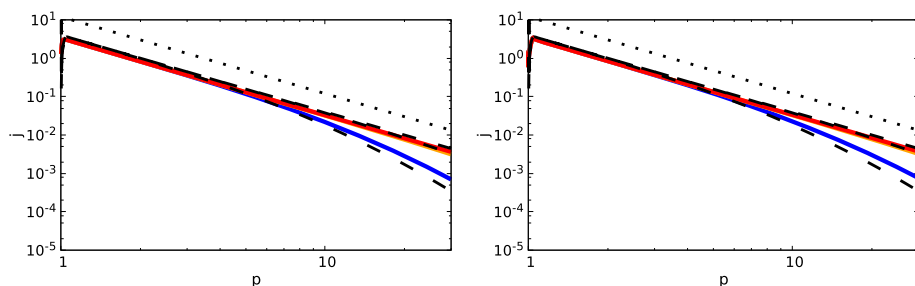


Fig. 22 Modified shock acceleration for $\nu = \frac{1}{2}$ and $\nu = \frac{2}{3}$. The times shown are $t = 10, 30, 100$. Adopted from Walter et al. (2022)

$$s = \ln \left(\frac{p}{p_0} \right) \quad (3.37)$$

with p_0 being the chosen reference momentum, U_1 and U_2 the upstream and downstream velocities of the shock characterised by the shock ratio $q = \frac{U_1}{U_2}$. The term f_s describes the adiabatic energy change caused by the change in velocity and Q was again a source that injects particles monoenergetically at the shock, so:

$$Q = S_0 \delta(r - r_s) \delta(s) H(t). \quad (3.38)$$

The velocity profile approximates a shock for growing values of γ and gives an ideal shock for $\gamma \rightarrow \infty$. A couple of example plots can be found in Fig. 22. There the difference in acceleration speed can be seen, as well as the fact, that the stationary solution remains the same.

3.3 Summary of Section 3

In this section we gave an overview of a nonlinear diffusion approach. Said diffusion approach was inspired by considerations by Bell (1978) or Ptuskin et al. (2008), resulting in a dependence of the diffusion coefficient on the spatial gradient of the energetic particles' distribution function. The resulting nonlinear partial differential equations were addressed by different mathematical techniques (e.g. Litvinenko et al. (2017), Litvinenko et al. (2019) or Walter et al. (2020)) as well as numerical simulations (same citations + Walter et al. (2022)). This nonlinear approach lead to anomalous features in the resulting particle distributions. One could find power-law structures in the spatial distribution and nonlinear time behaviours. Furthermore it was detected, that in the context of diffusive shock acceleration at a planar shock the stationary shock spectrum is not affected by a nonlinear diffusion process. However, the acceleration time scales are changed, when nonlinear diffusion is introduced. Future possible expansions of the here presented studies is e.g. the application onto spherical shocks.

4 Field Line Random Walk and Particle Decoupling, Transition from Subdiffusion to Normal Diffusion

4.1 Field Line Random Walk Theory

In field line random walk (FLRW) theory we describe the statistics of magnetic field lines in magnetohydrodynamic (MHD) turbulence. The most important application is the theory of perpendicular transport of energetic particles where it has been shown in the past that the field line diffusion coefficient directly impacts the particle motion (see, e.g., Webb et al. (2006), Shalchi (2010), Shalchi (2019), Shalchi (2020b), and Shalchi (2021b)).

Motivated by *Voyager 1* measurements it is often concluded that the solar wind and the very local interstellar medium are nearly incompressible (see Zank et al. (2019)). Therefore, the total magnetic field can be written as

$$\vec{B}(\vec{x}) = \delta B_x(\vec{x}) \hat{x} + \delta B_y(\vec{x}) \hat{y} + B_0 \hat{z} \quad (4.1)$$

and the corresponding magnetic field line equations are given by

$$dx = \frac{\delta B_x(\vec{x})}{B_0} dz \quad \text{and} \quad dy = \frac{\delta B_y(\vec{x})}{B_0} dz. \quad (4.2)$$

In Eqs. (4.1) and (4.2) we have used the constant mean magnetic field B_0 . Since the magnetic field components have to be evaluated along the field line, the problem of field line random walk is nonlinear and, thus, there is no simple way to describe FLRW in the general case. However, for slab turbulence, where by definition $\delta \vec{B}(\vec{x}) = \delta \vec{B}(z)$, the theory of FLRW is exact. A review of field line random walk theories was presented in Shalchi (2021a).

It is well-known that for short distances $z \rightarrow 0$, we find the initial ballistic regime

$$\langle (\Delta x)^2 \rangle = \frac{\delta B_x^2}{B_0^2} z^2. \quad (4.3)$$

A running field line diffusion coefficient can be defined via

$$d_{FL}(z) := \frac{1}{2} \frac{d}{dz} \langle (\Delta x)^2 \rangle \quad (4.4)$$

which can be used for diffusive as well as non-diffusive cases. If the field lines become diffusive in the limit $z \rightarrow \infty$, we find

$$\kappa_{FL} = \lim_{z \rightarrow \infty} d_{FL}(z) = \text{const.} \quad (4.5)$$

For incompressible three-dimensional turbulence, the properties of magnetic field lines are characterized by the *Kubo number* (see Kubo (1963))

$$K = \frac{\ell_{\parallel}}{\ell_{\perp}} \frac{\delta B_x}{B_0}. \quad (4.6)$$

In the latter formula, we have used the parallel and perpendicular correlation lengths of the turbulence, respectively. In the context of solar wind turbulence one often assumes a superposition of slab and two-dimensional modes (see Matthaeus et al. (1990)). Note, that slab turbulence corresponds to $K = 0$ and two-dimensional turbulence to $K = \infty$. In the

following, we construct a field line diffusion coefficient by employing simple heuristic arguments. The heuristic description of field line random walk was originally presented in Shalchi (2021a) but a more detailed version can be found in Shalchi (2024).

We remember that there is always an initial ballistic regime in which the field line mean square displacement is given by Eq. (4.3). In the considered regime the running field line diffusion coefficient (4.4) is then

$$d_{FL}(z) = \frac{\delta B_x^2}{B_0^2} z \quad (4.7)$$

corresponding to a linear increase with z . First, we consider the case of small Kubo numbers corresponding to slab or slab-like turbulence. In this case there is only one scale and that is the parallel correlation length ℓ_{\parallel} . If we expect that field lines behave diffusively for $z \geq \ell_{\parallel}$, it follows from Eq. (4.7) that

$$\kappa_{FL} = d_{FL}(z = \ell_{\parallel}) = \ell_{\parallel} \frac{\delta B_x^2}{B_0^2} \quad (4.8)$$

where we simply assumed that $d_{FL}(z)$ is a continuous function of z . Exact analytical theory predicts that for slab turbulence the diffusion coefficient is given by

$$\kappa_{FL} = L_{\parallel} \frac{\delta B_x^2}{B_0^2} \propto \ell_{\parallel} \frac{\delta B_x^2}{B_0^2} \quad (4.9)$$

where we have used the *parallel integral scale* L_{\parallel} . The form given by Eq. (4.9) is known as *quasi-linear* field line diffusion coefficient. Obviously using the simple arguments provided above gives us the correct scaling.

In the following, we construct a field line diffusion coefficient for the scenario of large Kubo numbers. In this case we expect that there is again only one scale but this is now the perpendicular correlation length ℓ_{\perp} . We expect the turnover from the ballistic regime to the diffusive regime as soon as

$$\langle (\Delta x)^2 \rangle \propto \ell_{\perp}^2. \quad (4.10)$$

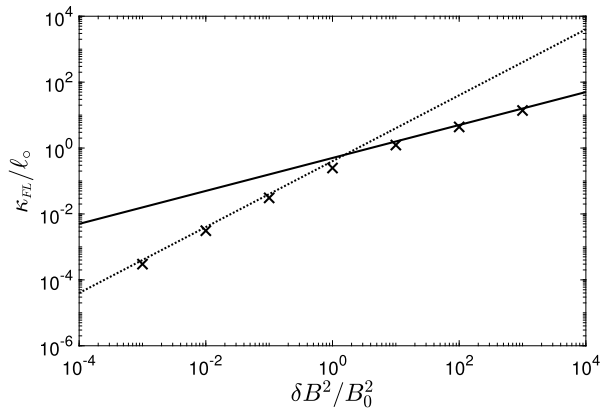
The latter condition simply means that field lines become diffusive as soon as the field line spread is so large that they experience the transverse structure of the turbulence. Therefore, we call the condition given by Eq. (4.10) the *transverse complexity condition*. In order to construct the field line diffusion coefficient, we assume that this condition is satisfied at $z = L_1$. Using this in Eqs. (4.3) and (4.7) yields

$$\ell_{\perp}^2 \propto \frac{\delta B_x^2}{B_0^2} L_1^2 \quad \text{as well as} \quad \kappa_{FL} = \frac{\delta B_x^2}{B_0^2} L_1. \quad (4.11)$$

From the first equation, one can easily derive $L_1 = \ell_{\perp} B_0 / \delta B_x$ telling us at which point along the z -axis field line diffusion is achieved. This relation can be used in the second equation to find

$$\kappa_{FL} = \frac{\delta B_x^2}{B_0^2} L_1 = \frac{\delta B_x^2}{B_0^2} \frac{B_0}{\delta B_x} \ell_{\perp} = \ell_{\perp} \frac{\delta B_x}{B_0} \quad (4.12)$$

Fig. 23 Field line diffusion coefficients versus the magnetic field ratio $\delta B^2/B_0^2$ as obtained from simulations performed for incompressible isotropic turbulence (crosses). The diffusion coefficients are divided by the bendover scale ℓ_o . The dashed line represents the quasi-linear scaling as given by Eq. (4.9) and the solid line corresponds to the nonlinear scaling as given by Eq. (4.12)



which is usually called the *nonlinear scaling*. To summarize, we expect to find the quasi-linear scaling (see Eqs. (4.8) or (4.9)) for small Kubo number turbulence and the nonlinear scaling (4.12) for large Kubo numbers.

Systematic analytical theories for FLRW have been developed in the past. Based on *Corrsin's independence hypothesis* (see Corrsin (1959)) and a diffusion approximation, Matthaeus et al. (1995) derived

$$\kappa_{FL} = \frac{1}{B_0^2} \int d^3k P_{xx}(\vec{k}) \frac{\kappa_{FL} k_{\perp}^2}{k_{\parallel}^2 + (\kappa_{FL} k_{\perp}^2)^2}. \quad (4.13)$$

The latter equation has to be understood as a nonlinear equation for the field line diffusion coefficient κ_{FL} . In Shalchi and Kourakis (2007a) the same assumptions have been made but the diffusion approximation was dropped. As a consequence, the following equation was found

$$\frac{d^2}{dz^2} \langle (\Delta x)^2 \rangle = \frac{2}{B_0^2} \int d^3k P_{xx}(\vec{k}) \cos(k_{\parallel} z) e^{-\frac{1}{2} \langle (\Delta x)^2 \rangle k_{\perp}^2}. \quad (4.14)$$

The latter equation can be solved analytically or numerically to obtain the field line mean square displacement $\langle (\Delta x)^2 \rangle$ as a function of parallel position z . From this one can derive a running diffusion coefficient via Eq. (4.4). Note, if we combine Eq. (4.14) with a diffusion approximation of the form $\langle (\Delta x)^2 \rangle = 2\kappa_{FL} |z|$, and after z -integrating the result, we find Eq. (4.13). Thus, Eq. (4.14) can be understood as a generalization of Eq. (4.13). Furthermore, Eq. (4.14) can also handle non-diffusive cases of field line random walk (see, e.g., Shalchi and Kourakis (2007a) and Shalchi and Kourakis (2007c)).

For large Kubo number turbulence, Eq. (4.13) predicts

$$\kappa_{FL} = L_U \frac{\delta B_x}{B_0} \propto \ell_{\perp} \frac{\delta B_x}{B_0} \quad (4.15)$$

where we have used the *ultra-scale* L_U . Note, that this scaling agrees with the nonlinear scaling (4.12) found by using simple heuristic arguments. In Fig. 23 we show an example plot demonstrating the different regimes of field line random walk as obtained from numerical simulations.

4.2 Parallel Diffusion of Energetic Particles

Energetic particles interacting with magnetohydrodynamic turbulence experience transport parallel with respect to the mean magnetic field. Parallel diffusion is a consequence of pitch-angle scattering which is described by the coefficient

$$D_{\mu\mu}(\mu) = \int_0^\infty dt \langle \dot{\mu}(t) \dot{\mu}(0) \rangle \quad (4.16)$$

where we have used the pitch-angle cosine μ . A detailed review of parallel transport, pitch-angle scattering, and nonlinear aspects of those processes can be found in Shalchi (2009).

The transport of energetic particles is described via partial differential equations. If we consider transport in phase-space and care only about the parallel motion of the particles, the simplest transport equation is (see, e.g., Shalchi (2009))

$$\frac{\partial F}{\partial t} + v\mu \frac{\partial F}{\partial z} = \frac{\partial}{\partial \mu} \left[D_{\mu\mu} \frac{\partial F}{\partial \mu} \right] \quad (4.17)$$

where we have used the phase-space distribution function $F = F(\mu, z, t)$ and the (conserved) particle speed v . Equation (4.17) corresponds to a *Sturm-Liouville problem* and describes a pitch-angle isotropization process. In the late-time limit, one finds a usual diffusion equation (see again Shalchi (2009) for details)

$$\frac{\partial M}{\partial t} = \kappa_{\parallel} \frac{\partial^2 M}{\partial z^2} \quad (4.18)$$

where $M = M(z, t)$ is the pitch-angle independent particle distribution function. Note, real transport equations are more complicated (see, e.g., Parker's transport equation as derived in Parker (1965)). Furthermore, one finds for the parallel spatial diffusion coefficient used in Eq. (4.18) the relation (see, e.g., Earl (1974))

$$\kappa_{\parallel} = \frac{v^2}{8} \int_{-1}^{+1} d\mu \frac{(1 - \mu^2)^2}{D_{\mu\mu}(\mu)}. \quad (4.19)$$

The simplest approach to obtain the pitch-angle scattering coefficient is to employ quasi-linear theory (see Jokipii (1966)). For a magnetostatic slab model, for instance, one finds (see, e.g., Shalchi (2009))

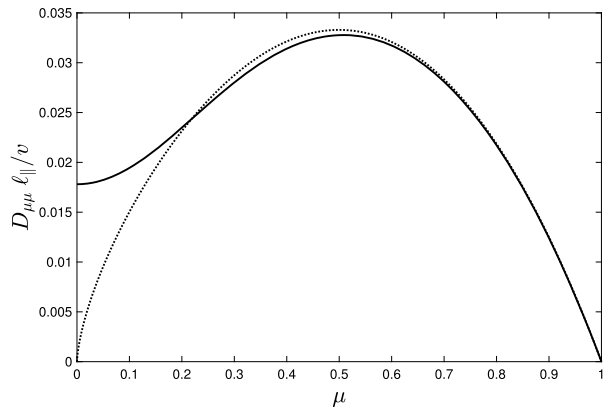
$$D_{\mu\mu} = \frac{\pi^2 \Omega^2}{B_0^2} (1 - \mu^2) \int_{-\infty}^{+\infty} dk_{\parallel} g^{slab}(k_{\parallel}) \left[\delta(v\mu k_{\parallel} + \Omega) + \delta(v\mu k_{\parallel} - \Omega) \right] \quad (4.20)$$

where we have used Dirac deltas and the gyro-frequency

$$\Omega = \frac{q B_0}{mc\gamma}. \quad (4.21)$$

In the latter formula, we have used the positive or negative electric charge of the particle q , its rest-mass m , the speed of light c , and the Lorentz factor γ . The *Larmor radius* is defined via $R_L = v/\Omega$ although this is really the gyro radius at $\mu = 0$. Furthermore, the function $g^{slab}(k_{\parallel})$ corresponds to the spectrum associated with the slab fluctuations. From Eq. (4.20) one can see that particles with given v , μ , and Ω interact only with specific parallel wave

Fig. 24 The pitch-angle diffusion coefficient $D_{\mu\mu}$ based on quasi-linear theory (dotted line) and second-order theory (solid line). The data is from Shalchi (2005) and was obtained for slab turbulence, a magnetic field ratio of $\delta B/B_0 = 0.25$, and a dimensionless rigidity of $R = R_L/\ell_{\parallel} = 0.0363$



numbers k_{\parallel} . This is called *gyro-resonance*. By considering Eq. (4.20), one can easily see that

$$D_{\mu\mu}(\mu = 0) = 0. \quad (4.22)$$

Note, this result is a consequence of the quasi-linear approximation. In reality, particles experience strong scattering at $\mu = 0$. This invalidity of quasi-linear theory is often called the *90° scattering problem*. However, this problem was already solved in Shalchi (2005) due to the development of *second-order quasi-linear theory* (see Fig. 24 for an example plot). Analytical forms of $D_{\mu\mu}$ based on second-order theory have been derived in Shalchi et al. (2009). Furthermore, the sharp resonance functions found in Eq. (4.20) are a consequence of quasi-linear theory. In reality, a particle with given properties interacts with all wave numbers. Therefore, the gyro-resonance picture strongly oversimplifies the mechanisms of pitch-angle scattering.

Regardless of what the pitch-angle scattering coefficient $D_{\mu\mu}$ is, the particle motion in the parallel direction starts as ballistic motion. At later times diffusion is restored and parallel transport is either described via the parallel diffusion coefficient κ_{\parallel} or the parallel mean free path which is defined via

$$\lambda_{\parallel} = \frac{3}{v} \kappa_{\parallel}. \quad (4.23)$$

The running particle diffusion coefficients in parallel and perpendicular directions can be defined via

$$d_{\parallel}(t) = \frac{1}{2} \frac{d}{dt} \langle (\Delta z)^2 \rangle \quad \text{and} \quad d_{\perp}(t) = \frac{1}{2} \frac{d}{dt} \langle (\Delta x)^2 \rangle, \quad (4.24)$$

respectively. A time-dependent formula for the parallel diffusion coefficient was obtained in Shalchi (2006), namely

$$d_{\parallel}(t) = \kappa_{\parallel} - \frac{3\kappa_{\parallel}^2}{v^2 t} \left[1 - e^{-v^2 t / (3\kappa_{\parallel})} \right]. \quad (4.25)$$

The latter formula was derived from Eq. (4.17) by employing the so-called *isotropic form* $D_{\mu\mu} = (1 - \mu^2)D$ which was derived from second-order theory in Shalchi et al. (2009). The parameter κ_{\parallel} used in Eq. (4.25) corresponds to the late-time parallel diffusion coefficient.

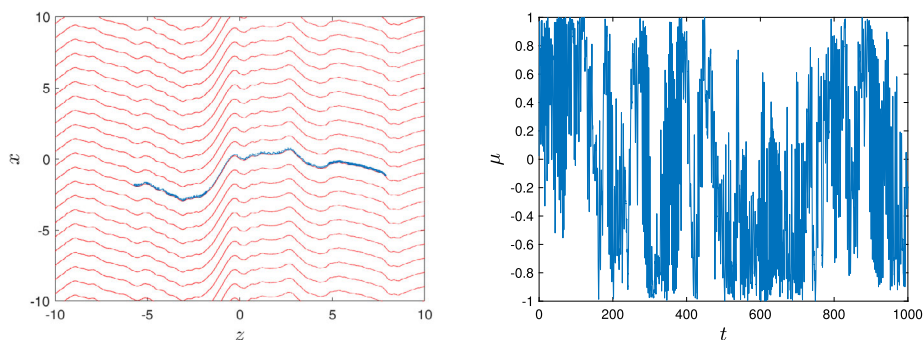


Fig. 25 Shown is a particle orbit obtained from test-particle simulations in slab turbulence where the magnetic field ratio satisfies $\delta B^2/B_0^2 = 1$ and for the particle rigidity we have set $R = R_L/\ell_{\parallel} = 0.1$. The left panel shows magnetic field lines (red) and the particle trajectory (blue). The right panel shows the corresponding pitch-angle cosine μ versus time

In Fig. 25 we depict the particle motion in slab turbulence as obtained from test-particle simulations. One can easily see that in reality pitch-angle scattering at $\mu = 0$ is very strong proving the invalidity of quasi-linear theory.

4.3 Perpendicular Diffusion of Energetic Particles

In the current section, we discuss particle transport across the mean magnetic field. Perpendicular transport can either be described by using simulations, heuristic arguments, or analytical theory. In the following, we review each approach and later we compare obtained results with each other.

4.3.1 Test-Particle Simulations

The most accurate description of perpendicular diffusion is achieved by employing test-particle simulations (see, e.g., Qin et al. (2002b) and Qin et al. (2002a) for some early work; see also Sect. 5.1.1). In this case we solve numerically the simplified *Newton-Lorentz equation* (1.8) neglecting a large-scale electric field

$$\frac{d\vec{p}}{dt} = q\vec{v} \times \vec{B}(\vec{x}) \quad (4.26)$$

where we have used *SI units*. For the incompressible case, the magnetic field can be generated via (see, e.g., Tautz (2010) for more details)

$$\delta\vec{B}(\vec{x}) = \sqrt{2}\delta B \sum_{n=1}^N A(k_n) \hat{\xi}_n \cos(\vec{k}_n \cdot \vec{x} + \beta_n) \quad (4.27)$$

where we have used the polarization vector

$$\hat{\xi}_n = \begin{pmatrix} -\sin\phi_n \\ \cos\phi_n \\ 0 \end{pmatrix}. \quad (4.28)$$

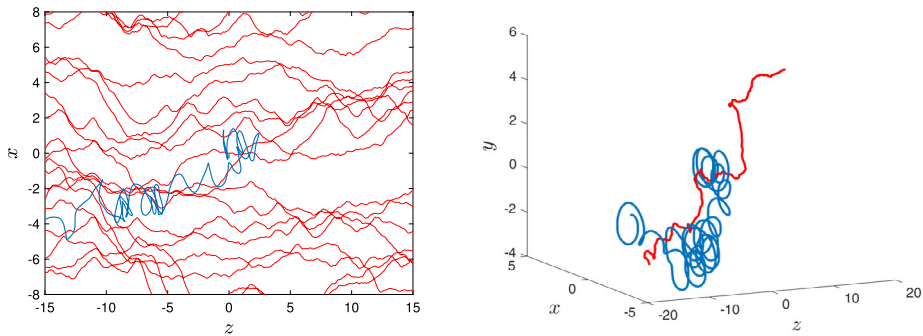


Fig. 26 Shown is a particle orbit obtained from test-particle simulations in two-component turbulence where the magnetic field ratio satisfies $\delta B^2/B_0^2 = 1$ and for the particle rigidity we have set $R = R_L/\ell_{\parallel} = 1.0$. The left panel shows magnetic field lines (red) and the particle trajectory (blue). The right panel shows the same scenario but as a three-dimensional plot

What the vector \vec{k}_n in Eq. (4.27) is depends on the considered turbulence model. For slab turbulence, for instance, we would simply use $\vec{k}_n = k_n \hat{z}$ where k_n is the corresponding wave number. For two-dimensional modes, on the other hand, we employ

$$\vec{k}_n = k_n \begin{pmatrix} \cos \phi_n \\ \sin \phi_n \\ 0 \end{pmatrix}. \quad (4.29)$$

Above we have used the total turbulent magnetic field δB , the spectrum $A^2(k_n)$, and the random numbers ϕ_n and β_n . The parameter N in Eq. (4.27) corresponds to the number of modes. Increasing this number improves numerical accuracy. However, one can usually work with only $N = 256$. This is at least sufficient if slab or two-dimensional turbulence is considered. The Newton-Lorentz equation (4.26) is then solved by using a numerical integration method such as a *Boris integrator* (see Boris (1970)). After this step, one finds the trajectories of the individual particles. From such orbits one can then compute the running diffusion coefficients in the different directions of space. In order to do this, one needs a huge number of particles such as 10^3 or even 10^5 for very accurate and smooth results. This needs to be done by using parallel computing (e.g., using *OpenMP* in C++). In Figs. 25 and 26 the reader can find example orbits obtained from the simulations discussed above.

4.3.2 Heuristic Arguments

One can try to understand the basic physics of perpendicular transport by using simple heuristic arguments (see Shalchi (2019)). First, we assume that particles follow magnetic field lines. This is true for turbulence without transverse structure meaning slab turbulence. Furthermore, we assume that the parallel motion is unperturbed meaning that it happens with constant parallel velocity

$$z = v_{\parallel} t \quad \text{with} \quad v_{\parallel} = v \mu = \text{const.} \quad (4.30)$$

If particles follow magnetic field lines and the field lines are diffusive, we can use

$$\langle (\Delta x)^2 \rangle = 2\kappa_{FL} |z| = 2v |\mu| \kappa_{FL} t. \quad (4.31)$$

From this we can read off the pitch-angle dependent perpendicular diffusion coefficient

$$D_{\perp}(\mu) = v |\mu| \kappa_{FL}. \quad (4.32)$$

By averaging over all μ , we find for the pitch-angle independent diffusion coefficient

$$\kappa_{\perp} = \frac{v}{2} \kappa_{FL} \quad (4.33)$$

and the perpendicular mean free path is in this case

$$\lambda_{\perp} = \frac{3}{v} \kappa_{\perp} = \frac{3}{2} \kappa_{FL}. \quad (4.34)$$

Characteristic for this result is that the perpendicular mean free path does not depend on particle energy/rigidity. The formula above is called the *Field Line Random Walk (FLRW) limit* because perpendicular transport is entirely controlled by the statistics of magnetic field lines.

However, in reality we have strong pitch-angle scattering and, therefore, the parallel motion is not unperturbed but diffusive. If particles follow field lines, we can still use

$$\langle (\Delta x)^2 \rangle = 2\kappa_{FL} |z|. \quad (4.35)$$

If parallel transport is diffusive, we can estimate

$$|z| \approx \sqrt{\langle (\Delta z)^2 \rangle} = \sqrt{2\kappa_{\parallel} t}. \quad (4.36)$$

Combining those two equations gives us

$$\langle (\Delta x)^2 \rangle \approx 2\kappa_{FL} \sqrt{2\kappa_{\parallel} t}. \quad (4.37)$$

A more systematic description of this type of transport yields (see, e.g., Webb et al. (2006) and Shalchi and Kourakis (2007b))

$$\langle (\Delta x)^2 \rangle = 4\kappa_{FL} \sqrt{\frac{\kappa_{\parallel} t}{\pi}}. \quad (4.38)$$

Equations (4.37) and (4.38) provide sub-diffusive transport of the form $\langle (\Delta x)^2 \rangle \propto \sqrt{t}$. We conclude that parallel diffusion suppresses perpendicular transport to a sub-diffusive level. For slab turbulence, compound sub-diffusion is the final state of perpendicular transport. In Fig. 25 we show an example trajectory of a particle in slab turbulence. Clearly one can see how the particle follows a single magnetic field line while experiencing strong changes of the pitch-angle. However, if we consider turbulence with transverse complexity, particles cannot follow field lines anymore. We assume that perpendicular diffusion is restored as soon as particles experience the transverse structure of the turbulence. In Fig. 26 we show as an example for such a scenario, magnetic field lines and a particle orbit for two-component turbulence.

In the following, we employ heuristic arguments in order to construct the perpendicular diffusion coefficient in turbulence with transverse structure. We assume that perpendicular diffusion is restored as soon as particles satisfy the *transverse complexity condition*

$$\langle (\Delta x)^2 \rangle \approx 2\ell_{\perp}^2. \quad (4.39)$$

Note, the factor 2 therein is arbitrary and could be omitted. Before condition (4.39) is satisfied, we have compound sub-diffusion and the corresponding running diffusion coefficient is given by

$$d_{\perp}(t) \approx \kappa_{FL} \sqrt{\frac{\kappa_{\parallel}}{2t}} \quad (4.40)$$

which is obtained after combining Eqs. (4.24) and (4.37). To construct the late-time perpendicular diffusion coefficient, we assume that diffusion is restored at time t_d and, thus, we find

$$\kappa_{\perp} \approx \kappa_{FL} \sqrt{\frac{\kappa_{\parallel}}{2t_d}} \quad (4.41)$$

where we simply have assumed that $d_{\perp}(t)$ is a continuous function of time. In order to find the time t_d , we combine Eqs. (4.37) and (4.39) to obtain

$$t_d \approx \frac{\ell_{\perp}^4}{2\kappa_{\parallel}\kappa_{FL}^2}. \quad (4.42)$$

The latter formula tells us how long it needs until normal diffusion is achieved. Equation (4.42) can be used in our formula for the diffusion coefficient (4.41) to find

$$\kappa_{\perp} \approx \kappa_{FL} \sqrt{\frac{\kappa_{\parallel}}{2t_d}} \approx \kappa_{FL} \sqrt{\frac{\kappa_{\parallel}^2 \kappa_{FL}^2}{\ell_{\perp}^4}} = \frac{\kappa_{FL}^2}{\ell_{\perp}^2} \kappa_{\parallel}. \quad (4.43)$$

This result has some similarity with the result found by Rechester and Rosenbluth (1978) and, thus, one could call this limit the CLRR (CollisionLess Rechester and Rosenbluth) limit as originally suggested in Shalchi (2015b). Equation (4.43) can easily be written as

$$\frac{\kappa_{\perp}}{\kappa_{\parallel}} \approx \frac{\kappa_{FL}^2}{\ell_{\perp}^2} \quad (4.44)$$

corresponding to a constant ratio of perpendicular and parallel diffusion coefficients. The recovery of normal diffusion due to transverse complexity is sometimes called *second diffusion*.

However, for weak pitch-angle scattering the above arguments are no longer valid because particles satisfy the transverse complexity condition before compound sub-diffusion is established. In this case, the parallel motion is still unperturbed in the parallel direction when the particles start to satisfy the transverse complexity condition and the perpendicular diffusion coefficient should be similar compared to the FLRW limit as given by Eqs. (4.33) and (4.34). Furthermore, there could be an extreme scenario where particles follow ballistic field lines while parallel transport is already diffusive. If the transverse complexity condition is satisfied before particles start to interact with diffusive field lines, one finds the so-called *fluid limit*

$$\frac{\kappa_{\perp}}{\kappa_{\parallel}} = \frac{\delta B_x^2}{B_0^2}. \quad (4.45)$$

Practically one finds CLRR and fluid limits for short parallel mean free paths and the FLRW limit for long parallel mean free paths. Figure 27 shows as an example a comparison with simulations. One can nicely see the turnover from CLRR to FLRW limits for an increasing parallel mean free path.

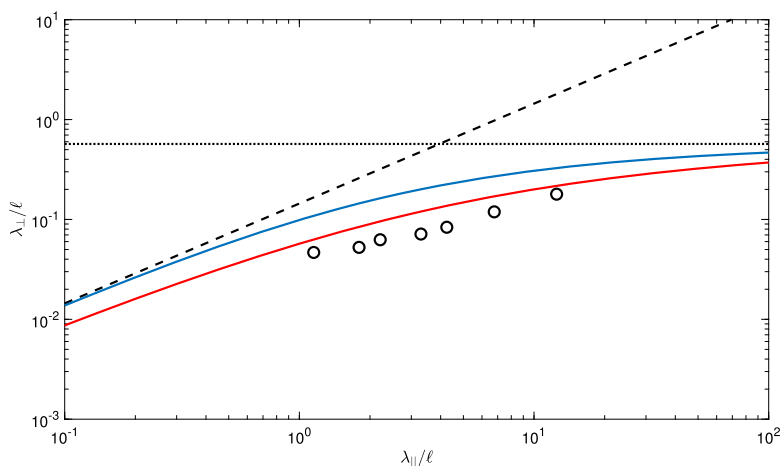


Fig. 27 The perpendicular mean free path versus the parallel mean free path for Goldreich-Sridhar turbulence. The latter model was proposed in Goldreich and Sridhar (1995). Shown are the test-particle simulations (black circles) performed by Sun and Jokipii (2011) as well as results obtained by employing the so-called *unified nonlinear transport theory* of Shalchi (2010) which are represented by the red solid line. The black dashed line corresponds to the CLRR limit given by Eq. (4.44) and the black dotted line corresponds to the FLRW limit. The blue solid line was obtained by employing the heuristic composite formula as given by Eq. (4.46). The field line diffusion coefficient is in this case $\kappa_{FL} = 0.38\ell$. More details can be found in Shalchi and Hussein (2015)

A *composite formula* containing FLRW and CLRR limits has been proposed in Shalchi (2019). According to this formula the perpendicular mean free path can be estimated via

$$\frac{\lambda_{\perp}}{\ell_{\perp}} \approx \frac{9\ell_{\perp}}{16\lambda_{\parallel}} \left[\sqrt{1 + \frac{8\kappa_{FL}\lambda_{\parallel}}{3\ell_{\perp}^2}} - 1 \right]^2. \quad (4.46)$$

For $\lambda_{\parallel} \rightarrow 0$, the latter formula yields Eq. (4.44) and for $\lambda_{\parallel} \rightarrow \infty$ the FLRW limit as given by Eq. (4.34). However, the fluid limit (4.45) is not contained in the composite formula.

The heuristic approach described above is based on the assumption of diffusive magnetic field lines. However, those heuristic arguments can also be developed for the case of super-diffusive field lines (see Shalchi (2020a)). Furthermore, the considerations presented above are based on the assumption of zero gyro radii. The effects of a finite Larmor radius have been discussed in Neuer and Spatschek (2006), Shalchi (2015a), Shalchi (2016), as well as Qin and Shalchi (2016).

4.3.3 Analytical Theories

In the following, we shall describe an analytical theory that contains the complete physics of perpendicular diffusion with the exception of finite Larmor radius effects. This approach was originally developed in Shalchi (2021b) where the reader can find more mathematical details. We start with the so-called *Chapman-Kolmogorov equation* (see Gardiner (1985) as well as Webb et al. (2006))

$$f_{\perp}(x, y, t) = \int_{-\infty}^{+\infty} dz f_{FL}(x, y, z) f_{\parallel}(z, t). \quad (4.47)$$

Here the perpendicular particle distribution function $f_{\perp}(x, y; t)$ is given as convolution integral of the field line distribution function $f_{FL}(x, y; z)$ and the parallel particle distribution function $f_{\parallel}(z; t)$. Note, that the formula above describes particles following magnetic field lines and does not include the transverse complexity effect. The latter effect will be incorporated later. Considering the second moment of Eq. (4.47) gives us (see, e.g., Shalchi and Kourakis (2007b))

$$\langle (\Delta x)^2 \rangle_P(t) = \int_{-\infty}^{+\infty} dz \langle (\Delta x)^2 \rangle_{FL}(z) f_{\parallel}(z; t) \quad (4.48)$$

where the subscript P emphasizes that the particle mean square displacement is considered. The parallel distribution function therein can be replaced by a usual Fourier representation of the form

$$f_{\parallel}(z; t) = \int_{-\infty}^{+\infty} dk'_{\parallel} F(k'_{\parallel}, t) e^{ik'_{\parallel} z}. \quad (4.49)$$

Using this in Eq. (4.48) yields

$$\langle (\Delta x)^2 \rangle_P(t) = \int_{-\infty}^{+\infty} dz \langle (\Delta x)^2 \rangle_{FL}(z) \int_{-\infty}^{+\infty} dk'_{\parallel} F(k'_{\parallel}, t) e^{ik'_{\parallel} z}. \quad (4.50)$$

For later considerations, it will be useful to rewrite this as

$$\begin{aligned} \langle (\Delta x)^2 \rangle_P &= - \int_{-\infty}^{+\infty} dk'_{\parallel} F(k'_{\parallel}, t) k'_{\parallel}{}^{-2} \\ &\times \int_{-\infty}^{+\infty} dz \left[\frac{d^2}{dz^2} \langle (\Delta x)^2 \rangle_{FL} \right] e^{ik'_{\parallel} z}. \end{aligned} \quad (4.51)$$

Therein we can use the field line random walk equation given by Eq. (4.14). Combining the latter equation with a field line diffusion approximation allows us to write Eq. (4.14) as

$$\frac{d^2}{dz^2} \langle (\Delta x)^2 \rangle_{FL} = \frac{2}{B_0^2} \int d^3 k P_{xx}(\vec{k}) \cos(k_{\parallel} z) e^{-\kappa_{FL} k_{\perp}^2 |z|}. \quad (4.52)$$

This can now directly be used in Eq. (4.51) to find

$$\begin{aligned} \langle (\Delta x)^2 \rangle_P &= - \frac{2}{B_0^2} \int_{-\infty}^{+\infty} dk'_{\parallel} F(k'_{\parallel}, t) k'_{\parallel}{}^{-2} \\ &\times \int d^3 k P_{xx}(\vec{k}) \int_{-\infty}^{+\infty} dz \cos(k_{\parallel} z) e^{-\kappa_{FL} |z| k_{\perp}^2 + ik'_{\parallel} z}. \end{aligned} \quad (4.53)$$

In the following, we omit the subscript P because the remaining mean square displacement is that of the particle and the field line mean square displacement no longer shows up in our equation. The z -integral in Eq. (4.53) can be solved and we obtain

$$\begin{aligned} \langle (\Delta x)^2 \rangle &= - \frac{2}{B_0^2} \int_{-\infty}^{+\infty} dk'_{\parallel} F(k'_{\parallel}, t) k'_{\parallel}{}^{-2} \\ &\times \int d^3 k P_{xx}(\vec{k}) \left[R_+(\vec{k}, k'_{\parallel}) + R_-(\vec{k}, k'_{\parallel}) \right] \end{aligned} \quad (4.54)$$

where we have used the *resonance functions*

$$R_{\pm}(\vec{k}, k'_{\parallel}) := \frac{\kappa_{FL} k_{\perp}^2}{(k_{\parallel} \pm k'_{\parallel})^2 + (\kappa_{FL} k_{\perp}^2)^2} \quad (4.55)$$

describing the coupling between particles and field lines.

The running diffusion coefficient, defined via Eq. (4.24), can also be written as (see Taylor 1922; Green 1951; Kubo 1957, and Shalchi 2011)

$$d_{\perp}(t) = \int_0^t d\tau \langle v_x(\tau) v_x(0) \rangle. \quad (4.56)$$

Note, in most articles the latter formula is used in the limit $t \rightarrow \infty$. However, Eq. (4.56) is more general and can be employed for non-diffusive cases as well. It follows from Eqs. (4.56) and (4.24) that the second derivative of the mean square displacement is equal to the *velocity auto-correlation function*

$$\langle v_x(t) v_x(0) \rangle = \frac{1}{2} \frac{d^2}{dt^2} \langle (\Delta x)^2 \rangle. \quad (4.57)$$

Therefore, in order to obtain this correlation function, we consider the second time-derivative of Eq. (4.54) and find

$$\begin{aligned} \frac{d^2}{dt^2} \langle (\Delta x)^2 \rangle &= -\frac{2}{B_0^2} \int_{-\infty}^{+\infty} dk'_{\parallel} \frac{d^2}{dt^2} F(k'_{\parallel}, t) k'_{\parallel}{}^{-2} \\ &\times \int d^3k P_{xx}(\vec{k}) \left[R_+(\vec{k}, k'_{\parallel}) + R_-(\vec{k}, k'_{\parallel}) \right]. \end{aligned} \quad (4.58)$$

For the parallel distribution function in Fourier space we can use (see, e.g., Shalchi (2020b))

$$F(k_{\parallel}, t) = \frac{1}{2\pi} \frac{1}{\omega_+ - \omega_-} [\omega_+ e^{\omega_- t} - \omega_- e^{\omega_+ t}] \quad (4.59)$$

where we have used the two parameters

$$\omega_{\pm} = -\frac{v}{2\lambda_{\parallel}} \pm \sqrt{\left(\frac{v}{2\lambda_{\parallel}}\right)^2 - \frac{1}{3} \left(v k_{\parallel}\right)^2}. \quad (4.60)$$

This result was derived from Eq. (4.17) by employing a two-dimensional subspace approximation. Alternatively, we can write Eq. (4.58) as

$$\begin{aligned} \frac{d^2}{dt^2} \langle (\Delta x)^2 \rangle &= \frac{1}{\pi B_0^2} \int_{-\infty}^{+\infty} dk'_{\parallel} \xi(k'_{\parallel}, t) \\ &\times \int d^3k P_{xx}(\vec{k}) \left[R_+(\vec{k}, k'_{\parallel}) + R_-(\vec{k}, k'_{\parallel}) \right] \end{aligned} \quad (4.61)$$

where now

$$\xi(k_{\parallel}, t) = \frac{v^2}{3} \frac{1}{\omega_+ - \omega_-} [\omega_+ e^{\omega_+ t} - \omega_- e^{\omega_- t}]. \quad (4.62)$$

The result derived above has to be understood as a generalized compound sub-diffusion approach where parallel transport is initially ballistic and becomes diffusive at later times. The magnetic field lines have similar properties in the sense that they are ballistic for short distances and become diffusive for larger distances. However, one important ingredient is missing in Eq. (4.61), namely the fact that particles no longer follow field lines as soon as the transverse complexity of the turbulence becomes important. We include the transverse complexity effect via a Gaussian and finally find the following differential equation

$$\begin{aligned} \frac{d^2}{dt^2} \langle (\Delta x)^2 \rangle &= \frac{1}{\pi B_0^2} \int_{-\infty}^{+\infty} dk_{\parallel} \xi(k_{\parallel}, t) \\ &\times \int d^3k P_{xx}(\vec{k}) \left[R_+(\vec{k}, k_{\parallel}') + R_-(\vec{k}, k_{\parallel}') \right] e^{-\frac{1}{2} \langle (\Delta x)^2 \rangle k_{\perp}^2}. \end{aligned} \quad (4.63)$$

Similar compared to the field line random walk equation (4.14), Eq. (4.63) corresponds to a second-order differential equation. However, Eq. (4.63) provides the perpendicular mean square displacement of particle orbits as a function of time t . The approach outlined above is called *Field-Line-Particle-Decorrelation (FLPD) theory* and was originally presented in Shalchi (2021b).

The theory described above is not very tractable analytically. A strong simplification can be achieved by using a diffusion approximation, meaning that we replace the particle mean square displacement on the right-hand-side of Eq. (4.63) by $\langle (\Delta x)^2 \rangle = 2\kappa_{\perp} t$. To continue we use this in Eq. (4.63) and time-integrate. After some algebra (see Shalchi (2021b) for details) we find

$$\begin{aligned} \kappa_{\perp} &= \frac{v^2}{6\pi B_0^2} \int_{-\infty}^{+\infty} dk_{\parallel}' \\ &\times \int d^3k P_{xx}(\vec{k}) \left[R_+(\vec{k}, k_{\parallel}') + R_-(\vec{k}, k_{\parallel}') \right] \\ &\times \frac{1}{v/\lambda_{\parallel} + v^2 k_{\parallel}'^2 / (3\kappa_{\perp} k_{\perp}^2) + \kappa_{\perp} k_{\perp}^2} \end{aligned} \quad (4.64)$$

which we call *diffusive FLPD theory*. Equation (4.63), on the other hand, is called *time-dependent FLPD theory*. One can show that for small Kubo number turbulence, Eq. (4.64) becomes equal compared to the so-called *Unified NonLinear Transport (UNLT) theory* developed in Shalchi (2010). For large Kubo number turbulence, on the other hand, a different result is obtained.

For the special case of two-dimensional turbulence, the components of the spectral tensor are given by

$$P_{nm}(\vec{k}) = g^{2D}(k_{\perp}) \frac{\delta(k_{\parallel})}{k_{\perp}} \left[\delta_{nm} - \frac{k_n k_m}{k_{\perp}^2} \right] \quad (4.65)$$

where $n, m = x, y$. All other tensor components are zero due to the fact that two-dimensional modes are incompressible. For the spectrum Shalchi and Weinhorst (2009) suggested to use the following form

$$g^{2D}(k_{\perp}) = \frac{2}{\pi} D(s, q) \delta B^2 \ell_{\perp} \frac{(k_{\perp} \ell_{\perp})^q}{[1 + (k_{\perp} \ell_{\perp})^2]^{(s+q)/2}}. \quad (4.66)$$

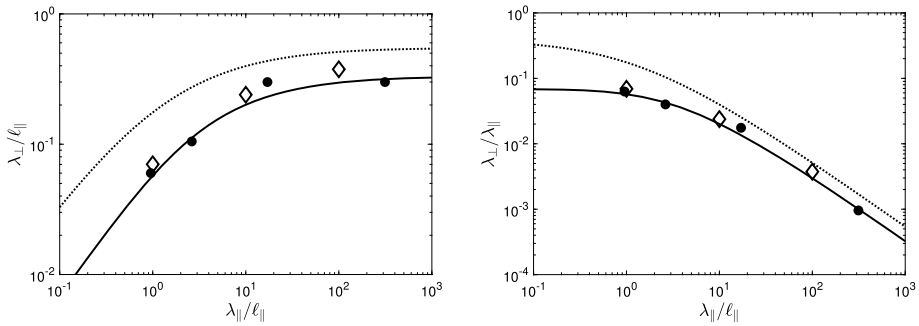


Fig. 28 Shown is a comparison of simulations with different analytical theories for slab/2D turbulence. The left panel shows the perpendicular mean free path versus the parallel mean free path and the right panel shows the ratio $\lambda_{\perp}/\lambda_{\parallel} \equiv \kappa_{\perp}/\kappa_{\parallel}$ versus the parallel mean free path. The solid lines correspond to the diffusive FLPD results as given by Eq. (4.68) and the dots represent the test-particle simulations published in Arendt and Shalchi (2020). The diamonds represent time-dependent FLPD theory as given by Eq. (4.63). For comparison we have also shown the NLGC/UNLT results without correction factor (see Eq. (4.69)), meaning that we have set $a^2 = 1$ (dotted lines). To obtain the visualized results the following parameter values have been used: $\delta B^2/B_0^2 = 1$, $\ell_{\perp} = \ell_{\parallel}$, $q = 3$, and a slab fraction of 20%

In the latter form we have used inertial and energy range spectral indexes s and q , respectively. The function $D(s, q)$ is due to normalization

$$D(s, q) = \frac{\Gamma\left(\frac{s+q}{2}\right)}{2\Gamma\left(\frac{s-1}{2}\right)\Gamma\left(\frac{q+1}{2}\right)}. \quad (4.67)$$

More details can be found elsewhere such as in Shalchi and Weinhorst (2009).

Using Eq. (4.65) in (4.64) yields

$$\kappa_{\perp} = \frac{\pi v^2}{3B_0^2} \int_0^{\infty} dk_{\perp} \frac{g^{2D}(k_{\perp})}{\frac{v\kappa_{FL}}{\sqrt{3}\kappa_{\perp}} k_{\perp} \sqrt{v/\lambda_{\parallel} + \kappa_{\perp} k_{\perp}^2} + v/\lambda_{\parallel} + \kappa_{\perp} k_{\perp}^2} \quad (4.68)$$

corresponding to diffusive FLPD theory for the case of two-dimensional turbulence. Analytical solutions of Eq. (4.68) have been discussed in Shalchi (2022).

Note, FLPD theory explicitly contains the field line diffusion coefficient κ_{FL} coming from the compound sub-diffusion phase of the transport. In the formal limit $\kappa_{FL} \rightarrow 0$, Eq. (4.68) would simplify to

$$\kappa_{\perp} = \frac{\pi v^2}{3B_0^2} \int_0^{\infty} dk_{\perp} \frac{g^{2D}(k_{\perp})}{v/\lambda_{\parallel} + \kappa_{\perp} k_{\perp}^2} \quad \text{for} \quad \kappa_{FL} \rightarrow 0. \quad (4.69)$$

This agrees with the two-dimensional limit of UNLT theory and the *nonlinear guiding center theory* (NLGC) developed by Matthaeus et al. (2003). However, the term with κ_{FL} in Eq. (4.68) significantly reduces the perpendicular diffusion coefficient and is, therefore, very important and must not be neglected (see, e.g., Fig. 28 of the current paper). In Table 1 we summarize the asymptotic limits contained in diffusive FLPD theory. For short parallel mean free paths and large Kubo numbers we find that particle transport is a combination of CLRR diffusion as given by Eq. (4.43) and the fluid limit given by Eq. (4.45) as demonstrated systematically in Shalchi (2022). This is a highly nonlinear regime where magnetic field

Table 1 Listed are the asymptotic limits contained in diffusive FLPD theory. The Kubo number is defined via Eq. (4.6) and the parallel mean free path λ_{\parallel} is an external parameter of the theory which needs to be provided. Usually λ_{\parallel} is obtained from simulations. The *hybrid regime* has to be understood as a mixture of CLRR (CollisionLess Rechester and Rosenbluth) and fluid limits. The reduced nonlinear FLRW limit is given by Eq. (4.72)

Parallel Mean Free Path	Kubo Number	Diffusive FLPD Theory
$\lambda_{\parallel}/\ell_{\parallel} \ll 1$	$K \ll 1$	CLRR Limit
$\lambda_{\parallel}/\ell_{\parallel} \gg 1$	$K \ll 1$	Classical FLRW Limit
$\lambda_{\parallel}/\ell_{\parallel} \ll 1$	$K \gg 1$	Hybrid Regime
$\lambda_{\parallel}/\ell_{\parallel} \gg 1$	$K \gg 1$	Reduced Nonlinear FLRW Limit

lines show nonlinear behavior and perpendicular transport is strongly influenced by parallel transport. For long parallel mean free paths and large Kubo numbers, on the other hand, we find a reduced FLRW limit where the field lines are still in the highly nonlinear regime. This limit can quickly be derived from Eq. (4.68). In the formal limit $\lambda_{\parallel} \rightarrow \infty$, the latter formula simplifies to

$$\kappa_{\perp} = \frac{v^2}{3(v\kappa_{FL}/\sqrt{3} + \kappa_{\perp})} \frac{\pi}{B_0^2} \int_0^{\infty} dk_{\perp} g^{2D}(k_{\perp}) k_{\perp}^{-2}. \quad (4.70)$$

The second factor therein, together with the integral, corresponds to the two-dimensional field line diffusion coefficient squared and, thus, we can write

$$\kappa_{\perp} = \frac{v^2}{3} \frac{\kappa_{FL}^2}{v\kappa_{FL}/\sqrt{3} + \kappa_{\perp}}. \quad (4.71)$$

The latter equation corresponds to a quadratic equation for κ_{\perp} which has a single physical solution and that is

$$\kappa_{\perp} = \frac{\sqrt{5}-1}{\sqrt{3}} \frac{v}{2} \kappa_{FL} \approx 0.71 \frac{v}{2} \kappa_{FL} \quad (4.72)$$

corresponding to a reduced field line random walk limit (compare with Eq. (4.33) of the current paper). The two limits obtained for small Kubo numbers are as described by diffusive UNLT theory as discussed in Shalchi (2015b) and Shalchi (2020b).

In Fig. 28 we show a comparison between different analytical theories and simulations for two-component turbulence. In previous work there was only agreement between theories and simulations if a correction factor, commonly called a^2 , was introduced and if this was assumed to be $a^2 = 1/3$. FLPD theory, on the other hand, agrees with simulations without the need of this factor nor does the theory contain any other free parameter.

4.4 Solar Energetic Particles and Transition to Diffusion

Solar energetic particles (SEPs) have provided an interesting testbed for understanding charged particle propagation in turbulent magnetic fields. As analyzed from the SEP observations, the parallel mean free path within the inner heliosphere is often considered to have the so-called Palmer consensus range of values from 0.01 to 0.3 au (Palmer 1982), with also considerably longer parallel mean free paths inferred (e.g. Torsti et al. 2004). As

most SEP events are observed with in situ instruments on spacecraft at distances less than 1 au, the transport of the observed SEPs, particularly the first-arriving SEPs is not necessarily diffusive or ballistic, which complicates analysis of SEP events.

Until recently, SEP transport has mostly been considered from the perspective of transport along the mean magnetic field, as the cross-field transport due to turbulence was considered negligible (e.g. Palmer 1982). This paradigm was challenged particularly by SEP events that were observed simultaneously with multiple spacecraft at large heliolongitudinal separation (e.g. Dresing et al. 2012). Models with the Fokker-Planck equation containing diffusion in velocity space, and spatial guiding centre diffusion across the mean field, have been extensively used to analyse the possible consequences of SEP transport in the inner heliosphere (e.g. Zhang et al. 2003; Dröge et al. 2010; He et al. 2011; Qin et al. 2013; Strauss and Fichtner 2015; Strauss et al. 2017).

4.4.1 Diffusion Description and First-Arriving Particles

The goal of analysis of SEP observations is often to deduce their source at or near the Sun, which predicates the necessity to understand the arrival of the first particles to the in situ instruments in the interplanetary space. However, spatial diffusion as a description is not physical for the first particles arriving at a distance from their source. This can be seen by inspecting the solution of a simple diffusion-convection equation for density $n(x, z, t)$ of particles propagating with velocity v along the z -axis while diffusing with diffusion coefficient κ along x -axis,

$$\frac{\partial n(x, z, t)}{\partial t} + v \frac{\partial n(x, z, t)}{\partial z} = \kappa \frac{\partial^2 n(x, z, t)}{\partial x^2}. \quad (4.73)$$

The solution to this equation, for an impulsive injection $n_0(x, z, t) = \delta(t)\delta(x)\delta(z)$, is given as

$$n(x, z, t) = \frac{n_0(0, z - vt, 0)}{2\sqrt{\pi\kappa t}} e^{-x^2/(4\kappa t)}. \quad (4.74)$$

As can be seen in Eq. (4.74), the velocity v of the particles only features in the distribution along the z -axis. In the direction of spatial diffusion (here along the x -axis, normal to the direction of convection), the solution is finite everywhere for any $t > 0$ for any non-zero diffusion coefficient κ . This clearly violates causality, which, for the given initial conditions, can be written as

$$n(x, z, t) \Big|_{\sqrt{x^2+z^2} > vt} = 0. \quad (4.75)$$

This causal limitation is outlined also in Chandrasekhar (1943), and reported in SEP simulations by Strauss and Fichtner (2015).

The causality problem has been recently addressed by several authors. Pei et al. (2006), Laitinen and Dalla (2019), Moradi and Li (2019) and Chhiber et al. (2021) analysed the lengthening of the path due to field-line random walk, with the goal to understand the delay caused by field-line random walk to the arrival of the first SEPs to the in-situ instruments in the interplanetary space. van den Berg et al. (2021) and Strauss et al. (2023) used essentially the same concept to derive a streaming-reduction factor for the streaming velocity. Chhiber et al. (2021), van den Berg et al. (2021) and Strauss et al. (2023) arrive to the same

solution for the effect of turbulence on the path length s or particle velocity v , compared to undisturbed path length s_0 or v_0 , as

$$\frac{s}{s_0} \sim \frac{v_0}{v} \sim \sqrt{1 + a \frac{\delta B^2}{B^2}},$$

for $\delta B^2 \ll B^2$, with the free parameter a depending on turbulence geometry for Chhiber et al. (2021) and considered as probability of the particle to follow the field line for Strauss et al. (2023). Unlike the other three studies, Laitinen and Dalla (2019) considered the random-walk as stochastic process, and derived the mean lengthening of the path as a mean of Wiener process as

$$\frac{s}{s_0} = 1 + a \frac{\delta B^2}{B^2},$$

where $a = [0, 1]$ is a geometric factor.

While the studies discussed above have shown some success in estimating the effect of field-line random walk on the first-arriving SEPs, it should be noted that the fundamental issue posed by spatial diffusion remains: The solution of Eq. (4.74) fails to fulfill the condition given by Eq. (4.75) for any non-zero v and κ .

4.4.2 Decoupling of SEPs from Turbulent Field Lines

An important question for the SEP transport in the inner heliosphere is whether they have had sufficient time to decouple from the random-walking field lines to become fully diffusive with respect to the mean magnetic field direction. As discussed above, the parallel mean free path of the SEPs can be a substantial fraction of the distance between the source and observer. Thus, a significant portion of the particles may have not scattered considerably. While the bulk properties of the particles might follow the diffusive behaviour, the first SEPs to arrive to the observer may still be following the random-walking field lines, rather than diffusing freely in space guided by the field-line random walk.

The behaviour of simulated particles analysed at fixed locations in space as opposed to analysed as the bulk reveals interesting details on the physics of SEP propagation in turbulent magnetic fields. Laitinen et al. (2013) analysed full-orbit simulated SEPs at 1 au from the particle source $Q = \delta(t)\delta(x)\delta(y)\delta(z)\delta(1 - \mu)$, in magnetic field configuration

$$\vec{B}(x, y, z) = B_0 \hat{z} + \delta \vec{B}(x, y, z)$$

with the magnetic fluctuations $\delta \vec{B}(x, y, z)$ defined as the often-used slab/2D composite model of turbulence (e.g. Giacalone and Jokipii 1999). The variance of particles along x -axis at $z = 1$ au is shown in Fig. 29 with the black curve. As can be seen, the evolution of the variance is characterised by a constant value for the first 10 hours, followed by a gradual transition towards a linear trend consistent of diffusive evolution. The constant value is at $\sigma^2(z = 1 \text{ au}) = 130 r_\odot^2$, consistent to that of the variance of the random-walking field lines, $\sigma_{FL}^2 = 2\kappa_{FL}z$, where $\kappa_{FL} = 2.1 \times 10^{10} \text{ cm}^2 \text{ s}^{-1}$ was obtained from the magnetic field configuration used in the simulations.

To compare the full-orbit simulations against diffusion-convection approach to particle transport, Laitinen et al. (2013) solved the variance at 1 au for a Fokker-Planck equation with pitch-angle and cross-field diffusion, with the diffusion coefficients obtained from the full-orbit particle simulations. As can be seen with the dashed red curve in Fig. 29, the variance

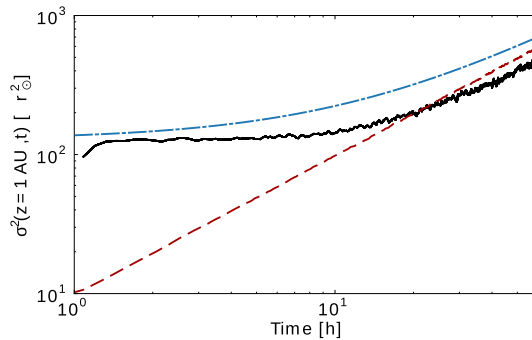
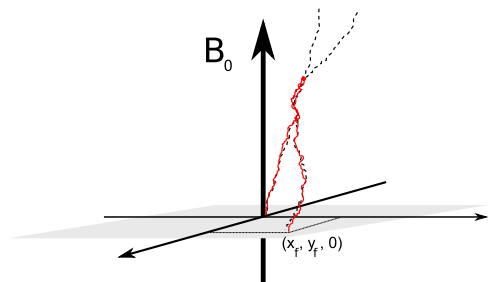


Fig. 29 Variance of particles along x -axis at $z = 1$ au, with z -axis along the background magnetic field, and particle source $Q = \delta(t)\delta(x)\delta(y)\delta(z)(1 - \mu)$. Black curve shows the variance obtained with full 3D simulations, whereas the dashed red curve shows the variance obtained with Fokker-Planck equation. The dash-dotted blue curve shows the variance consistent of diffusing population with initial Gaussian shape

Fig. 30 The scheme for analysing the decoupling of the particles from their initial field lines. The particles are injected at a given location (x_o, y_o, z_o) , and recorded when they next return to the original coordinate $z_f = z_o$ along the mean field, in z -direction



obtained with the Fokker-Planck equation shows a continuous linear trend in variance from the arrival of the first particles at $t = 1$ hr. Thus, the results of Laitinen et al. (2013) would seem to indicate that the diffusion description is not a valid description for SEPs in the early stages of an SEP event: rather, the SEPs, when arriving to 1 au, are still in the ballistic phase of their propagation, propagating deterministically along the stochastically-random walking field lines.

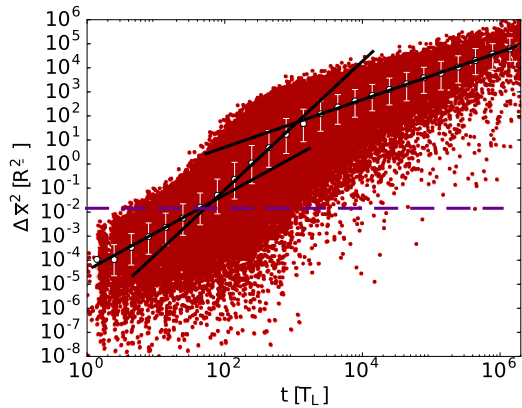
The second implication that can be drawn from the results of Laitinen et al. (2013) is the long duration of nearly constant $\sigma_x(z = 1 \text{ au})$ seen in Fig. 29. If we assume that the particles arrive at 1 au along random-walking field lines, but also diffuse with respect to these field lines, one would expect that the variance would be increasing linearly as

$$\sigma_x(z = 1 \text{ au})^2 = 2\kappa_{FL} z + 2\kappa_{\perp} t.$$

We have included this variance in Fig. 29 as the blue dash-dotted curve. As can be seen, the blue curve clearly deviates from the variance obtained from the full-orbit simulations. This deviation implies that the particles remain on their random-walking field lines for considerable time: only at long timescales can the cross-field propagation be considered diffusive.

The question of the decoupling of particles from random walking field lines was further investigated in Laitinen and Dalla (2017), where the simulation setup, again using 3D full-orbit test-particle simulations, allowed specifically to investigate the cross-field propagation of particles from their original field line. In the scheme, depicted in Fig. 30, the cross-field deviation of each particle from their original field line is recorded when the particle returns

Fig. 31 Deviation of 10 MeV protons in turbulent magnetic field. The Larmor radius of the protons is $0.13r_\odot$. The white symbols depict the median of deviations within a time range, and the error bars the upper and lower quartiles. The trends at short, intermediate and long timescales are shown with solid black curves



to the same location along the mean field, in the z -direction. In this way, a particle remaining coupled to its original random-walking field-line would deviate maximum 2 Larmor radii from its initial position.

Figure 31 depicts typical behaviour of the deviation in x -direction investigated in Laitinen and Dalla (2017). The scatter-plot (red circles) shows the square of the deviations for a simulation run of 10 MeV protons with $\delta B^2/B^2 = 0.316$ and slab fraction of 20%, as a function of a Larmor period T_L . The white symbols show the median deviations as a function of time, with the error bars showing the upper and lower quartiles, and the purple dashed curve shows the Larmor radius scale.

As can be seen, the evolution of the cross-field deviation of the particles can be divided into three timescales. At short timescales, the median deviation increases slightly superdiffusively, with $\Delta x^2 \propto x^\alpha$ where α varies between 1 and 2, depending on turbulence amplitude (Laitinen and Dalla 2017). When the median deviation reaches the Larmor radius scales, at $t \sim \tau_\parallel$, the parallel scattering time scale, the population begins to spread with increased superdiffusivity, with α between 3 and 4, until at $t \sim 10\tau_\parallel$ diffusive trend is reached (Laitinen and Dalla 2017).

To understand when the delayed decoupling of particles from their field lines causes the initially-wide, asymptotically diffusive SEP cross-field spread, as seen in Fig. 29, we must uncover what causes the three-phase evolution of the cross-field deviation shown in Fig. 31. Some recent research does provide suggestions for the reason of the uncovered behaviour of the particle deviations. Fraschetti and Jokipii (2011) investigated how particles propagate across the mean field due to stochastic drifts present in the fluctuating fields, as opposed to following random-walking field lines. The stochastic drifts can be considered as a mechanism that is responsible for the decoupling of particles from field lines. The trends due to the stochastic drift mechanism on the cross-field deviation of particles are shown in Fig. 32 with the magenta lines for isotropic (dashed curve) and slab-dominated (solid curve) turbulence, along with the deviations measured in the simulations with 2D-dominated (20% slab contribution, green symbols) and slab-dominated (99% slab contribution, blue symbols) (Laitinen and Dalla 2017).

As can be seen in Fig. 32, the simulations replicate the sub-diffusive Fraschetti and Jokipii (2011) slab trend well, whereas the 2D-dominated simulations show stronger tendency to superdiffusion, somewhat inconsistent with the Fraschetti and Jokipii (2011) result. However, the discrepancy may be caused by the use of different turbulence model (isotropic in Fraschetti and Jokipii (2011) as opposed to slab/2D composite model in Laitinen and Dalla (2017)).

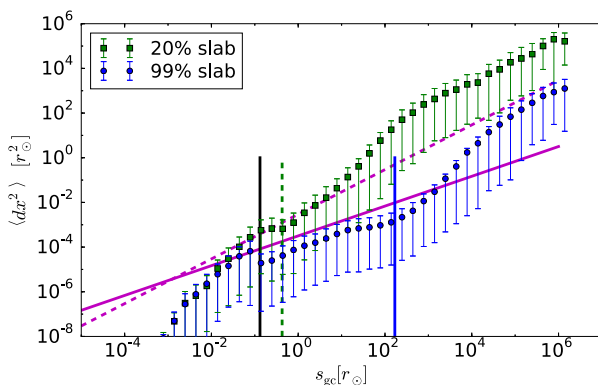


Fig. 32 The deviation of 10 MeV protons in 2D-dominated (green) and slab-dominated (blue) turbulence, as a function of the distance the particles have traveled. The dashed and solid magenta lines show the Frascchetti and Jokipii (2011) solutions for diffusion due to stochastic drifts for isotropic and slab turbulence models, respectively, and the dashed green and solid blue vertical lines the scale where neighbouring field lines separate exponentially, as derived by Ruffolo et al. (2004). The vertical black line shows the Larmor radius scale

The next crucial phase is the superdiffusive spreading of particles, which indicates the initiation of the decoupling of particles from their field lines. Laitinen and Dalla (2017) simulations suggested that the superdiffusive spreading starts when the median deviation of the particles reaches the particle Larmor radius scale. It could be thought then that the separation requires the particle to effectively drift away from its initial field line. The timescale for this separation then would be related to the slightly superdiffusive increase of the deviation during the first phase. This timescale concept is similar in heuristics as that suggested by Bieber and Matthaeus (1997), and also the suggestions where the relevant lengthscale would be the correlation scale as in Eq. (4.42). However the latter works relate the timescale to fieldline random walk, whereas the Laitinen and Dalla (2017) work suggest dependence only on the Larmor radius scale.

Another possible explanation for the decoupling comes from the similarity of the onset timescale of the superdiffusive phase with the parallel scattering timescale in 2D-dominated turbulence, reported by Laitinen and Dalla (2017). If we consider the parallel scattering as distinct “events”, it could be thought that the particle’s gyrocentre is scattered as well as the particles velocity along the magnetic field. However, scattering cannot be the sole reason for the decoupling of the particles from their field lines: in the simulation scheme used by Laitinen and Dalla (2017), all recorded particles scattered back, as per design. The scattering timescale, however, does imply a timescale where large changes in the (pitch-angle-dependent) gyroradius of the particles take place, which may in it self imply larger probability for the particle to decouple from its initial field line. As a caveat for the potential significance of the parallel scattering timescale, it should be noted that Laitinen and Dalla (2017) report much longer decoupling timescale in slab-dominated turbulence, of order $20\tau_{\parallel}$.

The decoupling could also be explained to be caused by the separation of the fieldlines themselves. Ruffolo et al. (2004) investigated the rate at which two neighbouring field lines separate. They found that neighbouring field lines separate initially slowly, until at length scales

$$\ell_g = \frac{\ell_c}{2} \frac{f_{sl}}{1 - f_{sl}}$$

where ℓ_c is the turbulence correlation scale and f_{sl} the slab fraction of the turbulence (in terms of turbulence variance), the field lines separate exponentially to reach the long-distance limit that is consistent with field-line random walk.

We show ℓ_g for the 2D- and slab-dominated cases in Fig. 32 with the dashed green and solid blue vertical curves, respectively. As can be seen, the slab ℓ_g coincides well with turnover to super-diffusive spreading seen in the simulations (blue symbols). However, ℓ_g doesn't seem to be consistent with the 2D simulated case (green symbols).

The final, time-asymptotic phase of the evolution of the cross-field deviation of the particles to diffusive trend, is more readily understandable. Whatever the process that decouples the particle from its original field line, at timescale τ_d , will take place again at that timescale, however stochastically, and this stochasticity will give rise to diffusive behaviour akin to that of the field lines.

4.5 Summary of Section 4

Over the years we have developed a more complete understanding of the physics of perpendicular transport. There is overall good agreement between simulations, heuristic arguments, and analytical theory (see, e.g., Figs. 27 and 28). This is in particular the case for two-component turbulence which is often used to approximate solar wind turbulence. Time-dependent FLDP theory contains initial ballistic, intermediate sub-diffusive, as well as final diffusive regimes. When normal diffusion is established, the analytical form of the perpendicular diffusion coefficient depends on the parallel mean free paths as well as the Kubo number (see Table 1 for more details).

Significant progress has been achieved in the theory of particle transport across the mean magnetic field (see Shalchi 2020b for a review, but also Shalchi 2021b). This concerns heuristic arguments as well as systematic analytical theory. Furthermore, detailed test-particle simulations can be performed for realistic turbulence models. FLDP theory shows remarkable agreement with simulations for the slab/2D model. Of course, the question arises whether FLDP theory is always correct and accurate. Furthermore, FLDP theory contains the field line diffusion coefficient (see, e.g., Eqs. (4.55), (4.63), and (4.64)). To date, it is unclear which field line diffusion coefficient has to be used for slab/2D turbulence. Is it the total diffusion coefficient found in this type of turbulence model or is it the field line diffusion coefficient associated with the two-dimensional modes? This problem does not occur in three-dimensional single mode turbulence where there is only one field line diffusion coefficient.

Although we presented, in the context of SEPs, some ideas on what can contribute to the decoupling of particles from their field lines, we do not have a complete understanding of how to model the initial phases of an SEP event. Laitinen et al. (2016) modelled the SEP transport as diffusion from random-walking paths instead of the mean field. While this produces a reasonable estimate for the process, it ignores the initial slow phase of the particle decoupling from the random-walking field lines. An improvement could be to consider a timescale, a finite “memory” for the particles of their past path. However, whether such a model would be mathematically tractable is a wholly different issue.

5 Insights from Full-Orbit Test Particle Simulations in Synthetic and MHD Turbulence

Understanding the influence of plasma turbulence on the propagation of fast charged particles, such as cosmic rays, is a fundamental challenge for heliophysics and astrophysics. As

already indicated in the previous chapters, studies of full-orbit particle tracing in synthetic or MHD turbulence can inform the transport regimes and coefficients of charged particle transport, which is often assumed to be diffusive. However, turbulence that exhibits non-Gaussian and non-local structures may also lead to non-diffusive transport behaviour. In this chapter, we will summarize some of the challenges associated with the full-orbit approach in synthetic turbulence and discuss features that arise when non-Gaussian structures are considered.

Cosmic ray (CR) transport characteristics depend on the efficiency and mechanism of their scattering in turbulent magnetic-fields. The correlation length ℓ of the turbulent cascade (Batchelor 1953) with energy spectrum $P(k)$ introduces several distinct transport regimes. CRs with $r_g \gg \ell$ undergo scattering by small angles of the order $\sim \ell/r_g$, leading to their diffusion coefficient scaling as $\kappa \propto E^2$ (Subedi et al. 2017), as observed in numerical simulations and laboratory experiments (Chen et al. 2020). We do not have a complete understanding of CR transport in the regime $r_g \lesssim \ell$, as the nature of the pitch-angle scattering mechanism is complex, with theories including “extrinsic” (cascading) and “intrinsic” (generated in kinetic instabilities) turbulence (see, e.g. Kempfski and Quataert (2022) and Hopkins et al. (2022) for recent overviews). Observations of this regime suggest, however, that $\kappa \propto E^\delta \propto r_g^\delta$ with $0.3 \lesssim \delta \lesssim 0.5$ (see Becker Tjus and Merten (2020) for a review).

Initially, Alfvénic turbulence was favored to explain these observations. However, subsequent studies argued for inefficient gyroresonance scattering in this scenario due to damping (Skilling 1975b; Hopkins et al. 2022), intermittency (Shukurov et al. 2017) and scale-dependent anisotropy (see, e.g., Goldreich and Sridhar 1995; Chandran 2000; Lithwick and Goldreich 2001; Cho and Vishniac 2000; Maron and Goldreich 2001; Cho and Lazarian 2003; Boldyrev 2006; Mason et al. 2006 and Schekochihin 2022 for a review), making fast MHD modes more attractive (Yan and Lazarian 2002) because they are believed to have an isotropic cascade (Cho and Lazarian 2002). Assuming an undamped, isotropic turbulent cascade, quasi-linear theory (QLT; Jokipii 1966) relates the parallel energy spectrum $P(k) \propto k_\parallel^\gamma$ to the CR diffusion coefficients scaling as $\kappa \propto E^{2-\gamma}$, consistent with observations in case of Kolmogorov ($\gamma = 5/3$; Kolmogorov 1941) and Iroshnikov-Kraichnan ($\gamma = 3/2$; Iroshnikov 1964; Kraichnan 1965) turbulence. The underlying assumption of QLT is that the mean free path $\lambda \sim \kappa/c \sim r_g/f(r_g)$ is determined by the fraction of the turbulent power located at gyroresonant scales, $f(r_g) = \int_{2\pi/r_g}^\infty dk P(k)/B^2 \leq 1$. In contrast to the approach adopted in QLT, CR pitch-angle changes could be introduced intermittently at sharp field bends with large curvature (Lemoine 2023; Kempfski et al. 2023; Malara et al. 2023). In this context, $f(r_g) \leq 1$ is determined by the volume-filling fraction of sharp field bends capable of scattering CRs, which requires additional characterization of the turbulent magnetic field beyond just the energy spectrum $P(k)$, such as the distribution of field line curvature. An even more efficient scattering mechanism is postulated in the theory of Bohm diffusion, with mean free paths of the order of the gyroradii, assuming a maximum volume-filling fraction $f \approx 1$ of scatter centers. Because of its small mean free paths and efficiency in isotropizing particles, this type of transport is often employed in acceleration models (Bell 2004; Blasi 2013; Brunetti and Jones 2014). It is important to note that acceleration models have limited predictability without a proper understanding of diffusion characteristics.

In addition to the impact of fluctuations on resonant scales, large-scale fluctuations, where most of the turbulent energy is stored, shape magnetic-field lines and large-scale magnetic mirrors that contribute to diffusivity (Felice and Kulsrud 2001; Beresnyak et al. 2011; Barreto-Mota et al. 2025). Large-scale fluctuations also introduce localized roughly ordered field lines, extending the applicability of QLT scaling results to the context of isotropic turbulence without a global guide field (Giacalone and Jokipii 1999; Subedi et al. 2017;

Dundovic et al. 2020; Reichherzer et al. 2022b; Kuhlen et al. 2022; Pezzi and Blasi 2023). Furthermore, in high-beta plasmas, kinetic instabilities grow thermal Larmor-scale magnetic fluctuations that introduce another small-angle scattering transport regime. In galaxy clusters, this may affect CRs up to TeV energies (Reichherzer et al. 2025; Ewart et al. 2024).

5.1 Issues with Current Full-Orbit Synthetic Models

Integrating particle trajectories through magnetic fields by solving the equation of motion can be achieved efficiently with various different numerical schemes. It has been shown that the statistical transport properties, such as the diffusion coefficient, converge for different schemes towards small step sizes for a given magnetic field snapshot.

While the numerical integration schemes are robust, there are various challenges in modelling realistic astrophysical turbulence. Most synthetic fields used in the astrophysical community are characterized by only the following few key properties.

1. The root mean squared strength $\delta B = \sqrt{\langle \delta \vec{B}^2(\vec{r}) \rangle}$. Typical values are $\delta B \sim 1 \mu\text{G}$ for the interstellar medium (ISM) and intracluster medium (ICM) (Govoni et al. 2017).
2. The distribution of magnetic energy $E(k)$, typically defined by a power-law in Fourier space, i.e.

$$E(k) = \frac{\delta B^2}{8\pi} k^{-\alpha} \frac{(\alpha - 1) k_{\min}^{\alpha-1}}{1 - (k_{\max}/k_{\min})^{\alpha-1}}, \quad (5.1)$$

between the injection wavenumber $k_{\min} = 2\pi/l_{\min}$ and the dissipation scale $k_{\max} = 2\pi/l_{\max}$. The correlation length indicates the scale over which the magnetic field varies and is defined as (Harari et al. 2015),

$$l_c = \frac{8\pi^2}{\delta B^2} \int_0^\infty \frac{dk}{k} E(k) = \frac{l_{\max}}{2} \frac{\alpha - 1}{\alpha} \frac{1 - (l_{\min}/l_{\max})^\alpha}{1 - (l_{\min}/l_{\max})^{\alpha-1}}. \quad (5.2)$$

Typical values are $l_{\max} \sim 10 \text{ pc}$ and $l_{\max} \sim 100 \text{ kpc}$ in the ISM and ICM (Kunz et al. 2022) respectively. In the heliosphere, typical values for l_{\max} will be of the order of the solar radius or smaller.

3. Different models and geometries of turbulence are employed in the theoretical and numerical modelling of astrophysical systems. Geometries range from one-dimensional (1D) to three-dimensional (3D) structures, with diverse theoretical frameworks like those developed by Kolmogorov, Kraichnan, Goldreich & Sridhar providing insights into their characteristics.
4. In astrophysical studies of CRs in synthetic turbulence, the probability density function (PDF) of turbulence is often assumed to be Gaussian without intermittency. Recent studies showed that intermittency is an important ingredient for realistic CR transport.

These properties comes with challenges that are discussed below.

5.1.1 Achieving Large Inertial Ranges

Realistic modelling of astrophysical turbulence over a wide range of wavelengths is crucial for studying regimes in astrophysical environments. Since current magnetohydrodynamic and particle-in-cell simulations only allow for limited energy ranges, synthetic magnetostatic turbulence models are often employed in astrophysical models (Mertsch 2020, see also Sect. 4.3.1).

The generation of synthetic magnetic turbulence with these characteristics used for CR studies is performed in the literature via (nested) grid and grid-less methods.

Grid Method The turbulent magnetic field vectors $\delta \vec{B}(\vec{r})$ are stored on a discrete grid with N^3 grid points (in 3D) with spacing s_s and a total grid box side length of $N \cdot s_s$. The sampling theorem constraints the fluctuations that fit into the grid box

$$l_{\min} \geq 2s_s, \quad l_{\max} \leq N \cdot s_s. \quad (5.3)$$

Thus, the inertial range is severely limited by the number of grid points N^3 that can be stored in the memory: $l_{\max}/l_{\min} \leq N$.

Nested-Grids Method To create larger inertial ranges of the turbulence cascade, nested grids are proposed in Giacinti et al. (2012). Individual grids with different dynamical ranges $l_{\min,i} - l_{\max,i}$ are combined to construct a larger dynamical range. In this approach, δB_i of each small interval between l_i and l_{i+1} is defined as

$$\delta B_i^2 = \delta B^2 \frac{l_{\max,i}^{\alpha-1} - l_{\min,i}^{\alpha-1}}{l_{\max}^{\alpha-1} - l_{\min}^{\alpha-1}}. \quad (5.4)$$

Continuation (usually periodically) of the individual grid boxes populates the entire spatial simulation volume with synthetic turbulence. An example of this is shown in Fig. 33.

Grid methods have the advantage of only interpolating the magnetic field at a desired location in each simulation step due to prior initialization on a discrete grid. This leads to fast calculation of particle trajectories but comes with the disadvantage that interpolation violates the divergence freedom of the magnetic field. Additionally, grids must be continued to prescribe the magnetic field in the entire simulation volume, causing the magnetic field structure to repeat itself on scales dictated by individual box sizes. This can result in numerical artefacts, which can be minimized by choosing smaller dynamical ranges than allowed by the sampling theorem and introducing a padding factor f_{pad} (Mertsch 2020). Specifically, $2f_{\text{pad}}s_s \lesssim l_{\min}$ and $l_{\max} \lesssim Ns_s/f_{\text{pad}}$. The grid sizes and fluctuation ranges of individual parts of the turbulence cascade are constrained by memory size and the padding factor.

Gridless Method Gridless methods sum over predefined plane waves at any arbitrary position \vec{r} via

$$\delta \vec{B}(\vec{r}) = \text{Re} \left(\sum_{n=0}^{N-1} \delta B_n^* e^{i\vec{k}_n \cdot \vec{r}} \right), \quad (5.5)$$

where the wavevectors are denoted by \vec{k}_n . Instead of precomputing and storing the turbulence on a discrete grid, the magnetic field vector can be computed at an arbitrary particle position r via

$$\delta \vec{B}(\vec{r}) = \sqrt{2} \delta B \sum_{n=1}^{n_m} \vec{\xi}_n A_n \cos \left(k_n \hat{k}_n \cdot \vec{r} + \beta_n \right), \quad (5.6)$$

with amplitudes A_n determined by the turbulence power spectrum as well as uniformly distributed phase factors β_n $[0, 2\pi[$, unit wavevectors \hat{k}_n , polarizations $\vec{\xi}_n$ satisfying $\hat{k}_n \cdot \vec{\xi}_n = 0$. By analyzing the turbulence's statistical properties and CR transport characteristics for

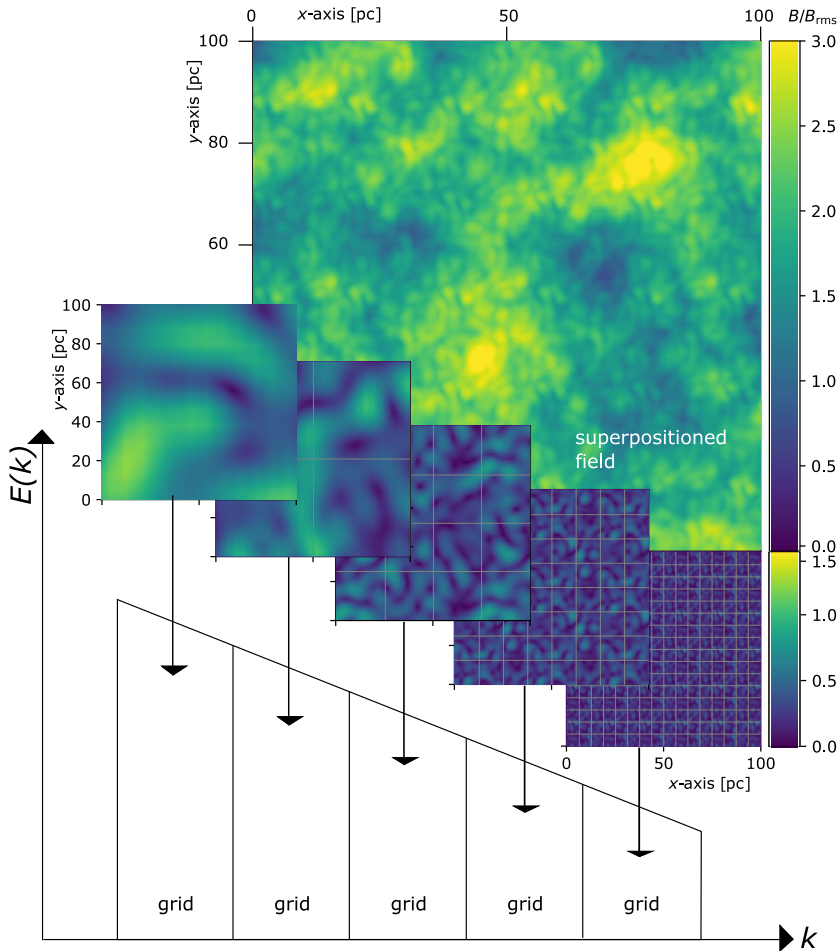


Fig. 33 Energy spectrum of combined turbulence and example magnetic-field slice plots in the simulation space of each part of the turbulent cascade. Superposition of the small slice plots of the periodically continued (boxes are separated by white bars) subgrids results in the large slice plot of the total field with a large inertial range. For visual purposes, the inertial range is chosen to be small with $l_{max}/l_{min} = 2$ for each subgrid. The padding factor $f_{pad} = 2$ results in only each third box being identical

different modes, Schlegel et al. (2020) conclude that 10 log-spaced wavemode decades of inertial range are sufficient.

We proceed with comparing the different approaches to generate large inertial ranges. To avoid issues with periodic continuation of tiny boxes and potential interpolation issues within the largest fields, we choose gridless turbulence at large and small scales. Within the central part of the inertial range, we use either gridless turbulence or nested grids. Figure 34 compares the structure functions S_2 for both models using different values for the wave modes and the padding. Panels a) and b) show the deviation from the theoretically expected structure function for Kolmogorov turbulence using the complete gridless and the combination of nested-grids and gridless turbulence, respectively. The analysis in the lower

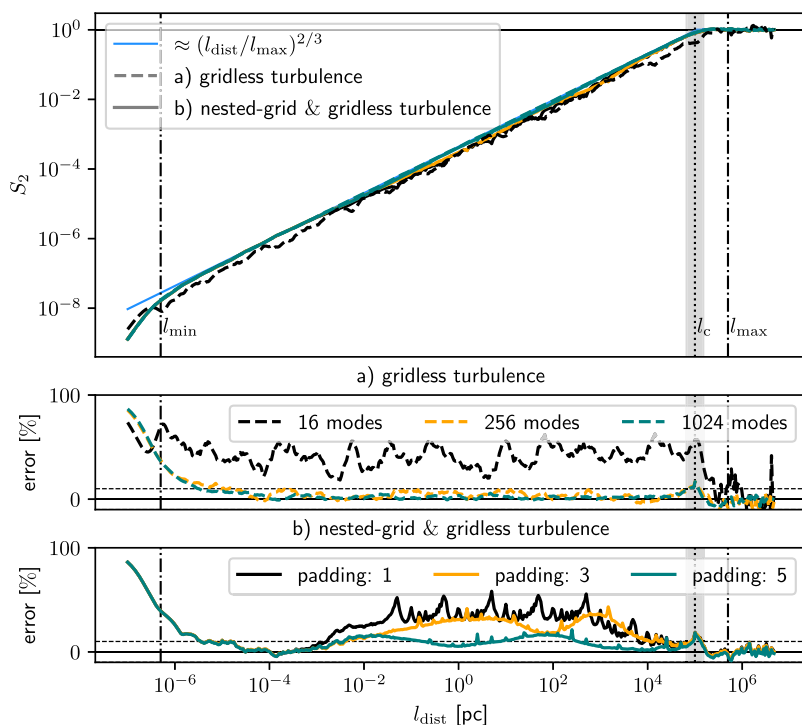


Fig. 34 Structure functions S_2 of different realizations and parameter combinations including panels a) and b) that show the deviation from theory prediction for Kolmogorov turbulence

panels reveals convergence towards theory with an increasing number of wave modes and large padding of nested grids.

5.1.2 Intermittency

Studying trajectories of particles in static snapshots of MHD-generated turbulence reveals anomalous transport properties, notably in disagreement with results obtained for the random-phase turbulence model underlying QLT (Shukurov et al. 2017; Lübke et al. 2024), such as superdiffusive transport in coherent structures and subdiffusion due to confinement in large-scale magnetic mirrors. The role of coherent structures in fast particle transport is discussed by Shukurov et al. (2017) and superdiffusive behavior is investigated by Hu et al. (2022). The role of magnetic mirrors in MHD turbulence is mentioned in Beresnyak et al. (2011) and further discussed by Lazarian and Xu (2021) and Zhang and Xu (2023), however a conclusive understanding of the role of magnetic mirrors in anomalous particle transport remains to be achieved, which is in part certainly due to the complicated nature of turbulent structures at work. Further, it was recently pointed out by Lemoine (2023) and Kempfski et al. (2023) that scattering occurs mainly due to sharp fieldline bends, which exhibit a distribution different from the usually employed models for magnetic turbulence. How CR transport is shaped by coherent structures and intermittent scattering in a turbulent dynamo without a mean field was recently explored by Lübke et al. (2025).

These properties are illustrated in Fig. 35 and noticeably affect the time-dependent transport behavior, as shown in Fig. 36, where particles in MHD turbulence exhibit an extended

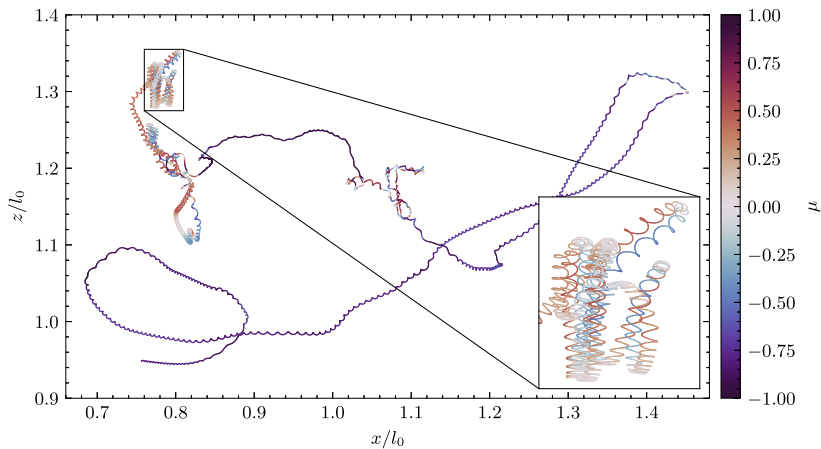


Fig. 35 Example trajectory of a charged particle with $r_g/l_0 = 0.004$ in isotropic MHD turbulence. The trajectory is color-coded by its instantaneous pitch-angle cosine $\mu = \cos \theta$. Notable are three distinct modes of transport: extensive fieldline wandering with mean free paths $\sim \mathcal{O}(l_0)$, sudden localized scattering events due to sharp magnetic fieldline bends, and localized confinement in magnetic bottles (highlighted in the inset)

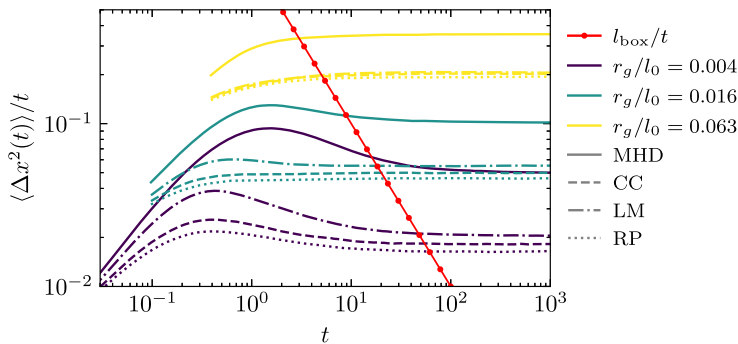


Fig. 36 Comparing the running mean squared displacements of different models for synthetic turbulence at three different particle gyroradii r_g . The red line indicates when the mean squared displacement crosses the size of the computational box with periodic boundaries. The MHD case is characterized by a pronounced bump due to superdiffusion along coherent structures, which dominates at early times, followed by transient subdiffusion due to long mirror confinement, before finally setting in diffusive equilibrium. Simple coherent structures introduced by the LM method reproduce this behavior somewhat at small particle gyroradii, and simple intermittent fields produced by the CC method closely resembles the well-known Gaussian RP method with only slightly increased diffusion

superdiffusive phase, followed by a transient subdiffusive phase, especially for low energy particles and small gyroradii, before settling in asymptotic diffusive behavior, which results from particles running repeatedly over the same periodic simulation box. Asymptotic diffusion coefficients obtained from MHD turbulence and several synthetic models, including the usual Gaussian random phases model, are shown in Fig. 37, which substantiates the overemphasis of random scattering in synthetic models. Note that these results account for differences in the spectra by also comparing the respective randomized-phase fields as shown in Lübke et al. (2024). The super- and subdiffusive transport characteristics can potentially be

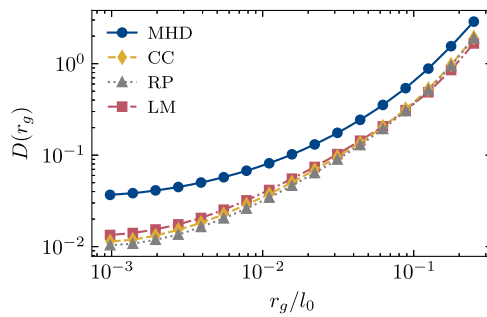


Fig. 37 Converged diffusion coefficients for charged test particles in different models for magnetic turbulence. Particles diffuse the fastest in MHD turbulence due to the presence of extended coherent structures, and the slowest in standard random phases (RP) turbulence. Including intermittency via a continuous cascade (CC) and simple coherent structures by Lagrangian mapping (LM) does not change the diffusion coefficients significantly from the RP case. Only at low r_g a slight enhancement is noticeable

described with modelling approaches discussed in Chap. 2. In this section we will discuss the shortcomings of the usually employed Gaussian synthetic turbulence fields and discuss the role of intermittency, i.e. broken scale invariance.

The vector field given by Eq. (5.5) approximates magnetic turbulence as a superposition of plane waves with random phases and a prescribed phenomenological power spectrum. It is essentially a Gaussian random field, which exhibits statistical self-similarity within the inertial range (i.e. statistical quantities such as averages of fluctuations $\langle f(\delta B_r) \rangle$ at scale r are scale-invariant). Despite being only a crude representation of realistic magnetic turbulence, it enjoys wide-spread recognition due to its conceptual simplicity (see Sect. 4 and, e.g., Giacalone and Jokipii 1999; Casse et al. 2001; Kulsrud 2020). On the other hand, one can invoke intermittency of magnetic turbulence, i.e. broken scale-invariance of statistical quantities caused by a locally non-uniform energy dissipation rate, which leads to the formation of coherent structures (e.g. vortex tubes in Navier-Stokes turbulence or current sheets in MHD turbulence, see, e.g., Frisch 1995; Grauer et al. 1994). Intermittency can be assessed through the scaling behavior of the structure functions of the field

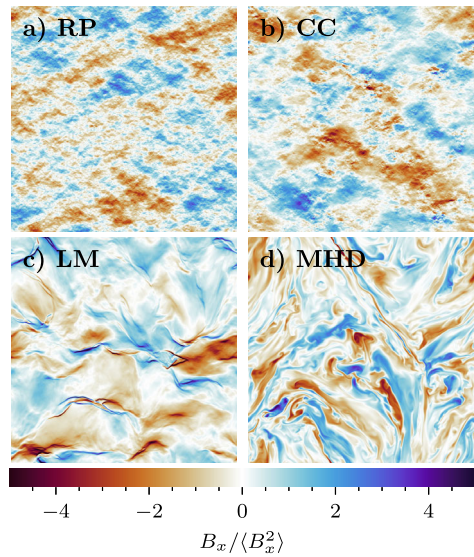
$$S_p(r) = \left\langle \left| \left(\vec{B}(\vec{x} + \vec{r}) - \vec{B}(\vec{x}) \right) \cdot \frac{\vec{r}}{r} \right|^p \right\rangle \propto r^{\zeta_p}, \quad (5.7)$$

where linear scaling $\zeta_p = H p$ indicates scale-invariance and nonlinear (i.e. anomalous) scaling $\zeta_p = H p + \phi(p)$ indicates intermittency.⁴ Such anomalous behavior is not only observed in simulations (e.g. Wan et al. 2016; Zhdankin et al. 2016), but also ubiquitously in the solar wind (e.g. Bruno and Carbone 2013; Chen et al. 2012; Sorriso-Valvo et al. 2017; Telloni et al. 2021; Roberts et al. 2022; Gomes et al. 2023).

While a Gaussian random field is uniquely defined by its mean and covariance functions, and thus is easy to synthesize, an intermittent random field has in principle infinitely many degrees of freedom, and thus finding a realistic and useful heuristic to guide and assess the construction of such a field is not a trivial task. Accordingly, there are several approaches found in the literature, some dealing with pure fluid turbulence (Juneja et al. 1994; Rosales

⁴For simplicity our discussion focuses on the longitudinal structure functions, i.e. the moments of the field fluctuations along the displacement vector \vec{r} . See, e.g., Germaschewski and Grauer (1999) for the role of perpendicular structure functions and Mallet et al. (2016) for field-aligned structure functions.

Fig. 38 Example slices of models for magnetic turbulence: random phases (RP), continuous cascade (CC), Lagrangian map (LM) and magnetohydrodynamics (MHD)



and Meneveau 2006, 2008; Chevillard et al. 2010; Pereira et al. 2016; Lübke et al. 2023; Li et al. 2024) and others focusing on magnetic turbulence (Subedi et al. 2014; Pucci et al. 2016; Malara et al. 2016; Durrive et al. 2020, 2022; Lübke et al. 2024; Maci et al. 2024).

As an example, we briefly present the considerations that led to the development of the synthetic field presented in Lübke et al. (2024).

1. Most of the above mentioned references utilize a discrete or continuous cascade algorithm, which mimics how energy density is inhomogeneously distributed while cascading down a hierarchy of scales, as described by a variety of phenomenological models of turbulent intermittency based on multiplicative cascades (see also Frisch (1995), Chap. 8). A convenient choice is a log-normal distribution for the energy dissipation rate according to Kolmogorov (1962), which can be expressed in terms of a continuous wavelet cascade (Muzy 2019).
2. This cascade algorithm can be embedded in a three-dimensional, vector-valued continuous wavelet transform to yield a divergence-free and intermittent vector field with the desired spectral properties, named the “continuous cascade” (CC) model (see Fig. 38b for an example). This model also fulfills the prescribed anomalous scaling of structure functions (see Fig. 39).
3. However, the CC field clearly lacks the intricate coherent structures and fast diffusion of test particles observed in MHD turbulence. This prompts the idea, inspired by Subedi et al. (2014), to generate two fields alongside each other, representing respectively the flow and magnetic field from MHD turbulence. Further, pressure-less Lagrangian mapping (LM) of grid points at each scale during the scale-by-scale generation of the CC fields is taken into account (originally due to Rosales and Meneveau (2006) in the context of fluid turbulence). In contrast to previous works, the cascade enhances the Lagrangian mapping, leading to strongly pronounced shock-like coherent structures with a Burgers-like scaling (see Figs. 38c and 39).

Despite the inclusion of intermittency and the successful generation of pronounced coherent structures, the CC and LM models achieve no substantial improvement in the transport of charged test particles towards the results from MHD, as shown in Figs. 36 and 37.

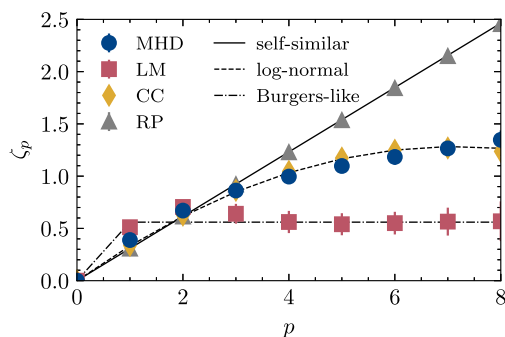


Fig. 39 Scaling exponents of structure functions $S_p(r) \sim r^{\zeta_p}$ of models for magnetic turbulence. The random phases (RP) field exhibits simple self-similar scaling akin to Kolmogorov (1941), the continuous cascade (CC) field realizes the log-normal model by Kolmogorov (1962), which provides for $p < 8$ a good fit to MHD turbulence (see also Grauer et al. (1994)), and the Lagrangian map (LM) model resembles Burger's turbulence with a constant scaling exponent (see, e.g., Bec and Khanin (2007) for an exposition)

This strongly suggests that the intermittency given by the structure function scaling is not sufficient information to reproduce the true complexity of magnetic turbulence. Instead, one needs to go beyond simple two-point statistics (such as the structure functions), and take geometric and topological properties into account when constructing synthetic fields. A useful geometric property is the fieldline curvature distribution, as utilized by Lübke et al. (2024), whereas topological tools such as persistence diagrams, Betti numbers and Minkowski functionals were employed by Makarenko et al. (2018b,a) and Henderson et al. (2019). A useful synthetic field for CR transport and modulation studies should also include scale-dependent anisotropy according to Goldreich and Sridhar (1995) and Boldyrev (2006), Mason et al. (2006).

5.1.3 Convergence of Diffusion Coefficient in Box-Based Simulations

The transport of CRs in turbulence undergoes several different regimes in time as shown in Fig. 40, where forced MHD simulations⁵ are used from Li et al. (2008). The initial ballistic phase leads to a linear increase of $\langle \Delta \mathbf{x}^2(t) \rangle / t$ with time and trajectory length. The gyromotion for low-energy CRs leads to deviation from this behaviour, as CRs return to the origin of the plane perpendicular to the local mean field, thus reducing the isotropic diffusion coefficient (blue lines in Fig. 40 for $l_{\text{traj}} \gtrsim 0.01 l_c$). This effect becomes significant in the perpendicular component of the diffusion coefficient of CRs in turbulence with a stronger mean field (Reichherzer et al. 2022a; Kuhlen et al. 2022). Figure 41 shows the anisotropic spatial displacement of CRs in a magnetic field with turbulence and a large-scale mean field.

Long-time diffusive behaviour emerges when CR travel over multiple ℓ_c , thus averaging the local field structure. Figure 40 illustrates differences in the time needed for the running diffusion coefficients to converge, with shortest times for $r_g \sim \ell_c$ and the need for significantly more time for low and high CR energies to reach steady state. Convergence in these cases appears only on scales much larger than the MHD turbulence boxes. This should be taken with care though, because in a realistic setting the structure of the magnetic field can probably not be viewed as a column of ideal turbulence cubes, nor should the average of a

⁵available from: http://turbulence.pha.jhu.edu/Forced_MHD_turbulence.aspx.

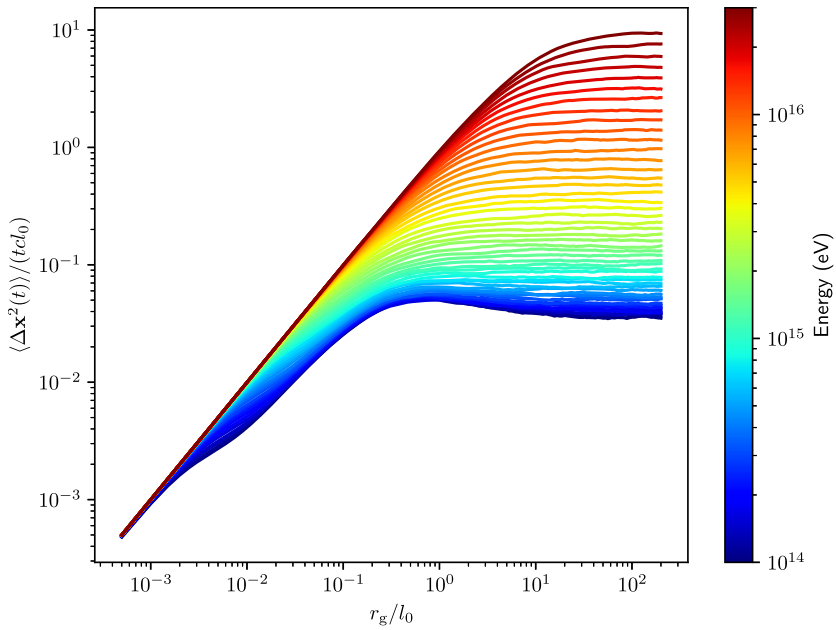
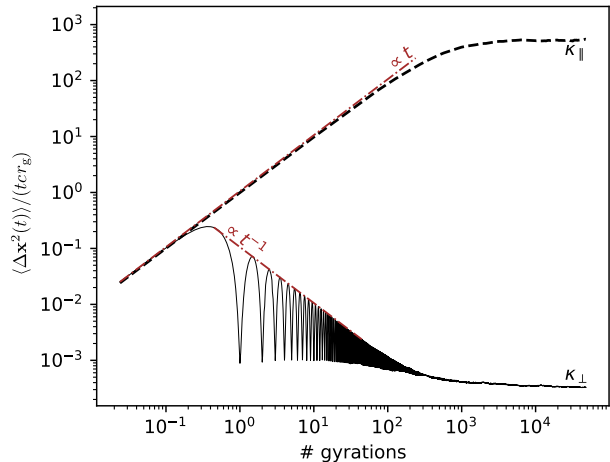


Fig. 40 Running diffusion coefficients of CRs with different energy in forced isotropic MHD turbulence (taken from the Johns Hopkins Turbulence Database; JHTDB)

Fig. 41 CRs with a specific energy in a synthetic magnetic field with turbulence and strong mean magnetic field, which defines the parallel and perpendicular diffusion coefficients that evaluate the spatial displacements along and perpendicular to the field. Both components scale with t and t^{-1} , respectively. Taken from Reichherzer (2022)



particle running multiple times over the same box be equated with the average of a particle running over multiple ℓ_c in a more realistic heterogeneous environment.

5.2 The Complications of Pitch-Angle Scattering

For most parts of this review, only unbounded spatial diffusion has been discussed, where the diffusive behaviour is classified in terms of the time dependence of the MSD as in Eq. (2). Pitch-angle scattering (see Sect. 4.2), however, is unique in the sense that the pitch-cosine

is bounded, i.e. $\mu \in [-1; 1]$, implying that the pitch-angle MSD $\langle(\Delta\mu)^2\rangle$ cannot be larger than 4. Full-orbit simulations do not only show the pitch-angle MSD saturating due to being bounded (something investigated extensively by Tautz et al. 2013; Tautz 2013), but also that the MSD oscillates initially (see, e.g., Kaiser et al. 1978; Tautz et al. 2013; Riordan and Pe'er 2019; van den Berg et al. 2024). This complicates the application of Eq. (2) to calculate a running diffusion coefficient for pitch-angle scattering from simulations: the running pitch-angle diffusion coefficient 1) will oscillate for short enough time scales due to the deterministic behaviour being decorrelated by pitch-angle diffusion, while it 2) will always show a t^{-1} behaviour for long enough times due to the saturation of the pitch-angle MSD (Tautz et al. 2013; Riordan and Pe'er 2019). Riordan and Pe'er (2019) show that the limited time interval when the running pitch-angle diffusion coefficient might be constant disappears under certain conditions: this happens, for example, when the turbulence strength increases and the MSD saturates quickly, yielding a practical problem for determining the pitch-angle diffusion coefficient from full-orbit simulations (see also the discussions and examples of van den Berg et al. 2024).

It is clear from this that the same criteria for identifying anomalous diffusion cannot be applied to pitch-angle scattering. It is therefore necessary to raise the question: how should anomalous diffusion be defined for pitch-angle scattering? In a more general context, it could be asked: how should anomalous diffusion be defined in a bounded domain? Since anomalous diffusion is associated with non-Gaussian statistics (as discussed after Eq. (2)), it might be possible to search for such probability distribution functions in the pitch-angle scattering time. Perri and Zimbardo (2012b), for example, calculate the pitch-angle scattering time expected from the resonance condition of QLT (see the discussion in Sect. 4.2) from observed magnetic field strengths and variances measured before a shock. Four events all showed scattering times with a Gaussian core transitioning to a power-law probability distribution. In another example, Perri et al. (2019) define the scattering time from full-orbit simulations as the time when the pitch-cosine changes sign (note that Pucci et al. 2016, requires two sign inversions) or when the pitch-angle changes by some predefined value. Power-law distributed scattering times are found for both of these definitions, with the power-law exponent being dependent on the definition of the scattering time. Such definitions of the pitch-angle scattering time are fairly *ad hoc* and therefore does not give a rigorous definition of anomalous diffusion on a bounded domain (i.e., it is, e.g., not clear if the QLT scattering time is a good estimate of the scattering time, given the theoretical limitations of QLT and the physical picture of the particle experiencing the total magnetic field without truly resonating with only a specific wavelength of the turbulence). Related to this is the finding of Tautz et al. (2013) that the probability distribution of pitch-cosine changes deviates from a Gaussian distribution at late times, although it is not clear if this is inherently due to signatures of anomalous diffusion or simply the relaxation of the probability distribution to a uniform distribution due to the saturation of $|\Delta\mu|$.

Zimbardo and Perri (2020) show that the temporal evolution of the pitch-angle distribution function from a delta injection, will be different between normal and anomalous diffusion, with anomalous diffusion having a distribution function that has a more intricate dependence on pitch-cosine and taking longer to relax to an isotropic distribution. When considering the pitch-angle distribution function observed *in situ*, there is always the uncertainty coming from the limited angular resolution of the instrument and the additional transport processes influencing the transport of the observed particles (e.g., focusing or continuous injection). It is, of course, much easier to construct the pitch-angle distribution function from full-orbit simulations. Perhaps better suited for identifying anomalous pitch-angle scattering, is then either the pitch-angle distribution or the pitch-angle correlation function.

Zimbardo and Perri (2020) additionally show that power-law scattering times could lead to a pitch-angle correlation function decaying as a power-law and not an exponential for isotropic pitch-angle scattering. The simulation results of Casse et al. (2001) and Fraschetti and Giacalone (2012) show for weak turbulence strengths that the pitch-angle correlation function has some oscillations due to deterministic behaviour before an exponential decorrelation. Fraschetti and Giacalone (2012) show in the presence of higher turbulence levels that the correlation function might show some initial exponential decay, but that there might then be an increase in the correlation followed by a decorrelation that is much slower than exponential. Overall, it is clear that more work, both theoretical and numerical, is needed when considering anomalous transport on the pitch-angle level.

5.3 Summary of Section 5

Numerically generated turbulent magnetic fields enable a deeper understanding of the transport properties of charged energetic particles in space plasmas. Integrating particle trajectories through magnetic fields is efficiently achieved using various numerical schemes, which robustly converge for different step sizes. However, modeling realistic astrophysical turbulence presents several challenges. Typically, synthetic fields in astrophysical studies are characterized by the root mean squared strength, the magnetic energy distribution defined by a power-law in Fourier space, different turbulence geometries, and an often assumed Gaussian probability density function for turbulence.

A major challenge is achieving large inertial ranges in synthetic turbulence models due to limitations in current simulations. Methods to address this are the grid and nested-grid methods. The grid method stores magnetic field vectors on a discrete grid, but it is constrained by memory and can introduce numerical artifacts. The nested-grid method uses multiple grids with different dynamic ranges to create larger inertial ranges, but also faces limitations. Gridless methods offer an alternative by summing predefined plane waves at any arbitrary position, potentially overcoming some limitations of grid methods. However, achieving realistic statistical properties and CR transport characteristics remains challenging. Recent studies suggest combining gridless and nested-grid methods for better results.

Intermittency poses additional challenges. It can be addressed by generating synthetic fields with multiplicative cascades to represent the non-uniform energy dissipation rate seen in turbulence. However, synthetic models still struggle to match the anomalous diffusion behavior observed in MHD simulations, indicating the need for more accurate geometric and topological modeling of coherent structures.

Additionally, incorporating a pitch-angle description adds another layer of complexity. In homogeneous and isotropic turbulence, pitch-angle scattering is typically modeled with a diffusion coefficient that depends on the particle's velocity and the turbulence spectrum. However, realistic turbulence often exhibits anisotropies and inhomogeneities, which complicates the pitch-angle diffusion process. Advanced models must consider these variations in pitch-angle scattering to accurately simulate CR transport. The resonance condition, which depends on the particle's gyro-radius and the turbulence wave spectrum, plays a significant role in pitch-angle diffusion. Yet, in current synthetic models, this aspect is often oversimplified, leading to discrepancies in predicting CR behavior compared to more detailed MHD simulations.

In conclusion, while current synthetic models provide valuable insights, they require further refinement to accurately replicate the complexity of astrophysical turbulence and its effects on cosmic ray transport. Future efforts should focus on enhancing the realism of these models by incorporating detailed statistical, geometric, and topological properties

of turbulence and improving the representation of pitch-angle scattering processes while exploring regimes of non-Gaussian diffusion.

6 Summary and Open Questions

This review explored the anomalous transport and acceleration of charged energetic particles in space and astrophysical plasmas, highlighting the deviations from traditional Gaussian diffusion models. The key points that were discussed included:

(1) Non-Gaussian Transport Models. Superdiffusion is characterized by the mean square displacement growing superlinearly with time, while subdiffusion grows sublinearly. These phenomena are contrasted with normal Gaussian diffusion, where displacement grows linearly with time. Models based on fractional diffusion-advection equations and non-Gaussian stochastic processes can be used to describe these features on a phenomenological level. Superdiffusive shock acceleration shows distinct spatial and energy spectra differences compared to normal diffusion, with power-law spatial profiles that exhibit harder energy spectra compared to standard diffusive shock acceleration.

(2) Nonlinear Diffusion Approaches. The nonlinear diffusion approach ties the diffusion coefficient to the spatial gradient of the particle distribution function. This leads to complex particle distributions, including power-law structures and nonlinear temporal behaviors. Although nonlinear diffusion does not alter the stationary shock spectrum it can significantly affect acceleration timescales and thus impact the results for transient and non-stationary shocks.

(3) Field Line Random Walk and Perpendicular Transport. Significant advances have been made in understanding perpendicular transport through simulations, heuristic arguments, and analytical theories. Time-dependent field-line-particle-decorrelation theory accurately describes initial ballistic, intermediate sub-diffusive, and final diffusive regimes. Despite progress, uncertainties remain, particularly in modeling the initial phases of solar energetic particle events and the appropriate field-line diffusion coefficients for different turbulence models.

(4) Numerical Full Orbit Simulations in Synthetic and MHD Turbulence. Simulating particle trajectories in turbulent magnetic fields reveals the complexity of their transport properties. Various numerical schemes efficiently integrate particle trajectories, but the primary challenge is to model realistic astrophysical turbulence. Current methods to construct synthetic turbulence, including grid and nested-grid techniques, have limitations in representing large inertial ranges. Combining these methods with gridless approaches shows promise, but challenges remain to match the diffusion behavior seen in MHD simulations. This is in part connected to aspects of intermittency and pitch-angle scattering. Addressing the non-uniform energy dissipation and structures in turbulence connected to intermittency and incorporating pitch-angle descriptions add complexity that, however, is characteristic of realistic turbulence. Anisotropies and inhomogeneities further complicate the pitch-angle diffusion process and resonance conditions.

Given the title of this review, we also conclude with a short list of open questions and new aspects that should be addressed in future work.

1. *What are the consequences of employing Levy walks, Levy flights, and tempered Levy flights for the transport and the acceleration of energetic particles?*

Since the form of the transport equation and, e.g., the resulting shock-accelerated energy spectra appear to depend on the choice of the Levy process used to describe the

anomalous scattering of the particles, it must be clarified whether one of the three mentioned processes is physically preferable for a given physical system or even in general.

2. *Does a generalized Ito lemma also exist for the case of Levy walks and tempered Levy flights?*

So far, the equivalence of a ‘fully fractional’ transport equation, i.e. one containing both a fractional diffusion and a fractional advection, to a system of stochastic differential equations has been established for the case of Levy flights but not for Levy walks and not for tempered Levy flights.

3. *How can a fractional advection be realized in a space- or astrophysical system?*

A fractional advection is usually associated with particle traps not being maintained by the considered flow but externally. It should be clarified how such external traps, which imply a Galilei-variant behaviour, can be realized in a given system.

4. *In what way is the anomalous transport obtained on the basis of nonlinear transport equations different from that resulting from fractional transport equations and why does it occur?*

While, for example, the accelerated spectra obtained with nonlinear transport equations are the same as for the linear case, the resulting spatial scalings exhibit an anomalous behaviour, i.e. power-laws rather than exponentials.

5. *Which turbulence characteristics lead to anomalous transport and why so, and what defines the temporal evolution characterized by an initial ballistic/superdiffusive, an intermediate subdiffusive, and an eventually Gaussian diffusive phase?*

The turbulence is affecting particle transport directly via scattering and indirectly via the transport of field lines to which the particles are attached to some degree. Two aspects remain unclear for various cases, so far: first, the dependence of the field line diffusion coefficient on the turbulence (in the sense that it is unclear which field line diffusion coefficient has to be used for slab/2D turbulence) and, second, what exactly may cause a decoupling of particles from ‘their’ field lines. Furthermore, while initial approaches exist, the consequences of intermittency as a result of structures like vortices and current sheets have to be explored quantitatively.

6. *What is a correct and efficient way to describe turbulence synthetically, i.e. not as a result from MHD modelling but rather by prescribing the turbulent fluctuations directly?*

More work is required to shed light on which properties of a magnetic field, like curvature or mirror structures, have to be incorporated in a synthetic generation of turbulence such that the latter resembles more realistically MHD turbulence and, thus, turbulence in real physical systems.

One can be optimistic that the next few years will witness progress regarding all of the above questions. In other words: we are living in an exciting time of growing understanding of the origin and consequences of anomalous transport and acceleration of charged energetic particles in space and astrophysical plasmas.

Acknowledgements We are grateful to the Deutsche Forschungsgemeinschaft (DFG) for financial support of the workshop and research activities via the project grants EF 98/4-1 and FI 706/26, as well as in the Collaborative Research Center SFB 1491. The work of PR was initially funded through a Gateway Fellowship and subsequently through the Walter Benjamin Fellowship by the Deutsche Forschungsgemeinschaft (DFG, German Research Foundation) — 518672034. TL acknowledges support from the UK Science and Technology Facilities Council (STFC) through grants ST/V000934/1 and ST/Y002725/1. JIR acknowledges financial support from NASA grants 80NSSC21K1319 and 80NSSC20K1783, and from the NSF grant EP-SCoR RII-Track-1 Cooperative Agreement OIA-2148653. AS acknowledges support by the Natural Sciences and Engineering Research Council (NSERC) of Canada. We acknowledge support from the International Space Science Institute (ISSI) in Bern, where FE, SP, JvdB, TL and JL are members of the ISSI International Team project #24-608 “Energetic Particle Transport in Space Plasma Turbulence”. GZ and

SP acknowledge support from the Italian PRIN 2022, project 2022294WNB entitled “Heliospheric shocks and space weather: from multispacecraft observations to numerical modeling”. Finanziato da Next Generation EU, fondo del Piano Nazionale di Ripresa e Resilienza (PNRR) Missione 4 “Istruzione e Ricerca” - Componente C2 Investimento 1.1, ‘Fondo per il Programma Nazionale di Ricerca e Progetti di Rilevante Interesse Nazionale (PRIN)’. GZ and SP further acknowledge the Space It Up project funded by the Italian Space Agency, ASI, and the Ministry of University and Research, MUR, under contract n. 2024-5-E.0 - CUP n.I53D2400060005. SP and GZ acknowledge support from the project ‘Data-based predictions of solar energetic particle arrival to the Earth: ensuring space data and technology integrity from hazardous solar activity events’ (CUP H53D23011020001) ‘Finanziato dall’Unione europea – Next Generation EU’ PIANO NAZIONALE DI RIPRESA E RESILIENZA (PNRR) Missione 4 “Istruzione e Ricerca” - Componente C2 Investimento 1.1, ‘Fondo per il Programma Nazionale di Ricerca e Progetti di Rilevante Interesse Nazionale (PRIN)’ Settore PE09.

Funding Information Open Access funding enabled and organized by Projekt DEAL.

Declarations

Competing Interests The authors declare that they have no conflicts of interest or competing interests in undertaking this work.

Open Access This article is licensed under a Creative Commons Attribution 4.0 International License, which permits use, sharing, adaptation, distribution and reproduction in any medium or format, as long as you give appropriate credit to the original author(s) and the source, provide a link to the Creative Commons licence, and indicate if changes were made. The images or other third party material in this article are included in the article’s Creative Commons licence, unless indicated otherwise in a credit line to the material. If material is not included in the article’s Creative Commons licence and your intended use is not permitted by statutory regulation or exceeds the permitted use, you will need to obtain permission directly from the copyright holder. To view a copy of this licence, visit <http://creativecommons.org/licenses/by/4.0/>.

References

- Achterberg A, Schure KM (2011) A more accurate numerical scheme for diffusive shock acceleration. *Mon Not R Astron Soc* 411(4):2628–2636. <https://doi.org/10.1111/j.1365-2966.2010.17868.x>
- Aerdker S, Merten L, Becker Tjus J, Walter D, Effenberger F, Fichtner H (2024) Numerical modeling of time dependent diffusive shock acceleration. *J Cosmol Astropart Phys* 2024(1):068. <https://doi.org/10.1088/1475-7516/2024/01/068>
- Aerdker S, Merten L, Effenberger F, Fichtner H, Becker Tjus J (2025) Superdiffusion of energetic particles at shocks: a Lévy flight model for acceleration. *Astron Astrophys* 693:15. <https://doi.org/10.1051/0004-6361/202451765>
- Alves Batista R, Becker Tjus J, Dörner J, Dundovic A, Eichmann B, Frie A, Heiter C, Hoerbe MR, Kampert K-H, Merten L, Müller G, Reichherzer P, Saveliev A, Schlegel L, Sigl G, van Vliet A, Winchen T (2022) CRPropa 3.2 - an advanced framework for high-energy particle propagation in extragalactic and galactic spaces. *J Cosmol Astropart Phys* 2022(9):035. <https://doi.org/10.1088/1475-7516/2022/09/035>
- Arendt V, Shalchi A (2020) Detailed test-particle simulations of energetic particles interacting with magnetized plasmas I. Two-component turbulence. *Adv Space Res* 66:2001–2023
- Baeumer B, Meerschaert MM (2010) Tempered stable Lévy motion and transient super-diffusion. *J Comput Appl Math* 233:2438–2448. <https://doi.org/10.1016/j.cam.2009.10.027>
- Barghouty AF, Schnee DA (2012) Anomalous transport of high-energy cosmic rays in galactic superbubbles. I. Numerical simulations. *Astrophys J* 749(2):178. <https://doi.org/10.1088/0004-637X/749/2/178>
- Barreto-Mota L, de Gouveia Dal Pino EM, Xu S, Lazarian A (2025) Cosmic ray diffusion in the turbulent interstellar medium: effects of mirror diffusion and pitch angle scattering. *Astrophys J* 988:269. <https://doi.org/10.3847/1538-4357/ade4c8>
- Batchelor GK (1953) The theory of homogeneous turbulence
- Bec J, Khanin K (2007) Burgers turbulence. *Phys Rep* 447(1):1–66. <https://doi.org/10.1016/j.physrep.2007.04.002>
- Becker Tjus J, Merten L (2020) Closing in on the origin of galactic cosmic rays using multimessenger information. *Phys Rep* 872:1–98. <https://doi.org/10.1016/j.physrep.2020.05.002>

- Bell AR (1978) The acceleration of cosmic rays in shock fronts. I. *Mon Not R Astron Soc* 182:147–156. <https://doi.org/10.1093/mnras/182.2.147>
- Bell AR (1983) Electron energy transport in ion waves and its relevance to laser-produced plasmas. *Phys Fluids* 26(1):279–284. <https://doi.org/10.1063/1.864018>
- Bell A (2004) Turbulent amplification of magnetic field and diffusive shock acceleration of cosmic rays. *Mon Not R Astron Soc* 353(2):550–558
- Bender CM, Milton KA, Pinsky SS, Simmons LM Jr (1989) A new perturbative approach to nonlinear problems. *J Math Phys* 30(7):1447–1455. <https://doi.org/10.1063/1.528326>
- Bender CM, Boettcher S, Milton KA (1991) A new perturbative approach to nonlinear partial differential equations. *J Math Phys* 32(11):3031–3038. <https://doi.org/10.1063/1.529047>
- Beresnyak A, Yan H, Lazarian A (2011) Numerical study of cosmic ray diffusion in magnetohydrodynamic turbulence. *Astrophys J* 728:60. <https://doi.org/10.1088/0004-637X/728/1/60>
- Bian NH, Emslie AG, Kontar EP (2017) The role of diffusion in the transport of energetic electrons during solar flares. *Astrophys J* 835(2):262. <https://doi.org/10.3847/1538-4357/835/2/262>
- Bieber JW, Matthaeus WH (1997) Perpendicular diffusion and drift at intermediate cosmic-ray energies. *Astrophys J* 485(2):655–659. <https://doi.org/10.1086/304464>
- Bieber JW, Wanner W, Matthaeus WH (1996) Dominant two-dimensional solar wind turbulence with implications for cosmic ray transport. *J Geophys Res* 101(A2):2511–2522. <https://doi.org/10.1029/95JA02588>
- Blasi P (2013) The origin of galactic cosmic rays. *Astron Astrophys Rev* 21:70. <https://doi.org/10.1007/s00159-013-0070-7>
- Blumen A, Klafter J, Zumofen G (1990) A stochastic approach to enhanced diffusion: Lévy walks. *Europhys Lett* 13:223. <https://doi.org/10.1209/0295-5075/13/3/006>
- Boldyrev S (2006) Spectrum of magnetohydrodynamic turbulence. *Phys Rev Lett* 96(11):115002
- Boris J (1970) Relativistic plasma simulation—optimization of a hybrid code. In: Proceedings of the fourth conference on numerical simulation of plasmas, Naval Research Laboratory, Washington, D.C., pp 3–67
- Brunetti G, Jones TW (2014) Cosmic rays in galaxy clusters and their nonthermal emission. *Int J Mod Phys D* 23:1430007–98. <https://doi.org/10.1142/S0218271814300079>
- Bruno R, Carbone V (2013) The solar wind as a turbulence laboratory. *Living Rev Sol Phys* 10(1):2. <https://doi.org/10.12942/lrsp-2013-2>
- Bruno R, Sorriso-Valvo L, Carbone V, Bavassano B (2004) A possible truncated-Lévy-flight statistics recovered from interplanetary solar-wind velocity and magnetic-field fluctuations. *Europhys Lett* 66(1):146–152. <https://doi.org/10.1209/epl/i2003-10154-7>
- Cairolì A, Klages R, Baule A (2018) Weak Galilean invariance as a selection principle for coarse-grained diffusive models. *Proc Natl Acad Sci USA* 115(22):5714–5719. <https://doi.org/10.1073/pnas.1717292115>
- Calvo I, Sánchez R, Carreras BA, van Milligen BP (2007) Fractional generalization of Fick's law: a microscopic approach. *Phys Rev Lett* 99(23):230603. <https://doi.org/10.1103/PhysRevLett.99.230603>
- Cartea Á, Del-Castillo-Negrete D (2007) Fluid limit of the continuous-time random walk with general Lévy jump distribution functions. *Phys Rev E* 76(4):041105. <https://doi.org/10.1103/PhysRevE.76.041105>
- Casse F, Lemoine M, Pelletier G (2001) Transport of cosmic rays in chaotic magnetic fields. *Phys Rev D* 65(2):023002. <https://doi.org/10.1103/PhysRevD.65.023002>
- Chambers JM, Mallows CL, Stuck BW (1976) A method for simulating stable random variables. *J Am Stat Assoc* 71(354):340–344. <http://www.jstor.org/stable/2285309>
- Chandran BDG (2000) Scattering of energetic particles by anisotropic magnetohydrodynamic turbulence with a Goldreich-Sridhar power spectrum. *Phys Rev Lett* 85(22):4656–4659. <https://doi.org/10.1103/PhysRevLett.85.4656>
- Chandrasekhar S (1943) Stochastic problems in physics and astronomy. *Rev Mod Phys* 15(1):1–89
- Chaves AS (1998) A fractional diffusion equation to describe Lévy flights. *Phys Lett A* 239(1–2):13–16. [https://doi.org/10.1016/S0375-9601\(97\)00947-X](https://doi.org/10.1016/S0375-9601(97)00947-X)
- Chen CHK, Mallet A, Schekochihin AA, Horbury TS, Wicks RT, Bale SD (2012) Three-dimensional structure of solar wind turbulence. *Astrophys J* 758(2):120. <https://doi.org/10.1088/0004-637X/758/2/120>
- Chen LE, Bott AFA, Tzeferacos P, Rigby A, Bell A, Bingham R, Graziani C, Katz J, Koenig M, Li CK, Petrasso R, Park H-S, Ross JS, Ryu D, White TG, Reville B, Matthews J, Meinecke J, Miniati F, Zweibel EG, Sarkar S, Schekochihin AA, Lamb DQ, Froula DH, Gregori G (2020) Transport of high-energy charged particles through spatially intermittent turbulent magnetic fields. *Astrophys J* 892(2):114. <https://doi.org/10.3847/1538-4357/ab7a19>
- Chevillard L, Robert R, Vargas V (2010) A stochastic representation of the local structure of turbulence. *Europhys Lett* 89(5):54002. <https://doi.org/10.1209/0295-5075/89/54002>
- Chhiber R, Matthaeus WH, Cohen CMS, Ruffolo D, Sonsnetree W, Tooprakai P, Seripienlert A, Chuychai P, Usmanov AV, Goldstein ML, McComas DJ, Leske RA, Szalay JR, Joyce CJ, Cummings AC, Roelof EC, Christian ER, Mewaldt RA, Labrador AW, Giacalone J, Schwadron NA, Mitchell DG, Hill ME, Wiedenbeck ME, McNutt RL, Desai MI (2021) Magnetic field line random walk and solar energetic

- particle path lengths. Stochastic theory and PSP/IS \odot IS observations. *Astron Astrophys* 650:26. <https://doi.org/10.1051/0004-6361/202039816>
- Cho J, Lazarian A (2002) Compressible sub-Alfvénic MHD turbulence in low- β plasmas. *Phys Rev Lett* 88(24):245001. <https://doi.org/10.1103/PhysRevLett.88.245001>
- Cho J, Lazarian A (2003) Compressible magnetohydrodynamic turbulence: mode coupling, scaling relations, anisotropy, viscosity-damped regime and astrophysical implications. *Mon Not R Astron Soc* 345(12):325–339. <https://doi.org/10.1046/j.1365-8711.2003.06941.x>
- Cho J, Vishniac ET (2000) The anisotropy of magnetohydrodynamic Alfvénic turbulence. *Astrophys J* 539(1):273–282. <https://doi.org/10.1086/309213>
- Corrsin S (1959) Progress report on some turbulent diffusion research. In: Landsberg HE, Van Mieghem J (eds) *Atmospheric diffusion and air pollution*. Advances in Geophysics, vol 6. Academic Press, New York, pp 161–164. [https://doi.org/10.1016/S0065-2687\(08\)60102-8](https://doi.org/10.1016/S0065-2687(08)60102-8)
- Decker RB (1983) Formation of shock-spike events at quasi-perpendicular shocks. *J Geophys Res* 88(A12):9959–9974. <https://doi.org/10.1029/JA088iA12p09959>
- del-Castillo-Negrete D (2006) Fractional diffusion models of nonlocal transport. *Phys Plasmas* 13(8):082308. <https://doi.org/10.1063/1.2336114>
- del-Castillo-Negrete D, Carreras BA, Lynch VE (2004) Fractional diffusion in plasma turbulence. *Phys Plasmas* 11(8):3854–3864. <https://doi.org/10.1063/1.1767097>
- Dmitruk P, Matthaeus WH, Seenu N (2004) Test particle energization by current sheets and nonuniform fields in magnetohydrodynamic turbulence. *Astrophys J* 617(1):667–679. <https://doi.org/10.1086/425301>
- Drake JF, Swisdak M, Che H, Shay MA (2006) Electron acceleration from contracting magnetic islands during reconnection. *Nature* 443(7111):553–556. <https://doi.org/10.1038/nature05116>
- Dresing N, Gómez-Herrero R, Klassen A, Heber B, Kartavykh Y, Dröge W (2012) The large longitudinal spread of solar energetic particles during the 17 January 2010 solar event. *Sol Phys* 281(1):281–300. <https://doi.org/10.1007/s11207-012-0049-y>
- Dröge W, Kartavykh YY, Klecker B, Kovaltsov GA (2010) Anisotropic three-dimensional focused transport of solar energetic particles in the inner heliosphere. *Astrophys J* 709(2):912–919. <https://doi.org/10.1088/0004-637X/709/2/912>
- Drury LO (1983) An introduction to the theory of diffusive shock acceleration of energetic particles in tenuous plasmas. *Rep Prog Phys* 46(8):973
- Dundovic A, Pezzi O, Blasi P, Klassen A, Heber B, Kartavykh WH (2020) Novel aspects of cosmic ray diffusion in synthetic magnetic turbulence. *Phys Rev D* 102(10):103016. <https://doi.org/10.1103/PhysRevD.102.103016>
- Durrive J-B, Lesaffre P, Ferrière K (2020) Magnetic fields from multiplicative chaos. *Mon Not R Astron Soc* 496(3):3015–3034. <https://doi.org/10.1093/mnras/staa1514>
- Durrive J-B, Changmai M, Keppens R, Lesaffre P, Maci D, Momferatos G (2022) Swift generator for three-dimensional magnetohydrodynamic turbulence. *Phys Rev E* 106(2):025307. <https://doi.org/10.1103/PhysRevE.106.025307>
- Earl JA (1974) The diffusive idealization of charged-particle transport in random magnetic fields. *Astrophys J* 193:231
- Effenberger F, Litvinenko YE (2014) The diffusion approximation versus the telegraph equation for modeling solar energetic particle transport with adiabatic focusing I: isotropic pitch-angle scattering. *Astrophys J* 783(1):15. <https://doi.org/10.1088/0004-637X/783/1/15>
- Effenberger F, Aerdker S, Merten L, Fichtner H (2024) Superdiffusion of energetic particles at shocks: a fractional diffusion and Lévy flight model of spatial transport. *Astron Astrophys* 686:219. <https://doi.org/10.1051/0004-6361/202449334>
- Eliazar I, Klafter J (2011) Anomalous is ubiquitous. *Ann Phys* 326(9):2517–2531. <https://doi.org/10.1016/j.aop.2011.07.006>
- Ewart RJ, Reichherzer P, Bott AFA, Kunz MW, Schekochihin AA (2024) Cosmic-ray confinement in radio bubbles by micromirrors. *Mon Not R Astron Soc* 532(2):2098–2107. <https://doi.org/10.1093/mnras/stae1578>
- Falgarone E, Momferatos G, Lesaffre P (2015) The intermittency of ISM turbulence: what do the observations tell us? In: Lazarian A, de Gouveia Dal Pino EM, Melioli C (eds) *Magnetic fields in diffuse media*. Astrophysics and Space Science Library, vol 407, p 227. https://doi.org/10.1007/978-3-662-44625-6_9
- Felice GM, Kulsrud RM (2001) Cosmic-ray pitch-angle scattering through 90°. *Astrophys J* 553(1):198–210. <https://doi.org/10.1086/320651>
- Fichtner H, Stern R, Effenberger F (2014) Numerical modeling of anomalous transport of cosmic rays. In: Pogorelov NV, Audit E, Zank GP (eds) *8th international conference of numerical modeling of space plasma flows (ASTRONUM 2013)*. Astronomical society of the Pacific conference series, vol 488, p 17
- Fisk LA, Axford WI (1969) Anisotropies of solar cosmic rays *Sol Phys* 7(3):486–498. <https://doi.org/10.1007/BF00146151>

- Fraschetti F, Giacalone J (2012) Early-time velocity autocorrelation for charged particles diffusion and drift in static magnetic turbulence. *Astrophys J* 755(2):114. <https://doi.org/10.1088/0004-637X/755/2/114>
- Fraschetti F, Jokipii JR (2011) Time-dependent perpendicular transport of fast charged particles in a turbulent magnetic field. *Astrophys J* 734(2):83. <https://doi.org/10.1088/0004-637X/734/2/83>
- Fraternali F, Adhikari L, Fichtner H, Kim TK, Kleimann J, Oughton S, Pogorelov NV, Roytershteyn V, Smith CW, Usmanov AV, Zank GP, Zhao L (2022) Turbulence in the outer heliosphere. *Space Sci Rev* 218(6):50. <https://doi.org/10.1007/s11214-022-00914-2>
- Frisch U (1995) *Turbulence: the legacy of A.N. Kolmogorov*. Cambridge University Press, Cambridge. ISBN 9780521457132. <https://doi.org/10.1017/cbo9781139170666>
- Gardiner CW (1985) *Handbook of stochastic methods for physics, chemistry and the natural sciences*. Springer, Berlin
- Germaschewski K, Grauer R (1999) Longitudinal and transversal structure functions in two-dimensional electron magnetohydrodynamic flows. *Phys Plasmas* 6(10):3788–3793. <https://doi.org/10.1063/1.873642>
- Giacalone J (2012) Energetic charged particles associated with strong interplanetary shocks. *Astrophys J* 761:28. <https://doi.org/10.1088/0004-637X/761/1/28>
- Giacalone J, Jokipii JR (1999) The transport of cosmic rays across a turbulent magnetic field. *Astrophys J* 520:204–214
- Giacalone J, Fahr H, Fichtner H, Florinski V, Heber B, Hill ME, Kóta J, Leske RA, Potgieter MS, Rankin JS (2022) Anomalous cosmic rays and heliospheric energetic particles. *Space Sci Rev* 218(4):22. <https://doi.org/10.1007/s11214-022-00890-7>
- Giacinti G, Kachelrieß M, Semikoz DV, Sigl G (2012) *J Cosmol Astropart Phys* 2012(7):031. <https://doi.org/10.1088/1475-7516/2012/07/031>
- Goldreich P, Sridhar S (1995) Toward a theory of interstellar turbulence. II. Strong alfvénic turbulence. *Astrophys J* 438:763
- Gomes LF, Gomes TFP, Rempel EL, Gama S (2023) Origin of multifractality in solar wind turbulence: the role of current sheets. *Mon Not R Astron Soc* 519(3):3623–3634. <https://doi.org/10.1093/mnras/stac3577>
- Govoni F, Murgia M, Vacca V, Loi F, Girardi M, Gastaldello F, Giovannini G, Feretti L, Paladino R, Carretti E, Concu R, Melis A, Poppi S, Valente G, Bernardi G, Bonafede A, Boschini W, Brienza M, Clarke TE, Colafrancesco S, de Gasperin F, Eckert D, Enßlin TA, Ferrari C, Gregorini L, Johnston-Hollitt M, Junklewitz H, Orrù E, Parma P, Perley R, Rossetti M, Taylor GB, Vazza F (2017) Sardinia radio telescope observations of Abell 194. The intra-cluster magnetic field power spectrum. *Astron Astrophys* 603:122. <https://doi.org/10.1051/0004-6361/201630349>
- Grauer R, Krug J, Marliani C (1994) Scaling of high-order structure functions in magnetohydrodynamic turbulence. *Phys Lett A* 195(5):335–338. [https://doi.org/10.1016/0375-9601\(94\)90038-8](https://doi.org/10.1016/0375-9601(94)90038-8)
- Greco A, Matthaeus WH, Servidio S, Chuychai P, Dmitruk P (2009) Statistical analysis of discontinuities in solar wind ACE data and comparison with intermittent MHD turbulence. *Astrophys J Lett* 691(2):111–114. <https://doi.org/10.1088/0004-637X/691/2/L111>
- Green MS (1951) Brownian motion in a gas of noninteracting molecules. *J Chem Phys* 19:1036
- Harari D, Mollerach S, Roulet E (2015) Anisotropies of ultrahigh energy cosmic ray nuclei diffusing from extragalactic sources. *Phys Rev D* 92(6):063014. <https://doi.org/10.1103/PhysRevD.92.063014>
- He H-Q, Qin G, Zhang M (2011) Propagation of solar energetic particles in three-dimensional interplanetary magnetic fields: in view of characteristics of sources. *Astrophys J* 734(2):74. <https://doi.org/10.1088/0004-637X/734/2/74>
- Henderson R, Makarenko I, Bushby P, Fletcher A, Shukurov A (2019) Statistical topology and the random interstellar medium. *J Am Stat Assoc* 115(530):625–635. <https://doi.org/10.1080/01621459.2019.1647841>
- Hoang GT, Bourdelle C, Pégourié B, Schunke B, Artaud JF, Bucalossi J, Clairet F, Fenzi-Bonizec C, Garbet X, Gil C, Guirlet R, Imbeaux F, Lasalle J, Loarer T, Lowry C, Travère JM, Tsironi E (2003) Particle pinch with fully noninductive lower hybrid current drive in tore supra. *Phys Rev Lett* 90(15):155002. <https://doi.org/10.1103/PhysRevLett.90.155002>
- Hopkins PF, Squire J, Butsky IS, Ji S (2022) Standard self-confinement and extrinsic turbulence models for cosmic ray transport are fundamentally incompatible with observations. *Mon Not R Astron Soc* 517(4):5413–5448. <https://doi.org/10.1093/mnras/stac2909>
- Hu Y, Lazarian A, Xu S (2022) Superdiffusion of cosmic rays in compressible magnetized turbulence. *Mon Not R Astron Soc* 512(2):2111–2124. <https://doi.org/10.1093/mnras/stac319>
- Ida K, Shi Z, Sun HJ, Inagaki S, Kamiya K, Rice JE, Tamura N, Diamond PH, Dif-Pradalier G, Zou XL, Itoh K, Sugita S, Gürcan OD, Estrada T, Hidalgo C, Hahn TS, Field A, Ding XT, Sakamoto Y, Oldenburger S, Yoshinuma M, Kobayashi T, Jiang M, Hahn SH, Jeon YM, Hong SH, Kosuga Y, Dong J, Itoh S-I (2015) Towards an emerging understanding of non-locality phenomena and non-local transport. *Nucl Fusion* 55(1):013022. <https://doi.org/10.1088/0029-5515/55/1/013022>

- Iroshnikov PS (1964) Turbulence of a conducting fluid in a strong magnetic field. *Sov Astron* 7:566
- Islaker H, Pisokas T, Vlahos L, Anastasiadis A (2017b) Particle acceleration and fractional transport in turbulent reconnection. *Astrophys J* 849(1):35. <https://doi.org/10.3847/1538-4357/aa8ee8>
- Islaker H, Vlahos L, Constantinescu D (2017a) Fractional transport in strongly turbulent plasmas. *Phys Rev Lett* 119(4):045101. <https://doi.org/10.1103/PhysRevLett.119.045101>
- Islaker H, Archontis V, Vlahos L (2019) Particle acceleration and heating in regions of magnetic flux emergence. *Astrophys J* 882(1):57. <https://doi.org/10.3847/1538-4357/ab30c6>
- Itô K (1951) On a formula concerning stochastic differentials. *Nagoya Math J* 3:55–65. <https://doi.org/10.1017/S0027763000012216>
- Ito K, Miyazaki S (2003) Crossover between anomalous superdiffusion and normal diffusion in oscillating convection flows. *Prog Theor Phys* 110(5):875–887. <https://doi.org/10.1143/PTP.110.875>
- Johlander A, Schwartz SJ, Vaivads A, Khotyaintsev YV, Gingell I, Peng IB, Markidis S, Lindqvist P-A, Ergun RE, Merklund GT, Plaschke F, Magnes W, Strangeway RJ, Russell CT, Wei H, Torbert RB, Paterson WR, Gershman DJ, Dorelli JC, Avanzo LA, Lavraud B, Saito Y, Giles BL, Pollock CJ, Burch JL (2016) Rippled quasiperpendicular shock observed by the magnetospheric multiscale spacecraft. *Phys Rev Lett* 117(16):165101
- Jokipii JR (1966) Cosmic-ray propagation. I. Charged particles in a random magnetic field. *Astrophys J* 146:480. <https://doi.org/10.1086/148912>
- Juneja A, Lathrop DP, Sreenivasan KR, Stolovitzky G (1994) Synthetic turbulence. *Phys Rev E* 49(6):5179–5194. <https://doi.org/10.1103/PhysRevE.49.5179>
- Kaiser TB, Birmingham TJ, Jones FC (1978) Computer simulation of the velocity diffusion of cosmic rays. *Phys Fluids* 21:361–373. <https://doi.org/10.1063/1.862234>
- Kajdić P, Preisser L, Blanco-Cano X, Burgess D, Trotta D (2019) First observations of irregular surface of interplanetary shocks at ion scales by cluster. *Astrophys J Lett* 874(2):13
- Kath WL, Cohen DS (1982) Waiting-time behavior in a nonlinear diffusion equation. *Stud Appl Math* 67(2):79–105. <https://doi.org/10.1002/sapm198267279>
- Kempski P, Quataert E (2022) Reconciling cosmic ray transport theory with phenomenological models motivated by Milky-Way data. *Mon Not R Astron Soc* 514(1):657–674. <https://doi.org/10.1093/mnras/stac1240>
- Kempski P, Fielding DB, Quataert E, Galishnikova AK, Kunz MW, Philippov AA, Ripperda B (2023) Cosmic ray transport in large-amplitude turbulence with small-scale field reversals. *Mon Not R Astron Soc* 525(4):4985–4998. <https://doi.org/10.1093/mnras/stad2609>
- Kirk JG, Duffy P, Gallant YA (1996) Stochastic particle acceleration at shocks in the presence of braided magnetic fields. *Astron Astrophys* 314:1010–1016. <https://doi.org/10.48550/arXiv.astro-ph/9604056>
- Klafter J, Blumen A, Shlesinger MF (1987) Stochastic pathway to anomalous diffusion. *Phys Rev A* 35:3081–3085. <https://doi.org/10.1103/PhysRevA.35.3081>
- Kolmogorov A (1941) The local structure of turbulence in incompressible viscous fluid for very large Reynolds' numbers. *Dokl Akad Nauk SSSR* 30:301–305
- Kolmogorov AN (1962) A refinement of previous hypotheses concerning the local structure of turbulence in a viscous incompressible fluid at high Reynolds number. *J Fluid Mech* 13(1):82–85. <https://doi.org/10.1017/S0022112062000518>
- Kraichnan RH (1965) Inertial-range spectrum of hydromagnetic turbulence. *Phys Fluids* 8(7):1385–1387. <https://doi.org/10.1063/1.1761412>
- Kruells WM, Achterberg A (1994) Computation of cosmic-ray acceleration by Ito's stochastic differential equations. *Astron Astrophys* 286:314–327
- Kubo R (1957) Statistical-mechanical theory of irreversible processes. *J Phys Soc Jpn* 12:570
- Kubo R (1963) Stochastic Liouville equations. *J Math Phys* 4:174
- Kuhlen M, Phan VHM, Mertsch P (2022) Diffusion of relativistic charged particles and field lines in isotropic turbulence. *arXiv e-prints*, [arXiv:2211.05881](https://arxiv.org/abs/2211.05881). <https://doi.org/10.48550/arXiv.2211.05881>
- Kulsrud RM (2020) Plasma physics for astrophysics. Princeton University Press, Princeton. <https://doi.org/10.2307/j.ctvzsmf0w>
- Kunz MW, Jones TW, Zhuravleva I (2022) Plasma physics of the intracluster medium. In: Bambi C, Sanganelo A (eds) *Handbook of X-ray and gamma-ray astrophysics*, pp 5049–5090. https://doi.org/10.1007/978-981-19-6960-7_125
- Lagutin AA, Volkov NV (2024) Where are the pevatrons that form the knee in the spectrum of the cosmic ray nucleon component around 4 PeV? *Phys At Nucl* 86(6):1076–1082. <https://doi.org/10.1134/S1063778824010307>
- Laitinen T, Dalla S (2017) Energetic particle transport across the mean magnetic field: before diffusion. *Astrophys J* 834(2):127. <https://doi.org/10.3847/1538-4357/834/2/127>
- Laitinen T, Dalla S (2019) From Sun to interplanetary space: what is the pathlength of solar energetic particles? *Astrophys J* 887(2):222. <https://doi.org/10.3847/1538-4357/ab54c7>

- Laitinen T, Dalla S, Marsh MS (2013) Energetic particle cross-field propagation early in a solar event. *Astrophys J Lett* 773:29–34
- Laitinen T, Kopp A, Effenberger F, Dalla S, Marsh MS (2016) Solar energetic particle access to distant longitudes through turbulent field-line meandering. *Astron Astrophys* 591:18. <https://doi.org/10.1051/0004-6361/201527801>
- Lazarian A, Xu S (2021) Diffusion of cosmic rays in MHD turbulence with magnetic mirrors. *Astrophys J* 923(1):53. <https://doi.org/10.3847/1538-4357/ac2de9>
- le Roux JA (2022) Investigating superdiffusive shock acceleration at a parallel shock with a fractional Parker equation for energetic-particle interaction with small-scale magnetic flux ropes. *Astrophys J* 930(2):125. <https://doi.org/10.3847/1538-4357/ac62d0>
- le Roux JA (2023) Parallel and momentum superdiffusion of energetic particles interacting with small-scale magnetic flux ropes in the large-scale solar wind. *Astrophys J* 945(1):60. <https://doi.org/10.3847/1538-4357/acb821>
- le Roux JA (2024) A tempered fractional kinetic transport theory for energetic particle interaction with quasi-two-dimensional turbulence in the large-scale solar wind. *Astrophys J* 968(2):112. <https://doi.org/10.3847/1538-4357/ad42a0>
- le Roux JA, Zank GP (2021) A focused transport-based kinetic fractional diffusion-advection equation for energetic particle trapping and reconnection-related acceleration by small-scale magnetic flux ropes in the solar wind. *Astrophys J* 913(2):84. <https://doi.org/10.3847/1538-4357/abf3c6>
- le Roux JA, Zank GP, Khabarova OV (2018) Self-consistent energetic particle acceleration by contracting and reconnecting small-scale flux ropes: the governing equations. *Astrophys J* 864(2):158. <https://doi.org/10.3847/1538-4357/aad8b3>
- Lemoine M (2023) Particle transport through localized interactions with sharp magnetic field bends in MHD turbulence. *J Plasma Phys* 89(5):175890501. <https://doi.org/10.1017/S0022377823000946>
- Lévy P (1926) Calcul des probabilités. *Rev Métaphys Morale* 33(3):3–6
- Li Y, Perlman E, Wan M, Yang Y, Meneveau C, Burns R, Chen S, Szalay A, Eyink G (2008) A public turbulence database cluster and applications to study Lagrangian evolution of velocity increments in turbulence. *J Turbul* 9:31. <https://doi.org/10.1080/14685240802376389>
- Li C, Deng W, Zhao L (2019) Well posedness and numerical algorithm for the tempered fractional differential equations. *Discrete Contin Dyn Syst, Ser B* 29(4):1989–2015. <https://doi.org/10.3934/dcdsb.2019026>
- Li T, Biferale L, Bonaccorso F, Scarpolini MA, Buzzicotti M (2024) Synthetic Lagrangian turbulence by generative diffusion models. *Nat Mach Intell* 6:393–403. <https://doi.org/10.1038/s42256-024-00810-0>
- Lin R (1974) Non-relativistic solar electrons. *Space Sci Rev* 16(1–2):189–256
- Lin RP (2005) Relationship of solar flare accelerated particles to solar energetic particles (SEPs) observed in the interplanetary medium. *Adv Space Res* 35(10):1857–1863. <https://doi.org/10.1016/j.asr.2005.02.087>
- Lischke A, Pang G, Gulian M, Song F, Glusa C, Zheng X, Mao Z, Cai W, Meerschaert MM, Ainsworth M, Karniadakis GE (2020) What is the fractional Laplacian? A comparative review with new results. *J Comput Phys* 404:109009. <https://doi.org/10.1016/j.jcp.2019.109009>
- Lithwick Y, Goldreich P (2001) Compressible magnetohydrodynamic turbulence in interstellar plasmas. *Astrophys J* 562(1):279–296. <https://doi.org/10.1086/323470>
- Litvinenko YE, Effenberger F (2014) Analytical solutions of a fractional diffusion-advection equation for solar cosmic-ray transport. *Astrophys J* 796(2):125. <https://doi.org/10.1088/0004-637X/796/2/125>
- Litvinenko YE, Fichtner H, Walter D (2017) Anomalous transport of cosmic rays in a nonlinear diffusion model. *Astrophys J* 841(1):57. <https://doi.org/10.3847/1538-4357/aa71ba>
- Litvinenko YE, Walter D, Fichtner H (2019) A nonlinear energetic particle diffusion model with a variable source. *AIP Adv* 9(5):055005. <https://doi.org/10.1063/1.5090953>
- Lübke J, Friedrich J, Grauer R (2023) Stochastic interpolation of sparsely sampled time series by a super-statistical random process and its synthesis in Fourier and wavelet space. *J Phys Complex* 4(1):015005. <https://doi.org/10.1088/2632-072X/acb128>
- Lübke J, Effenberger F, Wilbert M, Fichtner H, Grauer R (2024) Towards synthetic magnetic turbulence with coherent structures. *Europhys Lett* 146(4):43001. <https://doi.org/10.1209/0295-5075/ad438f>
- Lübke J, Reichherzer P, Aerdker S, Effenberger F, Wilbert M, Fichtner H, Grauer R (2025) Modeling cosmic-ray transport: magnetized versus unmagnetized motion in astrophysical magnetic turbulence. *arXiv e-prints arXiv:2505.18155*. <https://doi.org/10.48550/arXiv.2505.18155>
- Luce TC, Petty CC, de Haas JCM (1992) Inward energy transport in tokamak plasmas. *Phys Rev Lett* 68(1):52–55. <https://doi.org/10.1103/PhysRevLett.68.52>
- Luciani JF, Mora P, Virmont J (1983) Nonlocal heat transport due to steep temperature gradients. *Phys Rev Lett* 51(18):1664–1667. <https://doi.org/10.1103/PhysRevLett.51.1664>
- Maci D, Keppens R, Bacchini F (2024) BxC Toolkit: Generating tailored turbulent 3D magnetic fields. *Astrophys J Suppl* 273:11. <https://doi.org/10.3847/1538-4365/ad4bdf>

- Magdziarz M, Weron A (2007) Competition between subdiffusion and Lévy flights: a Monte Carlo approach. *Phys Rev E* 75(5):056702. <https://doi.org/10.1103/PhysRevE.75.056702>
- Mainardi F, Mura A, Pagnini G, Gorenflo R (2007) Sub-diffusion equations of fractional order and their fundamental solutions. In: Taş K, Tenreiro Machado JA, Baleanu D (eds) *Mathematical methods in engineering*. Springer, Dordrecht, pp 23–55. https://doi.org/10.1007/978-1-4020-5678-9_3
- Makarenko I, Bushby P, Fletcher A, Henderson R, Makarenko N, Shukurov A (2018a) Topological data analysis and diagnostics of compressible magnetohydrodynamic turbulence. *J Plasma Phys* 84(4). <https://doi.org/10.1017/s0022377818000752>
- Makarenko I, Shukurov A, Henderson R, Rodrigues LFS, Bushby P, Fletcher A (2018b) Topological signatures of interstellar magnetic fields – I. Betti numbers and persistence diagrams. *Mon Not R Astron Soc* 475(2):1843–1858. <https://doi.org/10.1093/mnras/stx3337>
- Malara F, Di Mare F, Nigro G, Sorriso-Valvo L (2016) Fast algorithm for a three-dimensional synthetic model of intermittent turbulence. *Phys Rev E* 94(5):053109. <https://doi.org/10.1103/PhysRevE.94.053109>
- Malara F, Perri S, Giacalone J, Zimbardo G (2023) Energetic particle dynamics in a simplified model of a solar wind magnetic switchback. *Astron Astrophys* 677:69. <https://doi.org/10.1051/0004-6361/202346990>
- Malkov M, Giacalone J, Guo F (2024) Flat spectra of energetic particles in interplanetary shock precursors. *Astrophys J* 973(1):27. <https://doi.org/10.3847/1538-4357/ad631e>
- Mallet A, Schekochihin AA, Chandran BDG, Chen CHK, Horbury TS, Wicks RT, Greenan CC (2016) Measures of three-dimensional anisotropy and intermittency in strong Alfvénic turbulence. *Mon Not R Astron Soc* 459(2):2130–2139. <https://doi.org/10.1093/mnras/stw802>
- Maron J, Goldreich P (2001) Simulations of incompressible magnetohydrodynamic turbulence. *Astrophys J* 554(2):1175–1196. <https://doi.org/10.1086/321413>
- Mason J, Cattaneo F, Boldyrev S (2006) Dynamic alignment in driven magnetohydrodynamic turbulence. *Phys Rev Lett* 97(25):255002
- Matthaeus WH, Goldstein ML, Aaron RD (1990) Evidence for the presence of quasi-two-dimensional nearly incompressible fluctuations in the solar wind. *J Geophys Res* 95:20673
- Matthaeus WH, Gray PC, Pontius DH Jr, Bieber JW (1995) Spatial structure and field-line diffusion in transverse magnetic turbulence. *Phys Rev Lett* 75:2136–2139
- Matthaeus WH, Qin G, Bieber JW, Zank GP (2003) Nonlinear collisionless perpendicular diffusion of charged particles. *Astrophys J* 590:53
- Merten L, Aerdker S (2025) Modeling cosmic-ray transport: a CRPropa based stochastic differential equation solver. *Comput Phys Commun* 311:109542. <https://doi.org/10.1016/j.cpc.2025.109542>
- Merten L, Becker Tjus J, Fichtner H, Eichmann B, Sigl G (2017) CRPropa 3.1—a low energy extension based on stochastic differential equations. *J Cosmol Astropart Phys* 2017(6):046. <https://doi.org/10.1088/1475-7516/2017/06/046>
- Mertsch P (2020) Test particle simulations of cosmic rays. *Astrophys Space Sci* 365(8):135. <https://doi.org/10.1007/s10509-020-03832-3>
- Metzler R, Klafter J (2000) The random walk’s guide to anomalous diffusion: a fractional dynamics approach. *Phys Rep* 339(1):1–77. [https://doi.org/10.1016/S0370-1573\(00\)00070-3](https://doi.org/10.1016/S0370-1573(00)00070-3)
- Metzler R, Klafter J (2004) TOPICAL REVIEW: the restaurant at the end of the random walk: recent developments in the description of anomalous transport by fractional dynamics. *J Phys A, Math Gen* 37:161–208. <https://doi.org/10.1088/0305-4470/37/31/R01>
- Montroll EW, Weiss GH (1965) Random walks on lattices. II. *J Math Phys* 6(2):167–181. <https://doi.org/10.1063/1.1704269>
- Moradi A, Li G (2019) Propagation of scatter-free solar energetic electrons in a meandering interplanetary magnetic field. *Astrophys J* 887(1):102. <https://doi.org/10.3847/1538-4357/ab4f68>
- Müller N, Manz P, Ramisch M (2023) Nondiffusive particle transport in the stellarator experiment TJ-K. *Phys Plasmas* 30(9):092306. <https://doi.org/10.1063/5.0156125>
- Muzy J-F (2019) Continuous cascades in the wavelet space as models for synthetic turbulence. *Phys Rev E* 99(4):042113. <https://doi.org/10.1103/PhysRevE.99.042113>
- Nakanotani M, Zank GP, Zhao L (2022) Particle acceleration in an MHD-scale system of multiple current sheets. *Front Astron Space Sci* 9:954040. <https://doi.org/10.3389/fspas.2022.954040>
- Neuer M, Spatschek KH (2006) Diffusion of test particles in stochastic magnetic fields for small Kubo numbers. *Phys Rev E* 73:26404
- Palmer I (1982) Transport coefficients of low-energy cosmic rays in interplanetary space. *Rev Geophys* 20(2):335–351
- Paradisi P, Cesari R, Mainardi F, Tampieri F (2001) The fractional Fick’s law for non-local transport processes. *Phys A, Stat Mech Appl* 293(1):130–142. [https://doi.org/10.1016/S0378-4371\(00\)00491-X](https://doi.org/10.1016/S0378-4371(00)00491-X)
- Parker EN (1965) The passage of energetic charged particles through interplanetary space. *Planet Space Sci* 13(1):9–49. [https://doi.org/10.1016/0032-0633\(65\)90131-5](https://doi.org/10.1016/0032-0633(65)90131-5)

- Pecora F, Servidio S, Greco A, Matthaeus WH, McComas DJ, Giacalone J, Joyce CJ, Getachew T, Cohen CMS, Leske RA, Wiedenbeck ME, McNutt RL, Hill ME, Mitchell DG, Christian ER, Roelof EC, Schwadron NA, Bale SD (2021) Parker Solar Probe observations of helical structures as boundaries for energetic particles. *Mon Not R Astron Soc* 508(2):2114–2122. <https://doi.org/10.1093/mnras/stab2659>
- Pei C, Jokipii JR, Giacalone J (2006) Effect of a random magnetic field on the onset times of solar particle events. *Astrophys J* 641(2):1222–1226. <https://doi.org/10.1086/427161>
- Pereira RM, Garban C, Chevillard L (2016) A dissipative random velocity field for fully developed fluid turbulence. *J Fluid Mech* 794:369–408. <https://doi.org/10.1017/jfm.2016.166>
- Perri S (2018) Superdiffusion of relativistic electrons at supernova remnant shocks. *Plasma Phys Control Fusion* 60(1):014005. <https://doi.org/10.1088/1361-6587/aa8602>
- Perri S, Zimbardo G (2007) Evidence of superdiffusive transport of electrons accelerated at interplanetary shocks. *Astrophys J Lett* 671(2):177
- Perri S, Zimbardo G (2008a) Observations of anomalous transport of energetic electrons in the heliosphere. *Astrophys Space Sci Trans* 4(1):27–30. <https://doi.org/10.5194/astra-4-27-2008>
- Perri S, Zimbardo G (2008b) Superdiffusive transport of electrons accelerated at corotating interaction regions. *J Geophys Res Space Phys* 113:03107. <https://doi.org/10.1029/2007JA012695>
- Perri S, Zimbardo G (2009a) Ion and electron superdiffusive transport in the interplanetary space. *Adv Space Res* 44(4):465–470. <https://doi.org/10.1016/j.asr.2009.04.017>
- Perri S, Zimbardo G (2009b) Ion superdiffusion at the solar wind termination shock. *Astrophys J Lett* 693(2):118
- Perri S, Zimbardo G (2012a) Superdiffusive shock acceleration. *Astrophys J* 750(2):87. <https://doi.org/10.1088/0004-637X/750/2/87>
- Perri S, Zimbardo G (2012b) Magnetic variances and pitch-angle scattering times upstream of interplanetary shocks. *Astrophys J* 754(1):8. <https://doi.org/10.1088/0004-637X/754/1/8>
- Perri S, Zimbardo G (2015) Short acceleration times from superdiffusive shock acceleration in the heliosphere. *Astrophys J* 815(1):75. <https://doi.org/10.1088/0004-637X/815/1/75>
- Perri S, Zimbardo G, Effenberger F, Fichtner H (2015) Parameter estimation of superdiffusive motion of energetic particles upstream of heliospheric shocks. *Astron Astrophys* 578:2. <https://doi.org/10.1051/0004-6361/201425295>
- Perri S, Amato E, Zimbardo G (2016) Transport of relativistic electrons at shocks in shell-type supernova remnants: diffusive and superdiffusive regimes. *Astron Astrophys* 596:34. <https://doi.org/10.1051/0004-6361/201628767>
- Perri S, Pucci F, Malara F, Zimbardo G (2019) On the power-law distribution of pitch-angle scattering times in solar wind turbulence. *Sol Phys* 294(3):34. <https://doi.org/10.1007/s11207-019-1421-y>
- Perri S, Prete G, Malara F, Pucci F, Zimbardo G (2021) The influence of magnetic turbulence on the energetic particle transport upstream of shock waves. *Atmosphere* 12(4):508. <https://doi.org/10.3390/atmos12040508>
- Perri S, Bykov A, Fahr H, Fichtner H, Giacalone J (2022) Recent developments in particle acceleration at shocks: theory and observations. *Space Sci Rev* 218(4):26. <https://doi.org/10.1007/s11214-022-00892-5>
- Perrone D, Dendy R, Furno I, Sanchez R, Zimbardo G, Bovet A, Fasoli A, Gustafson K, Perri S, Ricci P, et al (2013) Nonclassical transport and particle-field coupling: from laboratory plasmas to the solar wind. *Space Sci Rev* 178(2–4):233–270. <https://doi.org/10.1007/s11214-013-9966-9>
- Petty CC, Luce TC (1994) Inward transport of energy during off-axis heating on the DIII-D tokamak. *Nucl Fusion* 34(1):121–130. <https://doi.org/10.1088/0029-5515/34/1/109>
- Pezzi O, Blasi P (2023) Galactic cosmic ray transport in the absence of resonant scattering. *Mon Not R Astron Soc* 529(1):13–18. <https://doi.org/10.1093/mnras/slad192>
- Pommois P, Zimbardo G, Veltri P (2007) Anomalous, non-Gaussian transport of charged particles in anisotropic magnetic turbulence. *Phys Plasmas* 14(1):012311. <https://doi.org/10.1063/1.2434795>
- Prete G, Perri S, Zimbardo G (2019) Influence of the transport regime on the energetic particle density profiles upstream and downstream of interplanetary shocks. *Adv Space Res* 63(8):2659–2671. <https://doi.org/10.1016/j.asr.2019.01.002>
- Prete G, Perri S, Zimbardo G (2021) Energetic particle fluxes at heliospheric shocks: evidences of superdiffusion and comparison between analytical and numerical modeling. *New Astron* 87:101605. <https://doi.org/10.1016/j.newast.2021.101605>
- Ptuskin VS, Zirakashvili VN, Plesser AA (2008) Non-linear diffusion of cosmic rays. *Adv Space Res* 42:486–490. <https://doi.org/10.1016/j.asr.2007.12.007>
- Pucci F, Malara F, Perri S, Zimbardo G, Sorriso-Valvo L, Valentini F (2016) Energetic particle transport in the presence of magnetic turbulence: influence of spectral extension and intermittency. *Mon Not R Astron Soc* 459(3):3395–3406. <https://doi.org/10.1093/mnras/stw877>

- Qin G, Shalchi A (2016) Numerical test of different approximations used in the transport theory of energetic particles. *Astrophys J* 823:23
- Qin G, Matthaeus WH, Bieber JW (2002a) Perpendicular transport of charged particles in composite model turbulence: recovery of diffusion. *Astrophys J Lett* 578:117–120
- Qin G, Matthaeus WH, Bieber JW (2002b) Subdiffusive transport of charged particles perpendicular to the large scale magnetic field. *Geophys Res Lett* 29:1048
- Qin G, Wang Y, Zhang M, Dalla S (2013) Transport of solar energetic particles accelerated by ICME shocks: reproducing the reservoir phenomenon. *Astrophys J* 766(2):74. <https://doi.org/10.1088/0004-637X/766/2/74>
- Ragot BR, Kirk JG (1997) Anomalous transport of cosmic ray electrons. *Astron Astrophys* 327:432–440
- Reames DV (1999) Particle acceleration at the sun and in the heliosphere. *Space Sci Rev* 90(3–4):413–491
- Rechester AB, Rosenbluth MN (1978) Electron heat transport in a tokamak with destroyed magnetic surfaces. *Phys Rev Lett* 40:38–41
- Reichherzer P (2022) Consideration of real-time effects for improved coordination of multi-messenger campaigns. PhD thesis. Ruhr-Universität Bochum. <https://doi.org/10.13154/294-9255>
- Reichherzer P, Becker Tjus J, Zweibel EG, Merten L, Pueschel MJ (2022a) Anisotropic cosmic ray diffusion in isotropic Kolmogorov turbulence. *Mon Not R Astron Soc* 514(2):2658–2666. <https://doi.org/10.1093/mnras/stac1408>
- Reichherzer P, Merten L, Dörner J, Becker Tjus J, Pueschel MJ, Zweibel EG (2022b) Regimes of cosmic-ray diffusion in galactic turbulence. *SN Appl Sci* 4:15. <https://doi.org/10.1007/s42452-021-04891-z>
- Reichherzer P, Bott AFA, Ewart RJ, Gregori G, Kempinski P, Kunz MW, Schekochihin AA (2025) Efficient micromirror confinement of sub-tera-electronvolt cosmic rays in galaxy clusters. *Nat Astron* 9:438–448. <https://doi.org/10.1038/s41550-024-02442-1>
- Riesz M (1949) L'intégrale de Riemann-Liouville et le problème de Cauchy
- Riordan JD, Pe'er A (2019) Pitch-angle diffusion and Bohm-type approximations in diffusive shock acceleration. *Astrophys J* 873(1):13. <https://doi.org/10.3847/1538-4357/aaffd2>
- Roberts OW, Alexandrova O, Sorriso-Valvo L, Vörös Z, Nakamura R, Fischer D, Varsani A, Escoubet CP, Volwerk M, Canu P, Lion S, Yearby K (2022) Scale-dependent kurtosis of magnetic field fluctuations in the solar wind: a multi-scale study with cluster 2003–2015. *J Geophys Res Space Phys* 127(9):e2021JA029483. <https://doi.org/10.1029/2021JA029483>
- Rosales C, Meneveau C (2006) A minimal multiscale Lagrangian map approach to synthesize non-Gaussian turbulent vector fields. *Phys Fluids* 18(7):075104. <https://doi.org/10.1063/1.2227003>
- Rosales C, Meneveau C (2008) Anomalous scaling and intermittency in three-dimensional synthetic turbulence. *Phys Rev E* 78(1):016313. <https://doi.org/10.1103/PhysRevE.78.016313>
- Ruffolo D, Matthaeus WH, Chuychai P (2003) Trapping of solar energetic particles by the small-scale topology of solar wind turbulence. *Astrophys J Lett* 597(2):169–172. <https://doi.org/10.1086/379847>
- Ruffolo D, Matthaeus WH, Chuychai P (2004) Separation of magnetic field lines in two-component turbulence. *Astrophys J* 614(1):420–434. <https://doi.org/10.1086/423412>
- Sánchez R, Carreras BA, Newman DE, Lynch VE, van Milligen BP (2006) Renormalization of tracer turbulence leading to fractional differential equations. *Phys Rev E* 74(1):016305. <https://doi.org/10.1103/PhysRevE.74.016305>
- Schekochihin AA (2022) MHD turbulence: a biased review. *J Plasma Phys* 88(5):155880501. <https://doi.org/10.1017/S0022377822000721>
- Schlegel L, Frie A, Eichmann B, Reichherzer P, Tjus JB (2020) Interpolation of turbulent magnetic fields and its consequences on cosmic ray propagation. *Astrophys J* 889(2):123. <https://doi.org/10.3847/1538-4357/ab643b>
- Schlickeiser R (1989) Cosmic-ray transport and acceleration. I. Derivation of the kinetic equation and application to cosmic rays in static cold media. *Astrophys J* 336:243. <https://doi.org/10.1086/167009>
- Servidio S, Greco A, Matthaeus WH, Osman KT, Dmitruk P (2011) Statistical association of discontinuities and reconnection in magnetohydrodynamic turbulence. *J Geophys Res Space Phys* 116(A9):09102. <https://doi.org/10.1029/2011JA016569>
- Shalchi A (2005) Second-order quasilinear theory of cosmic ray transport. *Phys Plasmas* 12:052905
- Shalchi A (2006) Analytical investigation of the two-dimensional Fokker-Planck equation. *Astron Astrophys* 448:809
- Shalchi A (2009) Nonlinear cosmic ray diffusion theories. *Astrophysics and Space Science Library*, vol 362. Springer, Berlin. <https://doi.org/10.1007/978-3-642-00309-7>
- Shalchi A (2010) A unified particle diffusion theory for cross-field scattering: subdiffusion, recovery of diffusion, and diffusion in three-dimensional turbulence. *Astrophys J Lett* 720:127–130
- Shalchi A (2011) Applicability of the Taylor-Green-Kubo formula in particle diffusion theory. *Phys Rev E* 83:046402


- Shalchi A (2015a) Finite gyroradius corrections in the theory of perpendicular diffusion 1. Suppressed velocity diffusion. *Adv Space Res* 56:1264
- Shalchi A (2015b) Perpendicular diffusion of energetic particles in collisionless plasmas. *Phys Plasmas* 22:010704
- Shalchi A (2016) Finite gyroradius corrections in the theory of perpendicular diffusion 2. Strong velocity diffusion. *Adv Space Res* 57:431
- Shalchi A (2019) Heuristic description of perpendicular diffusion of energetic particles in astrophysical plasmas. *Astrophys J Lett* 881:27
- Shalchi A (2020a) Heuristic description of perpendicular particle transport in turbulence with super-diffusive magnetic field lines. *Astrophys J* 898:135
- Shalchi A (2020b) Perpendicular transport of energetic particles in magnetic turbulence. *Space Sci Rev* 216:23. <https://doi.org/10.1007/s11214-020-0644-4>
- Shalchi A (2021a) Field line random walk in magnetic turbulence. *Phys Plasmas* 28:120501
- Shalchi A (2021b) Perpendicular diffusion of energetic particles: a complete analytical theory. *Astrophys J* 923:209
- Shalchi A (2022) The ratio of perpendicular and parallel diffusion coefficients of low-energy particles in turbulent space plasmas. *Astrophys J* 936:1
- Shalchi A (2024) Heuristic construction of field line random walk diffusion coefficients. *Adv Space Res* 73(1):1073–1082. <https://doi.org/10.1016/j.asr.2023.09.015>
- Shalchi A, Dosch A (2008) Nonlinear guiding center theory of perpendicular diffusion: derivation from the Newton-Lorentz equation. *Astrophys J* 685(2):971–975. <https://doi.org/10.1086/591518>
- Shalchi A, Hussein M (2015) Erratum to: benchmarking the unified nonlinear transport theory for Goldreich-Sridhar turbulence. *Astrophys Space Sci* 355:243–244
- Shalchi A, Kourakis I (2007a) Analytical description of stochastic field-line wandering in magnetic turbulence. *Phys Plasmas* 14:092903
- Shalchi A, Kourakis I (2007b) A new theory for perpendicular transport of cosmic rays. *Astron Astrophys* 470:405
- Shalchi A, Kourakis I (2007c) Random walk of magnetic field lines for different values of the energy range spectral index. *Phys Plasmas* 14:112901
- Shalchi A, Weinhorst B (2009) Random walk of magnetic field lines: subdiffusive, diffusive, and superdiffusive regimes. *Adv Space Res* 43:1429–1435
- Shalchi A, Škoda T, Tautz RC, Schlickeiser R (2009) Analytical description of nonlinear cosmic ray scattering: isotropic and quasilinear regimes of pitch-angle diffusion. *Astron Astrophys* 507:589
- Shebalin JV, Matthaeus WH, Montgomery D (1983) Anisotropy in MHD turbulence due to a mean magnetic field. *J Plasma Phys* 29(3):525–547. <https://doi.org/10.1017/S0022377800000933>
- Shlesinger MF, West BJ, Klafter J (1987) Levy dynamics of enhanced diffusion - application to turbulence. *Phys Rev Lett* 58:1100–1103. <https://doi.org/10.1103/PhysRevLett.58.1100>
- Shukurov A, Snodin AP, Seta A, Bushby PJ, Wood TS (2017) Cosmic rays in intermittent magnetic fields. *Astrophys J Lett* 839(1):16. <https://doi.org/10.3847/2041-8213/aa6aa6>
- Skilling J (1975a) Cosmic ray streaming - I. Effect of Alfvén waves on particles. *Mon Not R Astron Soc* 172:557–566. <https://doi.org/10.1093/mnras/172.3.557>
- Skilling J (1975b) Cosmic ray streaming - III. Self-consistent solutions. *Mon Not R Astron Soc* 173:255–269. <https://doi.org/10.1093/mnras/173.2.255>
- Sorriso-Valvo L, Carbone F, Leonardis E, Chen CHK, Šafránková J, Němeček Z (2017) Multifractal analysis of high resolution solar wind proton density measurements. *Adv Space Res* 59(6):1642–1651. <https://doi.org/10.1016/j.asr.2016.12.024>
- Stern R, Effenberger F, Fichtner H, Schäfer T (2014) The space-fractional diffusion-advection equation: analytical solutions and critical assessment of numerical solutions. *Fract Calc Appl Anal* 17(1):171–190
- Strang G (1968) On the construction and comparison of difference schemes. *SIAM J Numer Anal* 5(3):506–517. <https://doi.org/10.1137/0705041>
- Strauss RD, Effenberger F (2017) A hitch-hiker's guide to stochastic differential equations: solution methods for energetic particle transport in space physics and astrophysics. *Space Sci Rev* 212(1–2):151–192. <https://doi.org/10.1007/s11214-017-0351-y>
- Strauss RD, Fichtner H (2015) On aspects pertaining to the perpendicular diffusion of solar energetic particles. *Astrophys J* 801(1):29. <https://doi.org/10.1088/0004-637X/801/1/29>
- Strauss RDT, Dresing N, Engelbrecht NE (2017) Perpendicular diffusion of solar energetic particles: model results and implications for electrons. *Astrophys J* 837(1):43. <https://doi.org/10.3847/1538-4357/aa5df5>
- Strauss RD, van den Berg JP, Engelbrecht NE, Wijsen N (2023) On the causality problem in focused particle transport. *J Phys Conf Ser* 2544:012008. <https://doi.org/10.1088/1742-6596/2544/1/012008>
- Stroth U, Geist T, Koponen JP, Hartfuß H-J, Zeiler P (1999) ECRH and W7-as team, evidence for convective inward particle transport in a stellarator. *Phys Rev Lett* 82(5):928–931. <https://doi.org/10.1103/PhysRevLett.82.928>

- Subedi P, Chhiber R, Tessein JA, Wan M, Matthaeus WH (2014) Generating synthetic magnetic field intermittency using a minimal multiscale Lagrangian mapping approach. *Astrophys J* 796(2):97. <https://doi.org/10.1088/0004-637X/796/2/97>
- Subedi P, Sonsrrettee W, Blasi P, Ruffolo D, Matthaeus WH, Montgomery D, Chuychai P, Dmitruk P, Wan M, Parashar TN, Chhiber R (2017) Charged particle diffusion in isotropic random magnetic fields. *Astrophys J* 837(2):140. <https://doi.org/10.3847/1538-4357/aa603a>
- Sun P, Jokipii JR (2011) Charged particle transport in anisotropic magnetic turbulence. In: American geophysical union, fall meeting 2011. Am. Geophys. Union, Washington, p 1903
- Tateishi AA, Ribeiro HV, Lenzi EK (2017) The role of fractional time-derivative operators on anomalous diffusion. *Front Phys* 5:52. <https://doi.org/10.3389/fphy.2017.00052>
- Tautz RC (2010) A new simulation code for particle diffusion in anisotropic, large-scale and turbulent magnetic fields. *Comput Phys Commun* 181:71–77
- Tautz RC (2013) Pitch-angle scattering in magnetostatic turbulence. II. Analytical considerations and pitch-angle isotropization. *Astron Astrophys* 558:148. <https://doi.org/10.1051/0004-6361/201322143>
- Tautz RC, Dosch A, Effenberger F, Fichtner H, Kopp A (2013) Pitch-angle scattering in magnetostatic turbulence. I. Test-particle simulations and the validity of analytical results. *Astron Astrophys* 558:147. <https://doi.org/10.1051/0004-6361/201322142>
- Taylor GI (1922) Diffusion by continuous movements. *Proc Lond Math Soc* 20:196
- Telloni D, Sorriso-Valvo L, Woodham LD, Panasenco O, Velli M, Carbone F, Zank GP, Bruno R, Perrone D, Nakanotani M, Shi C, D'Amicis R, Marco RD, Jagarlamudi VK, Steinvall K, Marino R, Adhikari L, Zhao L, Liang H, Tenerani A, Laker R, Horbury TS, Bale SD, Pulupa M, Malaspina DM, MacDowall RJ, Goetz K, de Wit TD, Harvey PR, Kasper JC, Korreck KE, Larson D, Case AW, Stevens ML, Whittlesey P, Livi R, Owen CJ, Livi S, Louarn P, Antonucci E, Romoli M, O'Brien H, Evans V, Angelini V (2021) Evolution of solar wind turbulence from 0.1 to 1 au during the first Parker Solar Probe–Solar Orbiter radial alignment. *Astrophys J Lett* 912(2):21. <https://doi.org/10.3847/2041-8213/abf7d1>
- Torsti J, Riihonen E, Kocharov L (2004) The 1998 May 2–3 magnetic cloud: an interplanetary “highway” for solar energetic particles observed with SOHO/ERNE. *Astrophys J Lett* 600(1):83–86. <https://doi.org/10.1086/381575>
- Trenchi L, Bruno R, Telloni D, D'Amicis R, Marcucci MF, Zurbuchen TH, Weberg M (2013) Solar energetic particle modulations associated with coherent magnetic structures. *Astrophys J* 770(1):11. <https://doi.org/10.1088/0004-637X/770/1/11>
- Trotta EM, Zimbardo G (2011) Quasi-ballistic and superdiffusive transport for impulsive solar particle events. *Astron Astrophys* 530:130. <https://doi.org/10.1051/0004-6361/201016278>
- Trotta EM, Zimbardo G (2015) A numerical study of Lévy random walks: mean square displacement and power-law propagators. *J Plasma Phys* 81(1):325810108. <https://doi.org/10.1017/S0022377814000592>
- Trotta D, Burgess D, Prete G, Perri S, Zimbardo G (2020) Particle transport in hybrid PIC shock simulations: a comparison of diagnostics. *Mon Not R Astron Soc* 491(1):580–595. <https://doi.org/10.1093/mnras/stz2760>
- Tsallis C, Bukman DJ (1996) Anomalous diffusion in the presence of external forces: exact time-dependent solutions and their thermostatical basis. *Phys Rev E* 54(3):2197–2200. <https://doi.org/10.1103/PhysRevE.54.R2197>
- Vallaes V, Tyson RC, Lane WD, Deleersnijder E, Hanert E (2017) A Lévy-flight diffusion model to predict transgenic pollen dispersal. *J R Soc Interface* 14:20160889
- van den Berg JP, Engelbrecht NE, Wijsen N, Strauss RD (2021) On the turbulent reduction of drifts for solar energetic particles. *Astrophys J* 922(2):200. <https://doi.org/10.3847/1538-4357/ac2736>
- van den Berg JP, Els PL, Engelbrecht NE (2024) An evaluation of different numerical methods to calculate the pitch-angle diffusion coefficient from full-orbit simulations: disentangling a rope of sand. *Astrophys J* 977(2):174. <https://doi.org/10.3847/1538-4357/ad8b4a>
- van Milligen BP, Carreras BA, Sánchez R (2004) Uphill transport and the probabilistic transport model. *Phys Plasmas* 11(8):3787–3794. <https://doi.org/10.1063/1.1763915>
- Walter D, Fichtner H, Litvinenko Y (2020) A perturbative approach to a nonlinear advection-diffusion equation of particle transport. *Phys Plasmas* 27(8):082901. <https://doi.org/10.1063/5.0003582>
- Walter D, Effenberger F, Fichtner H, Litvinenko Y (2022) A nonlinear model of diffusive particle acceleration at a planar shock. *Phys Plasmas* 29(7):072302. <https://doi.org/10.1063/5.0094667>
- Wan M, Matthaeus WH, Roytershteyn V, Parashar TN, Wu P, Karimabadi H (2016) Intermittency, coherent structures and dissipation in plasma turbulence. *Phys Plasmas* 23(4). <https://doi.org/10.1063/1.4945631>
- Webb GM, Gleeson LJ (1977) Green's theorem and Green's functions for the steady-state cosmic-ray equation of transport. *Astrophys Space Sci* 50(1):205–223. <https://doi.org/10.1007/BF00648532>
- Webb G, Zank G, Kaghshvili EK, Le Roux J (2006) Compound and perpendicular diffusion of cosmic rays and random walk of the field lines. I. Parallel particle transport models. *Astrophys J* 651(1):211

- Yan H, Lazarian A (2002) Scattering of cosmic rays by magnetohydrodynamic interstellar turbulence. *Phys Rev Lett* 89(28):281102. <https://doi.org/10.1103/PhysRevLett.89.281102>
- Zaburdaev V, Denisov S, Klafter J (2015) Lévy walks. *Rev Mod Phys* 87(2):483–530. <https://doi.org/10.1103/RevModPhys.87.483>
- Zanette DH (1998) Macroscopic current in fractional anomalous diffusion. *Phys A, Stat Mech Appl* 252(1):159–164. [https://doi.org/10.1016/S0378-4371\(97\)00613-4](https://doi.org/10.1016/S0378-4371(97)00613-4)
- Zank GP, Matthaeus WH (1992) The equations of reduced magnetohydrodynamics. *J Plasma Phys* 48(1):85–100. <https://doi.org/10.1017/S002237780001638X>
- Zank GP, Matthaeus WH (1993) Nearly incompressible fluids. II: magnetohydrodynamics, turbulence, and waves. *Phys Fluids A* 5(1):257–273. <https://doi.org/10.1063/1.858780>
- Zank GP, Adhikari L, Hunana P, Shiota D, Bruno R, Telloni D (2017) Theory and transport of nearly incompressible magnetohydrodynamic turbulence. *Astrophys J* 835(2):147. <https://doi.org/10.3847/1538-4357/835/2/147>
- Zank GP, Nakanotani M, Webb GM (2019) Compressible and incompressible magnetic turbulence observed in the very local interstellar medium by Voyager 1. *Astrophys J* 88:116
- Zaslavsky GM (2002) Chaos, fractional kinetics, and anomalous transport. *Phys Rep* 371(6):461–580. [https://doi.org/10.1016/S0370-1573\(02\)00331-9](https://doi.org/10.1016/S0370-1573(02)00331-9)
- Zhang C, Xu S (2023) Numerical testing of mirror diffusion of cosmic rays. *Astrophys J Lett* 959(1):8. <https://doi.org/10.3847/2041-8213/ad0fe5>
- Zhang M, McKibben R, Lopate C, Jokipii J, Giacalone J, Kallenrode M-B, Rassoul H (2003) Ulysses observations of solar energetic particles from the 14 July 2000 event at high heliographic latitudes. *J Geophys Res: Space Physics* (1978–2012) 108(A4)
- Zhao L-L, Zank GP, Adhikari L, Nakanotani M, Telloni D, Carbone F (2020) Spectral features in field-aligned solar wind turbulence from Parker Solar Probe observations. *Astrophys J* 898(2):113. <https://doi.org/10.3847/1538-4357/ab9b7e>
- Zhdankin V, Boldyrev S, Uzdensky DA (2016) Scalings of intermittent structures in magnetohydrodynamic turbulence. *Phys Plasmas* 23(5):055705. <https://doi.org/10.1063/1.4944820>
- Zheng J, Hu Q (2018) Observational evidence for self-generation of small-scale magnetic flux ropes from intermittent solar wind turbulence. *Astrophys J Lett* 852(2):23. <https://doi.org/10.3847/2041-8213/aaa3d7>
- Zimbardo G (2003) Numerical simulation of anomalous plasma transport in the presence of magnetic turbulence. *Commun Nonlinear Sci Numer Simul* 8(3):443–453. [https://doi.org/10.1016/S1007-5704\(03\)00051-0](https://doi.org/10.1016/S1007-5704(03)00051-0)
- Zimbardo G, Perri S (2013) From Lévy walks to superdiffusive shock acceleration. *Astrophys J* 778(1):35
- Zimbardo G, Perri S (2018) Understanding the radio spectral indices of galaxy cluster relics by superdiffusive shock acceleration. *Mon Not R Astron Soc* 478(4):4922–4930. <https://doi.org/10.1093/mnras/sty1438>
- Zimbardo G, Perri S (2020) Non-Markovian pitch-angle scattering as the origin of particle superdiffusion parallel to the magnetic field. *Astrophys J* 903(2):105. <https://doi.org/10.3847/1538-4357/abb951>
- Zimbardo G, Veltri P, Pommois P (2000) Anomalous, quasilinear, and percolative regimes for magnetic-field-line transport in axially symmetric turbulence. *Phys Rev E* 61(2):1940–1948. <https://doi.org/10.1103/PhysRevE.61.1940>
- Zimbardo G, Pommois P, Veltri P (2006) Superdiffusive and subdiffusive transport of energetic particles in solar wind anisotropic magnetic turbulence. *Astrophys J Lett* 639(2):91
- Zimbardo G, Perri S, Effenberger F, Fichtner H (2017) Fractional Parker equation for the transport of cosmic rays: steady-state solutions. *Astron Astrophys* 607:7. <https://doi.org/10.1051/0004-6361/201731179>
- Zimbardo G, Prete G, Perri S (2020) Collisionless shocks as a diagnostic tool for understanding energetic particle transport in space plasmas. *Front Astron Space Sci* 7:16
- Zumofen G, Klafter J (1993) Scale-invariant motion in intermittent chaotic systems. *Phys Rev E* 47:851–863. <https://doi.org/10.1103/PhysRevE.47.851>

Publisher's Note Springer Nature remains neutral with regard to jurisdictional claims in published maps and institutional affiliations.

Authors and Affiliations

F. Effenberger¹  · D. Walter¹ · H. Fichtner¹ · S. Aerdker¹ · R. Grauer¹ · T. Laitinen² · J.A. le Roux³ · Y. Litvinenko¹ · J. Lübke¹ · S. Perri⁴ · P. Reichherzer⁵ · A. Shalchi⁶ · J.P. van den Berg⁷ · G. Zimbardo⁴

- ✉ F. Effenberger
frederic.effenberger@rub.de
- D. Walter
dw@tp4.rub.de
- H. Fichtner
hf@tp4.rub.de
- S. Aerdker
sophie@tp4.rub.de
- R. Grauer
grauer@tp1.rub.de
- T. Laitinen
tlmlaitinen@uclan.ac.uk
- J.A. le Roux
jar0013@uah.edu
- Y. Litvinenko
yuri@tp4.rub.de
- J. Lübke
jeremiah.luebke@rub.de
- S. Perri
silvia.perri@fis.unical.it
- P. Reichherzer
patrick.reichherzer@physics.ox.ac.uk
- A. Shalchi
andreas.shalchi@umanitoba.ca
- J.P. van den Berg
24182869@mynwu.ac.za
- G. Zimbardo
gaetano.zimbardo@fis.unical.it

- ¹ Ruhr-University Bochum, Bochum, Germany
- ² University of Central Lancashire, Preston, UK
- ³ University of Alabama in Huntsville, Huntsville, USA
- ⁴ University of Calabria, Rende, Italy
- ⁵ University of Oxford, Oxford, UK
- ⁶ University of Manitoba, Winnipeg, Canada
- ⁷ North-West University, Potchefstroom, South Africa